UNCLASSIFIED

CENTRAL RESEARCH LIBRARY
DOCUMENT COLLECTION

OAK RIDGE NATIONAL LABORATORY LIBRARY
3 4456 0024746 3

ORNL-1705
Progress
Cy. 4

PHYSICS DIVISION

SEMIANNUAL PROGRESS REPORT

FOR PERIOD ENDING MARCH 10, 1954

CENTRAL RESEARCH LIBRARY
DOCUMENT COLLECTION

LIBRARY LOAN COPY

DO NOT TRANSFER TO ANOTHER PERSON

If you wish someone else to see this document, send in name with document and the library will arrange a loan.

OAK RIDGE NATIONAL LABORATORY
OPERATED BY
CARBIDE AND CARBON CHEMICALS COMPANY
A DIVISION OF UNION CARBIDE AND CARBON CORPORATION
UCC
POST OFFICE BOX P
OAK RIDGE, TENNESSEE

UNCLASSIFIED

ORNL 1705

Copy No 4

C t t No W 7405 g 26

PHYSICS DIVISION

SEMIANNUAL PROGRESS REPORT

for Period Ending March 10 1954

A H Snell Director

Edited by
J L Fowler and E O Wollan
Associate Directors

DATE ISSUED

JUN 1 1954

OAK RIDGE NATIONAL LABORATORY
Op t d by
CARBIDE AND CARBON CHEMICALS COMPANY
A D o of U o C b de d C bon Co p t
Po t Off Box P
Oak R dge Te e e

3 4456 0024746 3

INTERNAL DISTRIBUTION

1 C E Center
2 Biology Library
3 Health Physics Library
4 5 Central Research Library
6 Reactor Experimental Engineering Library
7 11 Laboratory Records Department
12 Laboratory Records ORNL R C
13 C E Larson
14 L B Emlet (K 25)
15 J P Murray (Y 12)
16 A M Weinberg
17 E H Taylor
18 E D Shipley
19 E J Murphy
20 F C VonderLage
21 A H Snell
22 A Hollaender
23 J A Swartout
24 K Z Morgan
25 F L Culler
26 M T Kelley
27 E M King
28 E O Wollan
29 D W Cardwell
30 A S Householder
31 L D Roberts
32 R B Briggs
33 R N Lyon
34 W C Koehler
35 W K Ergen
36 E P Blizard
37 M E Rose
38 G E Boyd
39 Lewis Nelson
40 R W Stoughton
41 C E Winters
42 W H Jordan
43 E C Campbell
44 D S Billington
45 M A Bredig
46 R S Livingston
47 C P Keim
48 J L Meem
49 C E Clifford
50 G H Clewett
51 C D Susano
52 C J Borkowski
53 M J Skinner
54 M K Wilkinson
55 S Bernstein
56 P M Reyling
57 D D Cowen
58 W M Good
59 G C Williams
60 J L Fowler
61 R W Johnson
62 J R McNally Jr
63 R G Cochran
64 C L Storrs
65 P M Steir
66 J H Neiler
67 E P Wigner (consultant)
68 H A Bethe (consultant)
69 K Lark Horovitz (consultant)
70 Eugene Guth (consultant)
71 J G Daunt (consultant)
72 W M Breazeale (consultant)
73 E C Smith
74 C G Hull
75 P R Bell
76 G G Kelley
77 C C Harris
78 H G MacPherson (consultant)

EXTERNAL DISTRIBUTION

79 W G Pollard ORINS
80 W K H Panofsky Stanford University
81 L C Biedenharn Sloans Physics Laboratory
82 R F Bacher California Institute of Technology
83 84 Ohio State University Attn Professor of Naval Science
85 John Dunning Columbia University
86 Phillips Petroleum Co Attn Librarian
87 R L Heath American Cyanamid Co
88 S DeBenedetti Carnegie Institute of Technology
89 Massachusetts Institute of Technology Department of Electrical Engineering
90 A von Hippel Laboratory for Insulation Research MIT
91 M Goodrich Louisiana State University
92 Truman S Grey Massachusetts Institute of Technology
93 V C Wilson General Electric Co Schenectady
94 D S Hughes University of Texas
95 343 Given distribution as shown in TID 4500 under Physics Category

Physics Division quarterly progress reports previously issued in this series are as follows

ORNL 325 Supplement	December January and February 1948 1949
ORNL 366	Period Ending June 15 1949
ORNL 481	Period Ending September 25 1949
ORNL 577	Period Ending December 15 1949
ORNL 694	Period Ending March 15 1950
ORNL 782	Period Ending June 15 1950
ORNL 865	Period Ending September 20 1950
ORNL 940	Period Ending December 20 1950
ORNL 1005	Period Ending March 20 1951
ORNL 1092	Period Ending June 20 1951
ORNL 1164	Period Ending September 20 1951
ORNL 1278	Period Ending December 20 1951
ORNL 1289	Period Ending March 20 1952
ORNL 1365	Period Ending June 20 1952
ORNL 1415	Period Ending September 20 1952
ORNL 1496	Period Ending December 20 1952
ORNL 1620	Period Ending September 10 1953

CONTENTS

PUBLICATIONS vii

PAPERS PRESENTED AT MEETINGS viii

ANNOUNCEMENTS ix

SUMMARY 1

1 HIGH VOLTAGE PHYSICS 3

Polarization of Fast Neutrons 3
Differential Neutron Scattering Cross Section for Nitrogen 4
Levels in Be^8 and Be^9 from the $Li^6(He^3\ p)Be^8$ and $Li^7(He^3\ p)Be^9$ Reactions 5
Triton Yields from Lithium Isotopes 7
Excitation of Nuclei by the Coulomb Field of Protons 8
Gamma Ray Spectrum and Gamma Ray Yield from Boron Bombarded by Protons 11

2 RADIOACTIVITY AND NUCLEAR ISOMERISM 18

Angular Correlation of Gamma Rays 18
Broad Beam Gamma Attenuations 19

3 NEUTRON DIFFRACTION 31

Neutron Diffraction Studies on Iron at High Temperatures 31
Neutron–Magnetic Diffraction Study of the Perovskite Type Compounds $(La\ Ca)MnO_3$ 34
Search for Antiferromagnetism in the Silicides V_3Si Cr_3Si and Mo_3Si 39

4 LOW TEMPERATURE PHYSICS 40

An Approximate Partition Function for Certain Iron Group Salts at Low Temperatures 40
Method for Brute Force Polarization of Hydrogen Nuclei 40
Low Temperature Specific Heat Anomaly of $MnCl_2$ 41

5 HEAVY ION PHYSICS 43

Investigation of Electron Capture and Loss for Heavy Ions Passing Through Gases 43

6 NEUTRON PHYSICS 50

Demonstration of Neutron Spin from Bloch Alvarez Type of Experiment 50

7 THEORETICAL PHYSICS 52

Tabulation of Angular Momentum Functions 52
Machine Computation of High Energy Electron Scattering 52
Maximum Values for Resonance Cross Sections 52
Polarization from Isolated Resonances 52
Theory of Nuclear Reactions with Radioactive Products 53
Quantum Electrodynamics 53
Oscillation Frequencies of Charged Particles in Axially Symmetric Electrostatic Fields 53

PUBLICATIONS

F K McGowan Internal Conversion Electron Gamma Directional Angular Correlation of Bi^{207} *Phys Rev* **92** 524 (1953)

F K McGowan and E C Campbell Internal Conversion and Directional Angular Correlation of the Bi^{207} Gammas *Phys Rev* **92** 523 (1953)

W C Koehler and E O Wollan Neutron Diffraction Study of the Structure of the *A* form of the Rare Earth Sesquioxides *Acta Cryst* **6** 741 (1953)

C D Moak A Study of the $H^3 + He^3$ Reactions *Phys Rev* **92** 383 (1953)

A Simon Theory of Polarized Particles and Gamma Rays in Nuclear Reactions *Phys Rev* **92** 1050 (1953)

M E Rose Angular Correlation of Nuclear Radiations *Science* **118** 635 (1953)

G T Trammell Magnetic Scattering of Neutrons from Rare Earth Ions *Phys Rev* **92** 1387 (1953)

W C Koehler and E O Wollan Paramagnetic Scattering of Neutrons by Rare Earth Oxides *Phys Rev* **92** 1380 (1953)

E D Klema and F K McGowan Gamma Gamma Angular Correlation in Pd^{106} *Phys Rev* **92** 1469 (1953)

F K McGowan Measure of *K* Shell Internal Conversion Coefficients with a Coincidence Scintillation Spectrometer *Phys Rev* **93** 163 (1954)

R L Macklin and H E Banta The $Li^7(n\ t)$ Reaction *Science* **119** 350 (1954)

M E Rose Spherical Tensors in Physics *Proc Phys Soc (London)* **67A** 239 (1954)

R A Erickson and L D Roberts The Measurement and the Calculation of the Liquid Helium Vapor Pressure Temperature Scale from 1° to 4 2°K *Phys Rev* **93** 957 (1954)

F K McGowan Angular Correlations of Gamma Rays in Ta^{181} *Phys Rev* **93** 471 (1954)

M E Rose Mixed Gamma–Mixed Gamma Angular Correlations *Phys Rev* **93** 477 (1954)

PAPERS PRESENTED AT MEETINGS

R L Macklin and H E Banta *Li^7(d t)Li^6 Reaction* Meeting of the American Physical Society Chicago Nov 1953

W C Koehler and E O Wollan *Neutron Diffraction by Rare Earth Metals* Diffraction Conference Pittsburgh Nov 1953

P M Stier C F Barnett and G E Evans *Charge States of Ion Beams in Various Gases* Meeting of the American Physical Society Chicago Nov 1953

P H Stelson *Angular Distribution of α Particles from the Na^{23}(p α)Ne^{20} Reaction* Meeting of the American Physical Society Chicago Nov 1953

C H Johnson and C C Trail *Yields Near Threshold for* (p n) *Reactions in Intermediate Nuclei* Meeting of the American Physical Society Chicago Nov 1953

R A Erickson and L D Roberts *The Measurement and the Calculation of the Liquid Helium Vapor Pressure-Temperature Scale from 1 to 4 2°K* Third International Conference on Low Temperature Physics and Chemistry Houston Dec 1953

L D Roberts S Bernstein J W T Dabbs C P Stanford and T E Stephenson *The Interaction of Polarized Neutrons with Polarized Mn^{55} and with Polarized Sm^{149} Nuclei Part I Production of Nuclear Polarization* Meeting of the American Physical Society Chicago Nov 1953 and International Conference on Low Temperature Physics Houston Dec 1953

C P Stanford T E Stephenson L W Cochran and S Bernstein *Polarization of Neutrons* Meeting of the American Physical Society Chicago Nov 1953

S Bernstein L D Roberts C P Stanford J W T Dabbs and T E Stephenson *The Interaction of Polarized Neutrons with Polarized Mn^{55} and with Polarized Sm^{149} Nuclei Part II Observation of Nuclear Polarization* Meeting of the American Physical Society Chicago Nov 1953 and International Conference on Low Temperature Physics Houston Dec 1953

M K Wilkinson C G Shull L D Roberts and S Bernstein *Neutron Diffraction Investigations on Superconducting Elements* Meeting of the American Physical Society New York Jan 1954

P R Bell *The Total Absorption Spectrometer* Scintillation Counter Symposium Washington Jan 1954

J E Francis P R Bell and G G Kelley *Double Line Linear Amplifier* Scintillation Counter Symposium Washington Jan 1954

J E Sherwood T E Stephenson C P Stanford and S Bernstein *Stern-Gerlach Experiment on Polarized Neutrons,* Meeting of the American Physical Society New York Jan 1954

T A Love and F C Maienschein *Spectrum of a Po B Source* Meeting of the American Physical Society New York Jan 1954

F C Maienschein and T A Love *Gamma Ray Spectrum of the Bulk Shielding Reactor* Meeting of the American Physical Society New York Jan 1954

J Schenck and J H Neiler *Response of LiI(Eu) Activator to Fast Neutrons* Scintillation Counter Symposium Washington Jan 1954

H B Willard J K Bair and J D Kington *Angular Distributions of 0 2 1 5 Mev Neutrons Elastically Scattered by Light Nuclei* Meeting of the American Physical Society New York Jan 1954

H E Banta and R L Macklin *Search for Li^7(n t) Reaction* Meeting of the American Physical Society Austin Feb 1954

C G Shull and M K Wilkinson *Small Angle Neutron Scattering by Iron at High Temperatures* Meeting of the American Physical Society Detroit Mar 1954

M K Wilkinson and C G Shull *Neutron Diffraction Observations on Iron at High Temperatures* Meeting of the American Physical Society Detroit Mar 1954

ANNOUNCEMENTS

The following persons have been added to the staff of the Physics Division during the period R Stephenson (Basic Shielding Research) from Engineering and Maintenance Division J W Wampler (Shielding) J R Taylor (Shielding) E Beckham (Shielding) from Laboratory Protection Division C Cross (Criticality Experiments) and R W Peelle (Basic Shielding Research)

Transfers during this period were as follows W J Maynard (Shielding) transferred to Aircraft Reactor Experiment and R K Osborn (Theoretical Physics) transferred to ANP Division

Terminations V L DiRito and W E Kunz (High Voltage) M K Hullings (Shielding)

PHYSICS DIVISION
SEMIANNUAL PROGRESS REPORT

SUMMARY

HIGH-VOLTAGE PHYSICS

The polarized nature of neutrons resulting from reactions induced by unpolarized bombarding particles and unpolarized targets has been observed. The polarization of the $Li^7(p,n)Be^7$ neutrons has been ~~demonstrated~~ investigated with both carbon and oxygen as analyzers, and of the $T(p,n)He^3$ neutrons with an oxygen analyzer.

The differential cross section for the scattering of fast neutrons by nitrogen has been measured at several neutron energies below 1.54 Mev. Three of the neutron energies were between resonances, and the corresponding differential cross sections were essentially isotropic. One of the neutron energies corresponded to a resonance, and for these resonant neutrons the differential cross section showed forward scattering.

Further studies have been made on the energy levels in the Be^8 and Be^9 nuclei by bombarding the lithium isotopes with He^3. It now seems certain that the 3-Mev level in Be^8 is a single broad level and not two or more closely spaced levels. On the other hand, in the case of Be^9 the experiments show, with increasing likelihood, more levels up to 10-Mev excitation than are presently thought to exist.

Cross sections for the production of tritium have been measured by means of the activation technique described in an earlier report. The method has been extended to exothermic reactions as well as endothermic reactions with high bombarding energies. Results are given for the $Li^7(d,t)Li^6$ and $Li^6(d,t)Li^5$ reactions with the additional inclusion of the $Li^7(n,t)He^5$ reaction.

Electromagnetic excitation of nuclei by means of the coulomb field of charged particles has been employed to study low-lying states in the tantalum, gold, and thallium isotopes. New levels were found in the nuclei Ta^{180} and Au^{197}, while two hitherto unknown levels were found in Tl^{205}.

Proton-capture gamma-ray spectra have been studied with a 3 × 3 in. NaI crystal. With this crystal it has been possible to resolve the 16- and 12-Mev gamma rays from $B^{11}(p,\gamma)C^{12}$ and to observe how the modes of decay corresponding to these two gamma rays depend upon energy.

RADIOACTIVITY AND NUCLEAR ISOMERISM

The angular correlations of gamma rays in cascade have been measured with a sodium iodide coincidence scintillation spectrometer for certain excited states in Nd^{144}, Ba^{134}, Lu^{175}, Cs^{133}, and Eu^{153}. The angular correlation of the 54-kev x ray from ϵ-capture in Hf^{175} and the 342-kev gamma ray in Lu^{175} has also been measured. Investigations have been made of the gamma rays from Eu^{153} with a delayed sodium iodide scintillation spectrometer.

Measurements of gamma attenuation under broad-beam geometry are continuing, and a satisfactory method has been developed for analyzing the data. New data for the attenuation of the polonium-beryllium 4.44-Mev gamma rays in lead and in aluminum and of the Cs^{137} gamma rays in water are presented. An analysis of previously reported data gives close agreement with absorption coefficients given by NBS and with build-up factors calculated by NDA.

NEUTRON DIFFRACTION

The ferromagnetic properties of iron have been studied up to 1000°C. The increase in the diffuse magnetic scattering as one passes through the Curie point is much less than expected, but there is considerable magnetic small-angle scattering (1 to 5 deg) which can be accounted for on the basis of shrinking domain size which at the highest temperatures goes over into short-range order type of scattering.

Diffraction studies at temperatures ranging from 300 to 4°K on a series of mixed perovskite-type compounds, $(La,Ca)MnO_3$, show ferromagnetic properties over part of the composition range and several types of antiferromagnetic structures and mixtures of ferro- and antiferromagnetism over other composition ranges.

Several silicides of transition elements which had been predicted to be antiferromagnetic were found to show no measurable magnetic scattering.

Page No.	Column No.	Line No.	Errata
1	1	6	*for* . . . has been demonstrated *read* . . . has been investigated

SUMMARY

LOW TEMPERATURE PHYSICS

The specific heat of anhydrous manganous chloride has been measured from 1 3 to 4 2°K Sharp maxima are found at 1 8 and 2 0°K close to the magnetic susceptibility anomaly previously described

A proposal for the brute force polarization of protons is discussed

A calculation of the anisotropy of magnetic thermodynamic properties is given which is suitable for some paramagnetic ions of the iron group

HEAVY ION PHYSICS

Investigations of electron capture and loss by heavy ions passing through gases have been continued and extensive results are given of the measurement of the fraction of an ion beam in the various charge states Curves of the ratios of complementary cross sections calculable from these data are shown and qualitative interpretations are given

NEUTRON PHYSICS

That the spin of the neutron is indeed $\frac{1}{2}(h/2\pi)$ has been fully demonstrated in a magnetic resonance experiment in which magnetite single crystals were used as both polarizer and analyzer

THEORETICAL PHYSICS

Brief statements are made regarding some reaction theory problems involving resonance polarization maximum values of reaction cross sections and spectrum shapes There is a calculation of the oscillation frequencies of charged particles in axially symmetric electrostatic fields The status of some machine calculation problems having to do with general nuclear physics is briefly reported These include tabulation (by UNIVAC) of Racah and Clebsch Gordon coefficients and an investigation (by ORACLE) of the electron scattering for various nuclear models Computational work aimed at evaluating a novel formulation of quantum electrodynamics with thus far negative results is reported

1 HIGH VOLTAGE PHYSICS

POLARIZATION OF FAST NEUTRONS

H B Willard J K Bair
J D Kington

Blin Stoyle[1] and Simon and Welton[2] have pointed out that polarized particles may be produced in nuclear reactions by the interference of nuclear states involving spin orbit coupling Experimental verification for this effect includes the double scattering of protons by helium [3] the observation of polarized protons from the $D(d\ p)H^3$ reaction [4] the analysis of polarized neutrons from the $D(d\ n)He^3$ reaction by elastic scattering on carbon [5 6] and the preliminary work on polarization of neutrons from the $Li^7(p\ n)Be^7$ reaction analyzed by elastic scattering from oxygen [7]

In order to investigate the polarization of neutrons from several $(p\ n)$ reactions the geometry shown in Fig 1 1 has been employed Neutrons produced at angle θ (laboratory system) are elastically scattered by cylindrical samples and detected with a proton recoil counter at either $+\theta_2$ or $-\theta_2$ The ratio of scattering $(-\theta_2/+\theta_2)$ is given by

$$r_{\mp} = \frac{1 + P_1P_2}{1 - P_1P_2}$$

where P_1 is the polarization of the $(p\ n)$ reaction and P_2 is the polarization of the elastic scattering reaction The latter can be calculated from the data obtained by measuring the elastic scattering angular distribution of unpolarized neutrons Corrections were made for background and multiple scattering in the sample [8]

The asymmetry factor $r_{\mp}$ for the $Li^7(p\ n)Be^7$ reaction as analyzed by the 440 kev resonance in $O^{16}(n\ n)O^{16}$ was measured as a function of energy and angle the results are given in Fig 1 2 The oxygen analyzer was in the form of an H_2O cylinder 1 in in diameter and 4 in long It was placed 15 in from the Li^7 target which was 20 kev thick The neutron recoil counter subtended an average angle of 10 deg Assuming the analyzing resonance to be $J = 3/2$ with interference between p wave resonance and s wave potential scattering the

[1] R J Blin Stoyle *Proc Phys Soc* **64A** 700 (1951)

[2] A S mon nd T A Welton *Phys Rev* 89 886 (1953)

[3] M Heusinkveld and G Freier *Phys Rev* 85 80 (1952)

[4] G R Bishop J M Westhead G Preston and H H Halb n *Nature* 170 113 (1953)

[5] P H ber and E Baumgartne *Helv Phys Act* **XXXVI** 420 (1953)

[6] R Ricamo *Helv Phys Act* **XXXVI** 423 (1953)

[7] S E Darden R E Field and R K Ada *Bull Am Phys Soc* **28** No 6 27 (1953)

[8] M Walt PhD Thes s University of W sconsin 1953

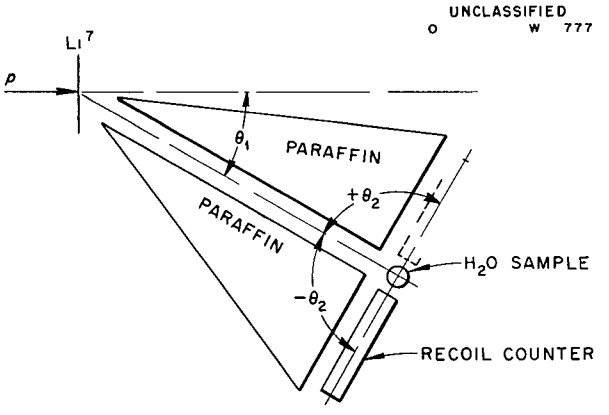

Fig 1 1 Geometrical Arrangement of Target Shields and Detector To Study Polarization of Neutrons from $Li^7(p\ n)Be^7$ Reaction

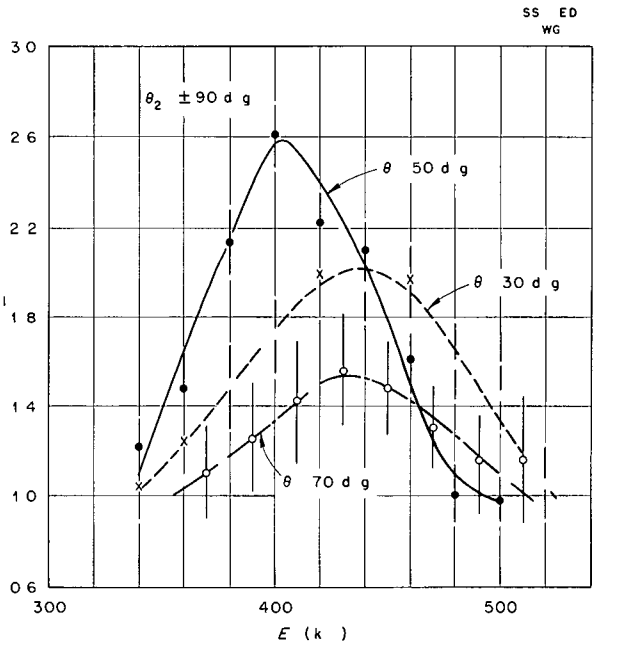

Fig 1 2 Asymmetry Factor $r_{\mp}$ of $Li^7(p\ n)Be^7$ Neutrons Analyzed by Elastic Scattering of Neutrons from O^{16}

maximum value of P_2 (90 deg) is about 0 83 at 400 kev From the observed value of $r_{\mp}$ this gives P_1 = 0 54 A resonance in carbon at 2 95 Mev (neutron energy) was also used for analyzing $Li^7(p\ n)Be^7$ at higher bombarding energies thus giving a maximum asymmetry of $r_{\mp}$ = 2 13 ± 0 11 The $T(p\ n)He^3$ reaction was also examined as to the polarization of the neutrons produced At θ_1 = 50 deg and a neutron energy of 400 kev scattering through θ_2 = 90 deg on an O^{16} analyzer yielded the value $r_{\mp}$ = 0 96 ± 0 05

DIFFERENTIAL NEUTRON SCATTERING CROSS SECTION FOR NITROGEN

J L Fowler C H Johnson

The differential cross section for the scattering of fast neutrons by nitrogen has been measured at several neutron energies below 1 54 Mev Neutrons were produced by bombarding a tritium gas target with protons from the 2 5 Mev Van de Graaff generator In computing the neutron energy a correction to the proton energy scale was made for the thickness of the gas target and the nickel target window The neutron-energy spread resulting from the stopping power of the target and nonuniformity of the foil was about 40 kev

A cylindrical scattering sample 3 cm in diameter and 12 cm long was placed at 0 deg to the proton beam with its axis perpendicular to the proton beam axis and 30 cm from the target The sample consisted of a thin walled can containing LiN_3 An identical can to be used for background measurements contained several equally spaced disks of lithium cut to match the lithium in the original sample Neutrons scattered by the sample were detected with a 1-atm propane recoil counter that was 1 in in diameter It was placed with its axis perpendicular to the axis of the scattering sample and with the center of its active volume approximately 13 5 cm from the center of the sample At each neutron energy the counter was biased to give a flat response for neutrons scattered at all angles from nitrogen A paraffin slab was placed to shield the counter from the direct neutron flux The scatterer paraffin and counter were supported by wires in order to reduce the background At each scattering angle neutrons were counted first with the LiN_3 sample in place and then with the background sample of lithium The sample and paraffin were then removed and neutrons were counted near 0 deg to the proton beam to determine the initial flux to the scatterer All measurements were monitored by a long counter At each counter position the necessary lengths were recorded for calculating the absolute cross section

Figure 1 3 shows the resulting angular distributions The four curves show the differential elastic scattering cross section in barns per steradian plotted against the cosine of the scattering angle in the center-of mass system The curve plotted vertically at the right of the figure is the known total cross section of nitrogen [9] The arrows connecting this curve to the angular distribution curves indicate the four neutron energies used

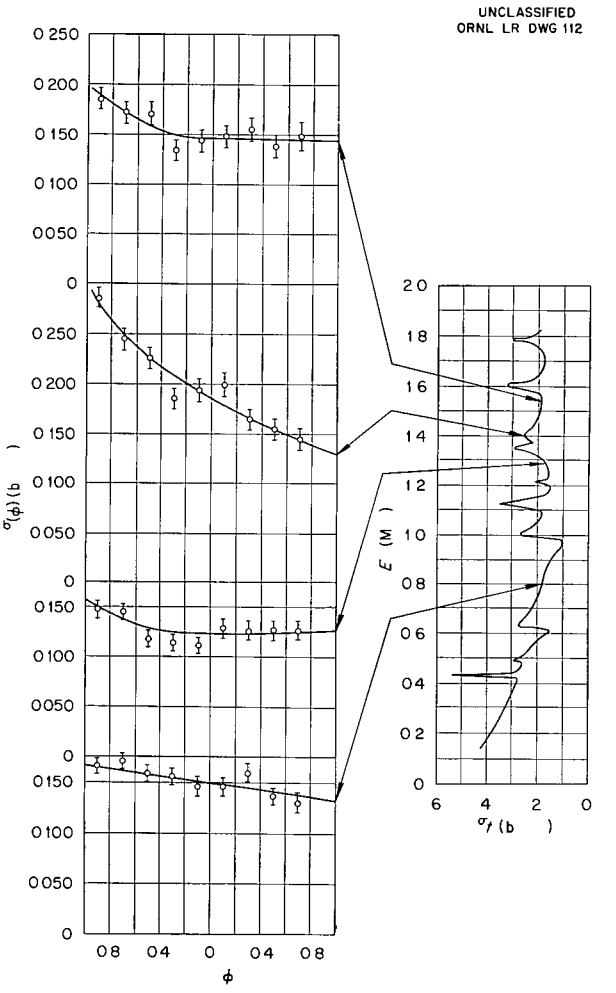

Fig 1 3 Differential Cross Section for Elastic Scattering of Neutrons from Nitrogen

[9] J J Hinchley P H Stelson and W M Preston *Phys Rev* 86 483 (1952)

namely 0 80 1 28 1 40 and 1 54 Mev Three of the angular distributions were obtained at energies relatively far removed from resonances these do not deviate strongly from isotropy The 1 40-Mev curve was obtained at a resonance and shows strong anisotropy with forward scattering of neu trons The integral of the differential cross section over all solid angle agrees with measured total cross section to within 3% The curves have not yet been corrected for multiple scattering in the sample

A primary reason for making these measurements was to check the range of validity of previous results[10] obtained by using a nitrogen recoil counter The two methods agree in the region of cos $\phi < 0\ 5$ For cos $\phi > 0\ 5$ that is for low energy nitrogen recoils the nitrogen counter gave an excessive number of counts The data enable the potential scattering phase shifts to be esti mated so that the interference between this and the resonance scattering which is used in analyzing the resonance scattering angular distributions can be found [10]

[10] J L Fowle C H Johnson and J R R se *Phys Rev* 91 441(A) (1953)

LEVELS IN Be^8 AND Be^9 FROM THE $Li^6(He^3\ p)Be^8$ AND $Li^7(He^3\ p)Be^9$ REACTIONS

W E Kunz C D Moak
W M Good

The 20 channel pulse analyzer was used to re investigate the charged particle spectra of the following reactions $Li^6(He^3\ p)Be^8$ $Li^7(He^3\ p)Be^9$ $Li^7(He^3\ d)Be^8$ and $Li^7(He^3\ \alpha)Li^6$ The target arrangement was identical to that described in the previous investigation of these reactions How ever the greatly improved analyzing efficiency made possible much improved statistics The results of the more recent measurements are shown in Figs 1 4 and 1 5

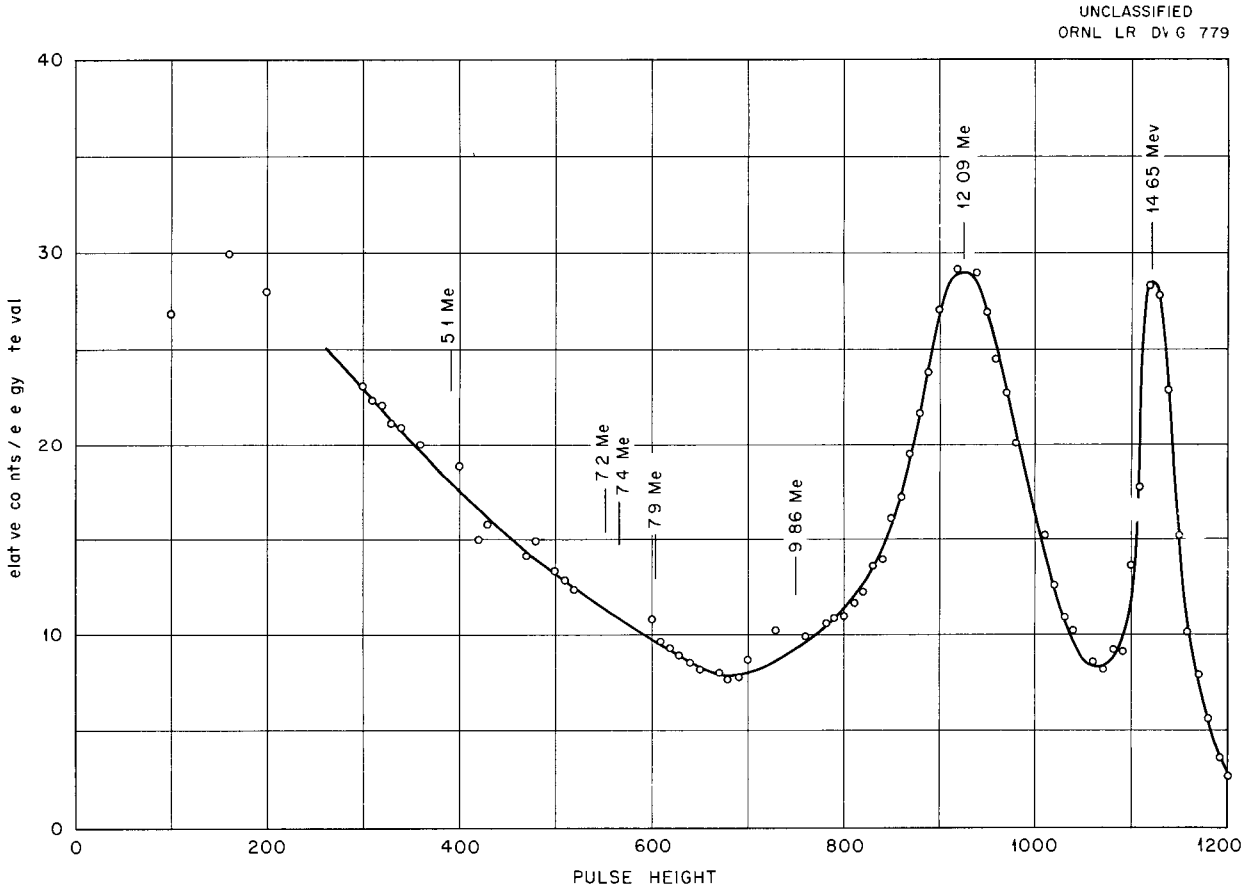

Fig 1 4 Spectrum of Protons from Reaction $Li^6(He^3\ p)Be^8$ 3 mils of Aluminum Absorber

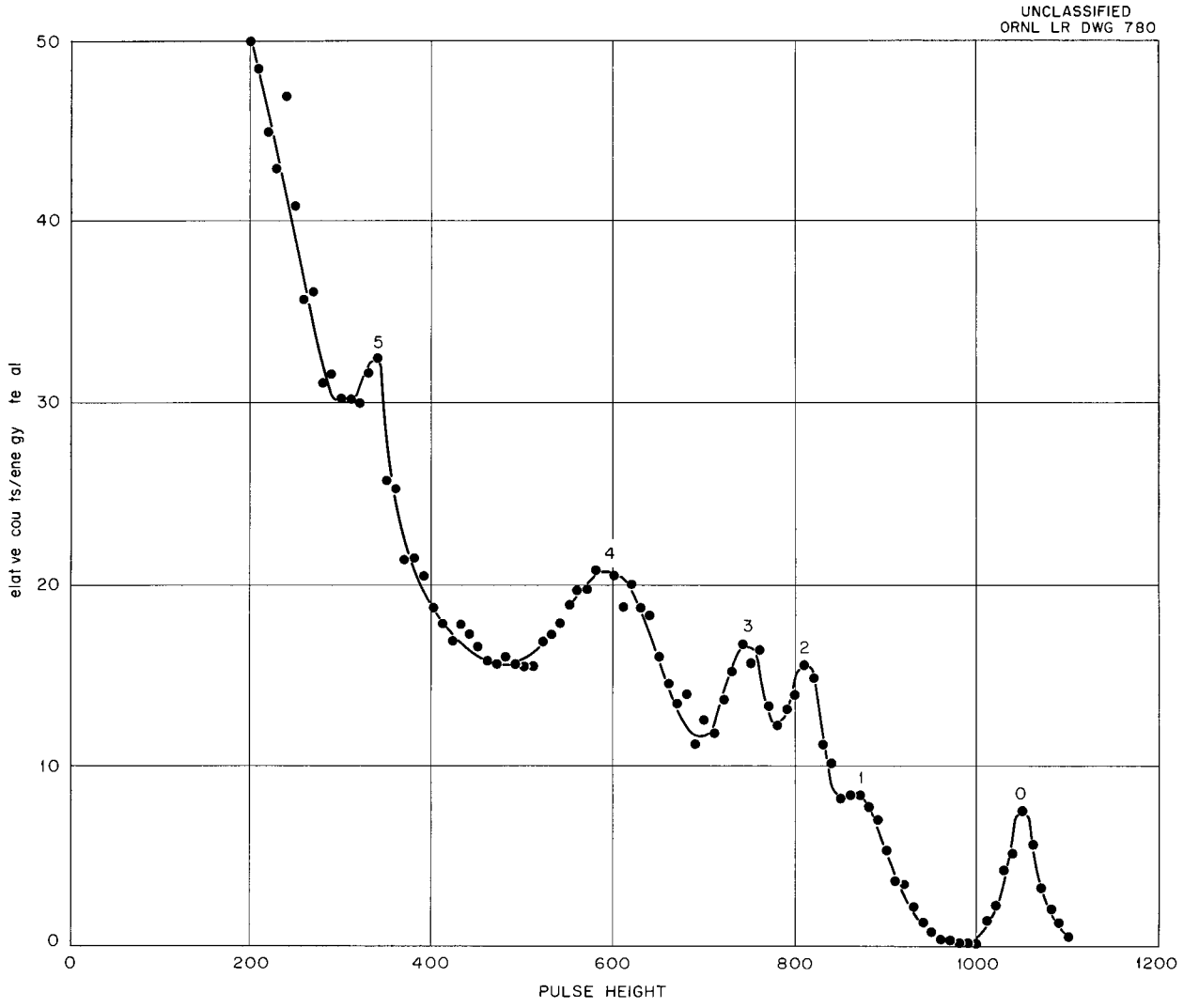

Fig 1 5 Spectrum of Protons from Reaction $Li^7(He^3\ p)Be^9$ 0 1 mil of Nickel Absorber

It was desirable to secure better statistics for the $Li^6(He^3\ p)Be^8$ spectrum in order to examine what has been reported to be structure in the second most energetic proton group and also to seek evidence for lesser energy proton groups of low intensity Figure 1 4 is interpreted as confirming the earlier result on $Li^6(He^3\ p)Be^8$ namely that only two groups of protons are evident In particu lar the second most-energetic proton group is cer tainly not several unresolved groups Furthermore the Li^6 sample contained 5% Li^7 and from what is known about the $Li^7(He^3\ p)Be^9$ reaction groups of low intensity are expected at energies of roughly 9 9 7 9 7 4 7 2 and 5 1 Mev

Figure 1 5 cannot be uniquely interpreted as yet because of some uncertainty in the response of NaI to deuterons When 4 mils of aluminum ab sorber is placed in front of the NaI crystal each of the groups 0 1 2 3 and 4 loses energy as though it were a proton However depending on the nature of the NaI response to deuterons groups 2 and 4 could conceivably be deuterons If groups 2 and 4 are assumed to be deuterons group 1 probably corresponds to the known level at 2 43 Mev in Be^9 Group 3 corresponding to 3 18 Mev in Be^9 appears to be a new level Group 5 is the alpha particle from $Li^7(He^3\ \alpha)Li^6$ and the con tinuum is the mode $Li^7(He^3\ He^4\ n\ p)He^4$

Beryllium 9 has been bombarded with He^3 and two reaction modes have been observed namely

$Be^9(He^3\ p)B^{11}$ and $Be^9(He^3\ \alpha)Be^8$ The proton spectrum of the mode $Be^9(He^3\ p)B^{11}$ closely resembles that of the reaction $B^{10}(d\ p)B^{11}$ described in the literature The $Be^9 + He^3$ reaction is being investigated further

TRITON YIELDS FROM LITHIUM ISOTOPES

R L Macklin H E Banta

Cross sections have been measured by the activation technique for tritium production in the lithium isotopes by deuterons and by reactor and polonium beryllium neutrons These measurements are a continuation from the $Li^7(d\ t)Li^6$ cross section measurements reported previously [11] The calibrations of the tritium recovery and counting apparatus previously employed have been refined The two methods gave results agreeing within 2½% well within their anticipated uncertainty The average value of the calibration constant was $6\ 70 \times 10^8$ tritons per count per second The reproducibility of the method was determined as ±2% standard deviation by simultaneous reactor exposures of a group of natural LiF targets

The measurement of the $Li^7(d\ t)Li^6$ reaction cross section was extended to higher energies (2 5 to 4 Mev) than in the previous experiments At the higher energies the energy of the tritons emitted at the back angles is too great for use of the aluminum overcoat technique Accordingly a modification of the target arrangement was devised (Fig 1 6) wherein all but a negligible fraction of the backward tritons were captured in an aluminum tube from which they were recovered in the same manner as were the forward tritons from each target

[11] R L Macklin and H E Bant *Phy Sem ann Prog Rep Sept 10 1953* ORNL 1620 p 5

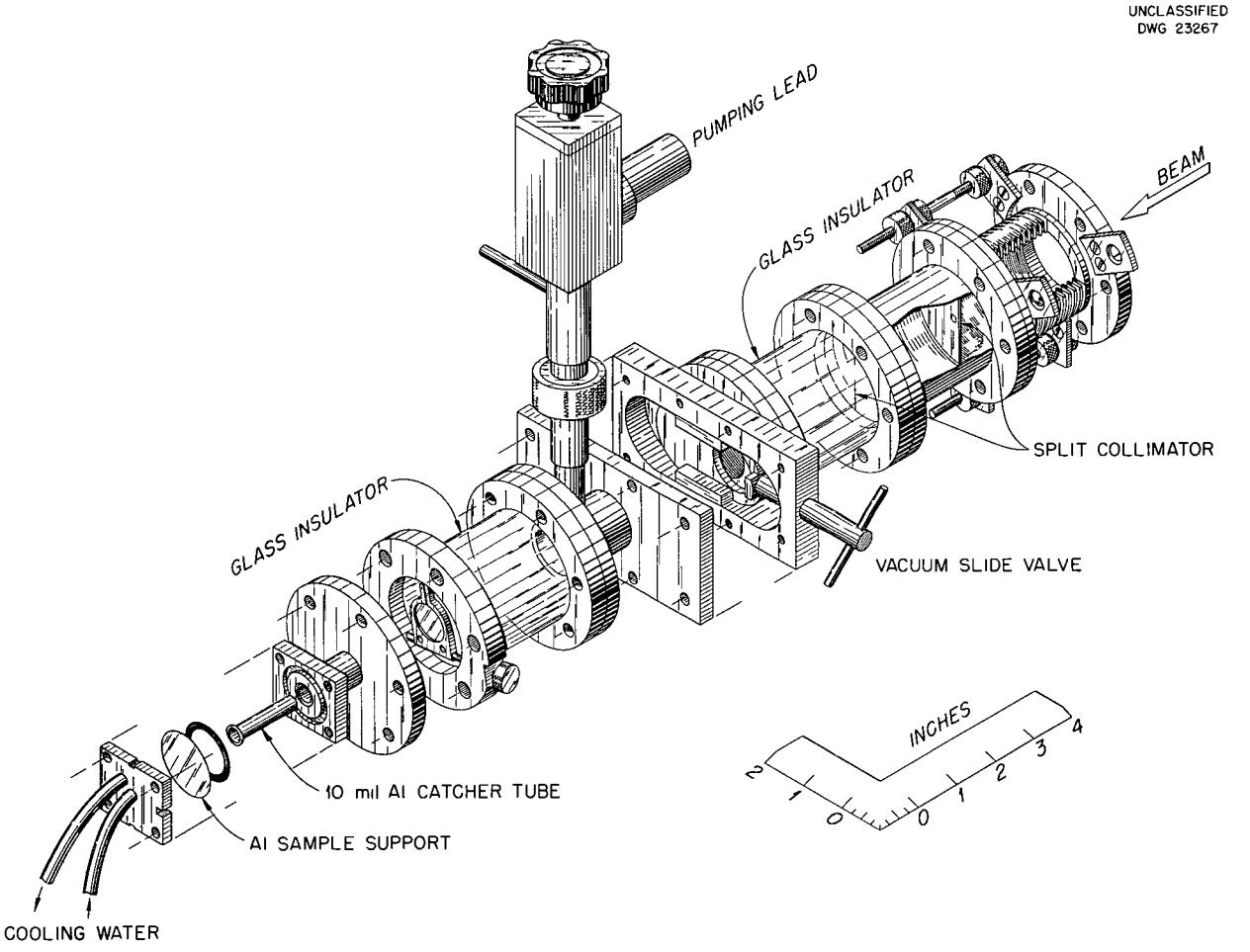

Fig 1 6 Deuteron Activation Apparatus

The cross section results on this reaction are incomplete and further experiments are required

The modified technique for high energy triton recovery has allowed the investigation of the cross section for the exoergic reactions $Li^6(d\ t)Li^5$ together with $Li^6(d\ t\ p)He^4$ The triton yield from 0 4 to 4 Mev is indicated in Fig 1 7 Pending further work with the modified triton recovery technique an uncertainty of perhaps 20% is indicated for the cross sections The results seem to show an excess of backward tritons at the lowest energies (0 4 to 0 6 Mev) and probably a forward excess above 1 Mev deuteron energy Uncertainty as to the end products of the reaction makes an exact calculation of the expected distribution and the self-absorption of the LiF targets impossible

The $Li^7(n\ t\ n)He^4$ reaction together with the $Li^7(n\ t)He^5$ reaction was detected using decigram samples of Li^7F from which the tritium was recovered by repeated fusion in hydrogen argon A cross section of 72 ± 18 millibarns was found for fission neutrons above 2 8 Mev [the computed threshold for $Li^7(n\ t\ n)He^4$] For polonium beryllium neutrons (broad maximum near 4 Mev) the cross section found was 30 ± 20 millibarns The $Li^6(n\ t)He^4$ contamination was evaluated by the simultaneous exposure of natural LiF in these experiments

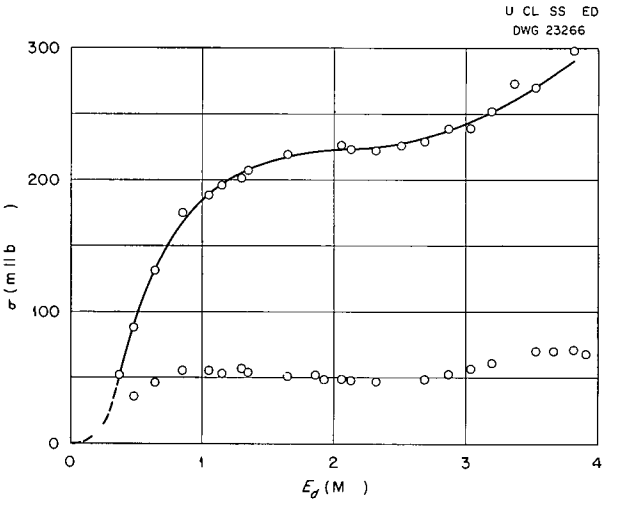

Fig 1 7 $Li^6(d\ t)$ Yield

EXCITATION OF NUCLEI BY THE COULOMB FIELD OF PROTONS

P H Stelson F K McGowan

When heavy nuclei are bombarded with charged particles having an energy appreciably below the coulomb barrier of the nucleus the short range nuclear forces cannot operate The collisions may however still give rise to nuclear excitations produced by the electric field of the impinging particles [12] The excitation cross sections can be expressed in terms of the same nuclear properties that determine the transition probabilities for electromagnetic radiative transitions Recently the feasibility of coulomb excitation has been exhibited by the observation[13] of gamma radiation following the nuclear excitation of Ta W and Pt

Bohr and Mottelson[14] have suggested that the method of coulomb excitation should provide a powerful tool for the study of nuclear collective properties According to their nuclear model which describes the nucleus in terms of the coupled motion of individual particles and surface oscillations low lying excited states of the collective type in contrast to single particle states should reveal themselves by especially large cross sections for coulomb excitation In addition from the explicit expressions for the angular distribution of the gamma radiation following coulomb excitation given by Alder and Winther [15] the angular momenta of the coulomb excited state and the final state after gamma ray emission may be inferred

An investigation of coulomb excitation of nuclei by protons from the 5 Mev Van de Graaff generator has been undertaken For the detection of the gamma radiation a scintillation spectrometer employing NaI crystals 1 5 in in diameter by 1 in thick has been used Differential pulse height spectra of the electromagnetic radiation from thick targets (thick to protons) of the heavier elements bombarded by 2 to 4 Mev protons have been observed at 0 deg to the incident protons

Figure 1 8 is the differential pulse height spectrum of the gamma radiation from tantalum for

[12] K A Ter M rtiro yan *Zhur Eksp i Teort Fiz* 22 284 (1952) Refe en e to othe theo et al p per on oulomb ex itat on e g ve n Append x IV of A Boh and B Mottel on *Dan Mat Fys Medd* 27 16 (1953)

[13] T H us and C Zupan c *Dan Mat Fys Medd* 28 1 (1953) C L McClell nd and C Goodman *Phys Rev* 91 760 (1953)

[14] A Bohr and B Mottelson *Dan Mat Fys Medd* 27 16 (1953)

[15] K Alder nd A Winther *Phys Rev* 91 1578 (1953)

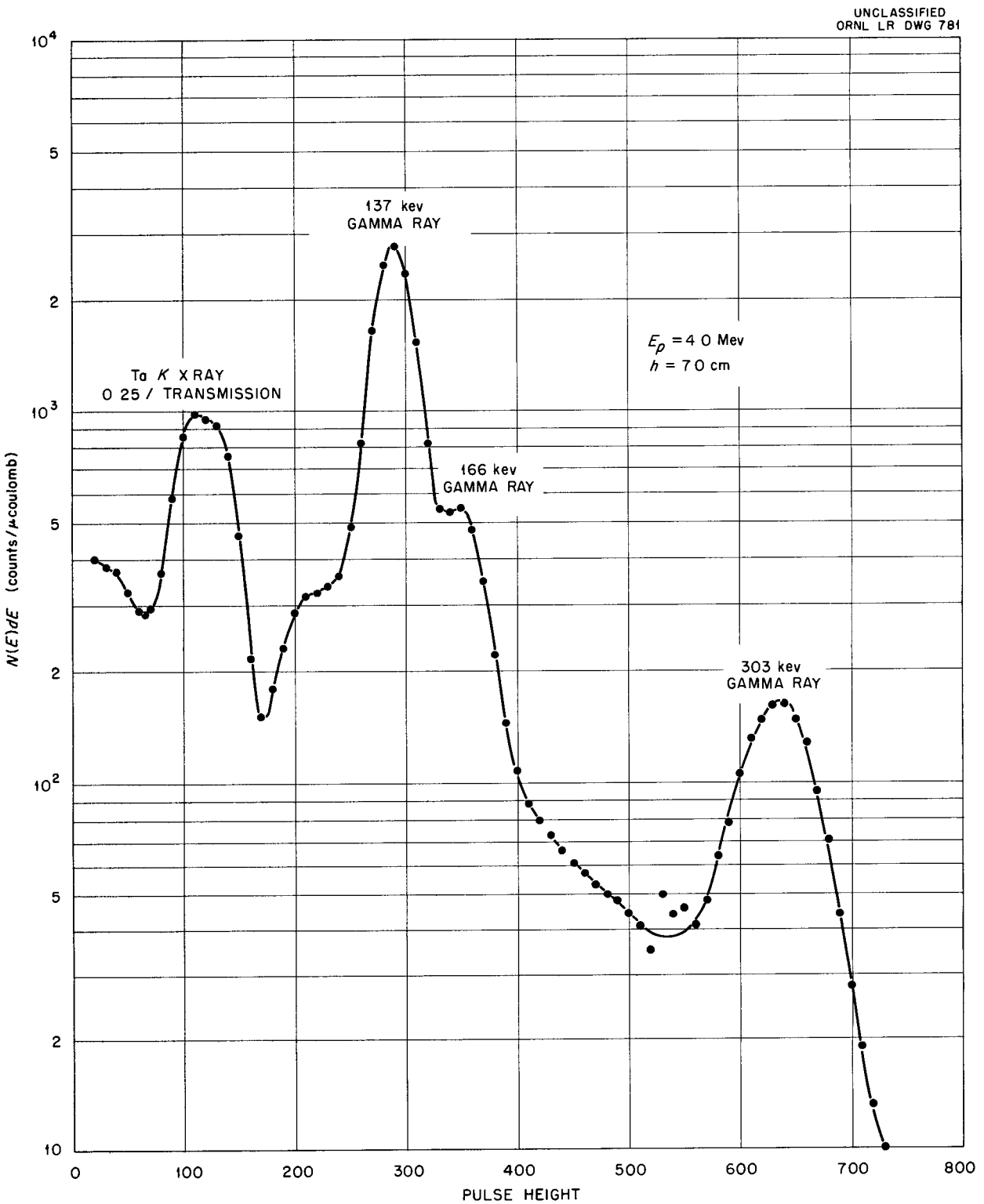

Fig 1 8 Pulse Spectrum in NaI from Gamma Rays Produced by Protons on Tantalum

E_p = 4 0 Mev A graded shield of 0 040 in of tin plus 0 005 in of copper was used to attenuate the K x rays from tantalum that result mostly from ionization in the K shell by the impinging protons The observed nuclear gamma rays of 137 166 and 303 kev result from the decay of 137 and 303 kev levels in tantalum excited by coulomb excitation Thick target yields of the gamma rays are given in Table 1 1 The 137 kev level was shown to exist from the beta decay of Hf^{181} but the 303 kev level in Ta^{181} is not populated by the beta decay directly or by gamma emission from higher levels in Ta^{181} From gamma gamma directional angular correlation and K shell internal conversion-coefficient measurements [16] the angular momentum of the 137 kev level is $9/2$ and the radiation from the decay of the state is $E2 + M1$ with the intensity ratio $E2/M1$ equal to 0 25 On the basis of this information the proton gamma angular distribution of the 137 kev gamma radiation resulting from direct coulomb excitation of the 137 kev level should be only about 1% anisotropic The proton gamma angular distributions of the 166 and 303 kev garima radiation have been measured and the data are being analyzed Both distributions are anisotropic

[16] F K McGowan *Phys Rev* 93 471 (1954)

TABLE 1 1 THICK TARGET YIELD OF GAMMA RAYS BY COULOMB EXCITATION

NUCLEUS	E_p (Mev)	E_γ (kev)	YIELD (g mma/μco lomb) $\times 10^{-5}$
T 181	2 6	137	4 3
T 181	4 0	137	20 4
T 181	2 6	166	0 25
T 181	4 0	166	2 5
Ta^{181}	2 6	303	0 18
Ta^{181}	4 0	303	1 8
A 197	4 0	192	0 60
A 197	4 0	282	2 4
Au^{197}	4 0	550	1 4
Tl^{205}	4 0	203	0 73
Tl^{203}	4 0	279	0 40
$Tl^{203\ 205}$	4 0	415	0 12

In order to measure excitation cross sections it would be desirable to use thin targets rather than to attempt to extract the cross sections from thick target yields For the heavier nuclei targets of a few mg/sq cm thick deposited on a backing material which does not exhibit any nuclear reaction or coulomb excitation by the impinging protons would be required A number of nuclei with closed or nearly closed shells were examined for coulomb excitation The elements Sn Pb and Bi all yielded in addition to the usual K x rays a continuum of electromagnetic radiation when irradiated with protons Typical differential pulse height spectra of the radiation from tin and bismuth for various proton energies are shown in Fig 1 9 The continuum observed from lead targets is similar to that from bismuth except that the pulse spectrum corresponding to 650 to 1400 kev of energy dissipated in the phosphor shows some structure which may be attributed to either coulomb excitation in lead or to low Z impurities in lead A nickel target also exhibited this same continuum and a few gamma rays from nuclear reactions for E_p = 2 83 Mev This source of radiation is not understood clearly except that it is coming from the target and the intensity dependence on the energy of the impinging proton excludes nuclear barrier penetration by the proton At the present bismuth appears to be the material best suited for target backing In any case the pulse height spectra of gamma rays resulting from coulomb excitation will be superimposed on this continuum of electromagnetic radiation

Gamma rays of 192 282 and 550 kev have been observed from Au^{197} and thick target yields are listed in Table 1 1 An interpretation of these gamma rays in terms of levels excited in Au^{197} by coulomb excitation is not complete Several low lying levels in Au^{197} are known from the ϵ capture decay of Hg^{197} however the 550 kev level is not populated by the decay of Hg^{197}

Curve 1 in Fig 1 10 is the differential pulse height spectrum of the gamma radiation from thallium for E_p = 4 0 Mev Thallium has two isotopes Tl^{203} (29 5%) and Tl^{205} (70 5%) From the beta decay of Hg^{203} and ϵ capture decay of Pb^{203} levels at 279 and 683 kev are known to exist in Tl^{203} No levels in Tl^{205} are known from radioactive decay The observed gamma rays of 279 and 415 kev are attributed to the decay of two levels excited in Tl^{203} by coulomb excitation

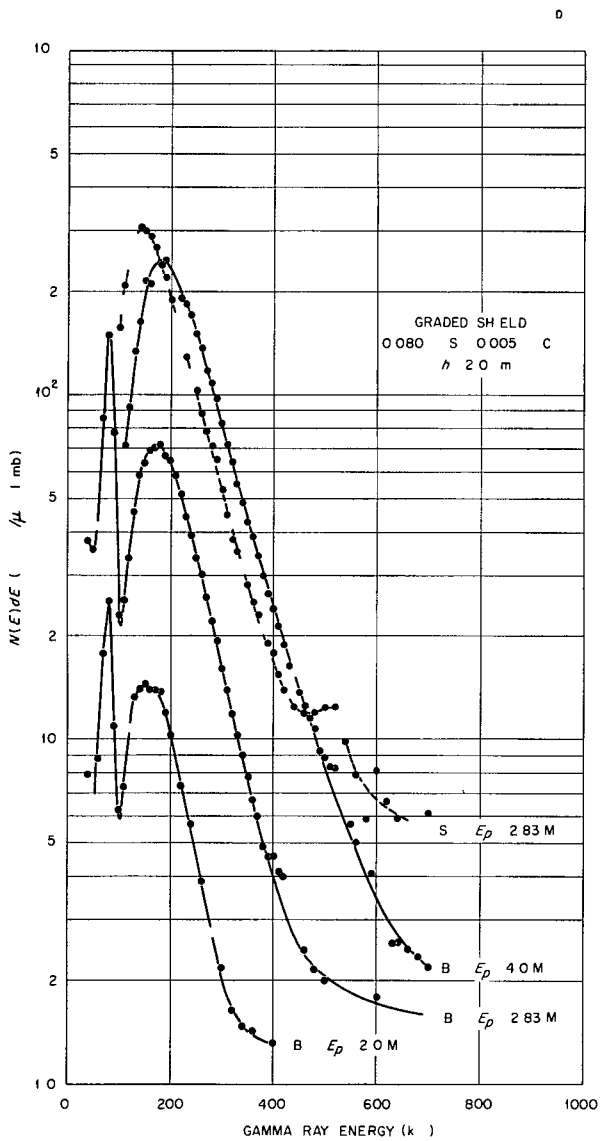

Fig 1 9 Pulse Spectrum in NaI from Gamma Radiation Produced by Protons on Tin and Bismuth

There is some evidence for the 683 kev cross over transition in the pulse spectrum The 203 kev gamma ray is probably to be attributed to an excited state in Tl^{205} Po ibly a second level exists at 630 kev In this case the peak at 415 kev could be composed of two gamma rays of nearly the same energy such that a gamma ray cascade of 415 and 203 kev exists in Tl^{205} Some coinci dence spectrometry measurements of the gamma rays should resolve these tentative conclusions Curve 2 in Fig 1 10 is the pulse spectrum of the continuum from a Bi^{209} target Thick target yields of the gamma rays from thallium have been ob tained from the data shown in Fig 1 10 on the assumption that the continuum from thallium is identical to that observed from bismuth Curve 3 in Fig 1 10 is the result of peeling off the con tinuum from the thallium data The apparent peak at 520 pulse height units is believed to be a false peak The true shape is probably the dashed section of the curve which represents the super position of the Compton recoil electron distri butions for the two cross over gamma ray transitions of about 630 and 683 kev The thick target yields are listed in Table 1 1

GAMMA RAY SPECTRUM AND GAMMA RAY YIELD FROM BORON BOMBARDED BY PROTONS

J K Bair H B Willard
J D Kington

A large 3 × 3 in NaI crystal mounted on a 3 in dia photo tube has recently been obtained This combination[17] has a full width at half maximum for the Cs^{137} photo peak of less than 8% Figure 1 11 shows the ThC 2 62 Mev gamma ray spectrum and $F^{19}(p\,\alpha\gamma)O^{16}$ spectrum (87% 6 13 Mev) taken with a $1\frac{1}{2} \times 2$ in NaI crystal Figure 1 12 shows the same spectra taken with the 3 × 3 in crystal The most striking feature of these data is the marked accentuation of the ThC full energy peak as obtained with the larger crystal In the case of the 6 13 Mev gamma ray this accentuation of the full energy peak is not so marked and the center peak corresponding to the escape of a single quantum of annihilation radiation appears to be considerably larger than would be expected

Figure 1 13 shows the pulse height spectra of the radiation resulting from the proton bombardment ot boron This curve was obtained in two separate runs having different window widths as shown for the low and high energy regions These differing resolutions were dictated by counting rate con siderations The two highest energy peaks are the result of the capture gamma ray going to the ground state and to the 4 43 Mev excited state in C^{12} No structure is apparent in the peaks resulting from these gamma rays either in the pulse height curves or in photographs taken of the pulses displayed on an oscilloscope screen The small irregularities

[17] Furn shed by N H Lazar

Fig 1 10 Pulse Spectrum in NaI of Gamma Radiation Produced by Protons on Natural Thallium

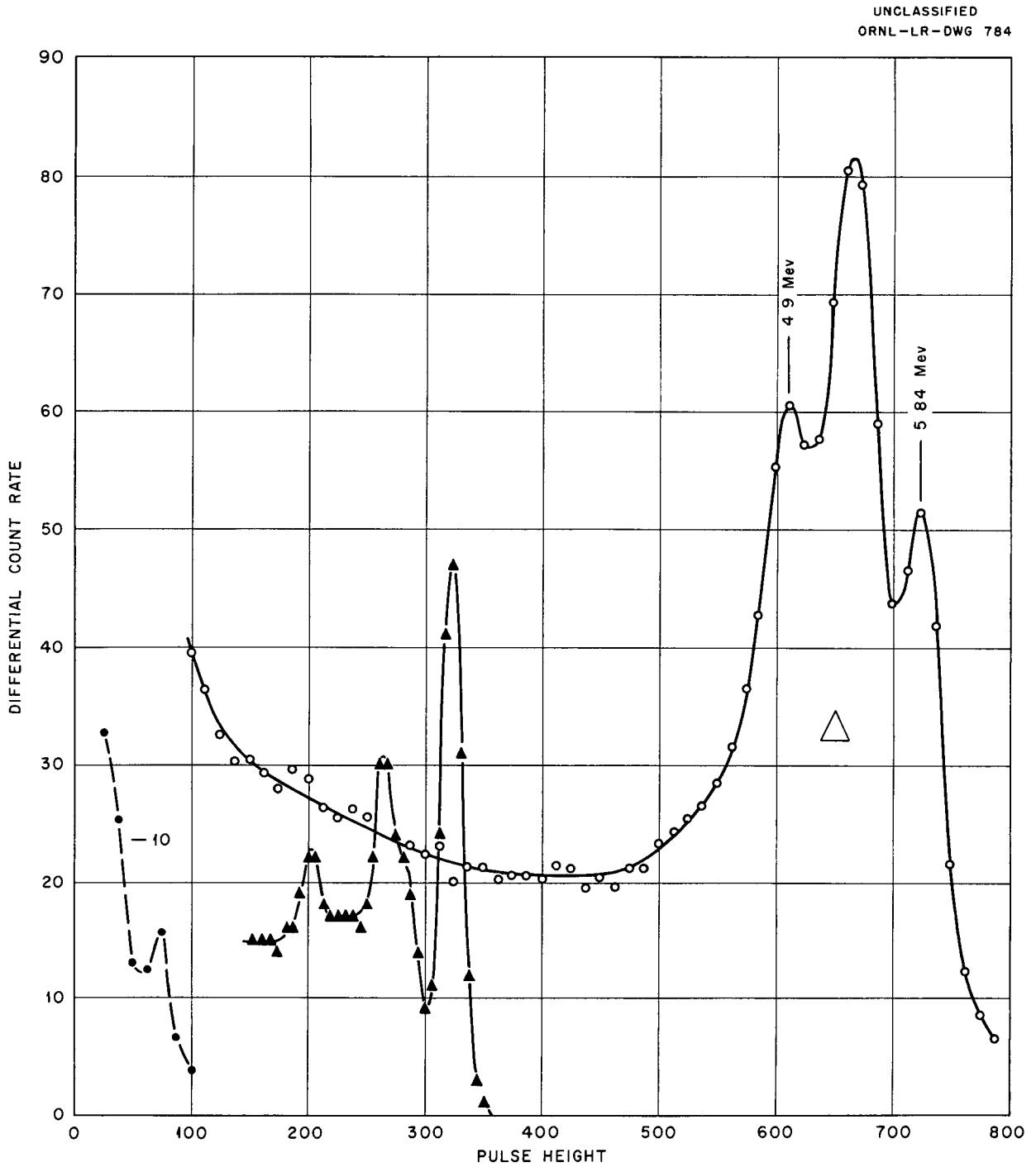

Fig 1 11 Pulse Spectrum Produced in a 1 5 × 2 in NaI Crystal by Gamma Rays of 2 62 and 6 13 Mev Energy

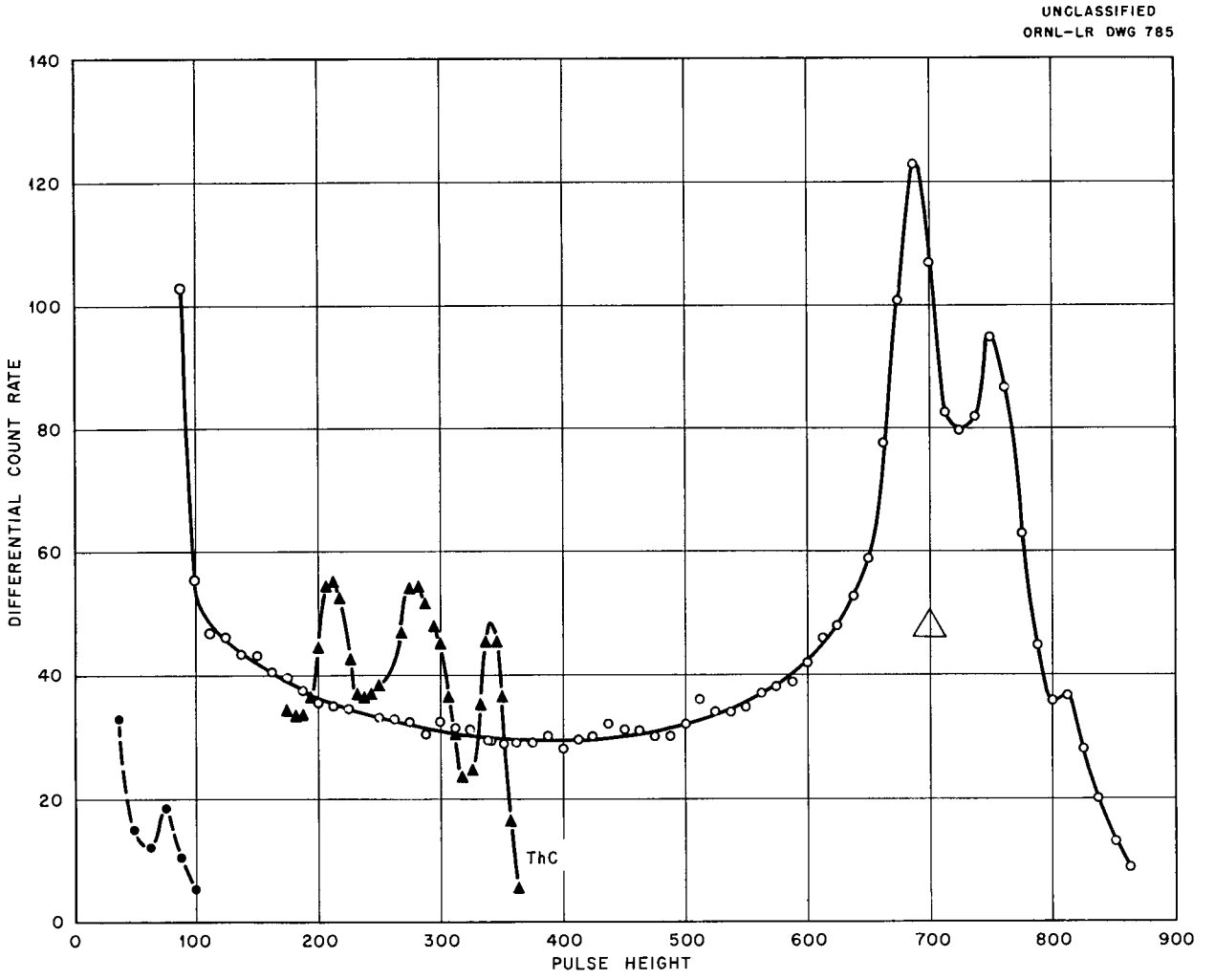

Fig 1 12 Pulse Spectrum Produced in a 3 × 3 in NaI Crystal by Gamma Rays of 2 62 and 6 13 Mev Energy

in the curve at pulse heights of 250 to 350 are believed to be due to target impurities probably fluorine Figure 1 14 shows a more detailed spectra of these reaction products in the region below 3 Mev together with Cs^{137} and ThC calibrations Peak I 0 72 Mev results from the $B^{10}(p\ p\gamma)B^{10-}$ reaction leaving B^{10} at a known level at 718 ± 5 kev peak II 1 00 Mev is of unknown origin probably an impurity but is not due to B^{10} peaks IV and V are the single escape and Compton peak corresponding to peak VI 2 14 Mev which is the full energy peak resulting from the $B^{11}(p\ p^{1})B^{11*}$ reaction leaving B^{11} at a known level at 2 138 Mev The peak corresponding to 2 14 Mev with the escape of both annihilation radiations is masked by peak II

The $B^{11}(p\ \gamma)C^{12}$ gamma ray yield has been extended to proton energies of about 4 Mev Figure 1 15 shows the yield of gamma rays at 0 and 90 deg to the proton beam Curves II and IV are for the transition to the ground state curves I and III are for the transition through the level in C^{12} at 4 43 Mev Further work is in progress to extend these data to higher energies

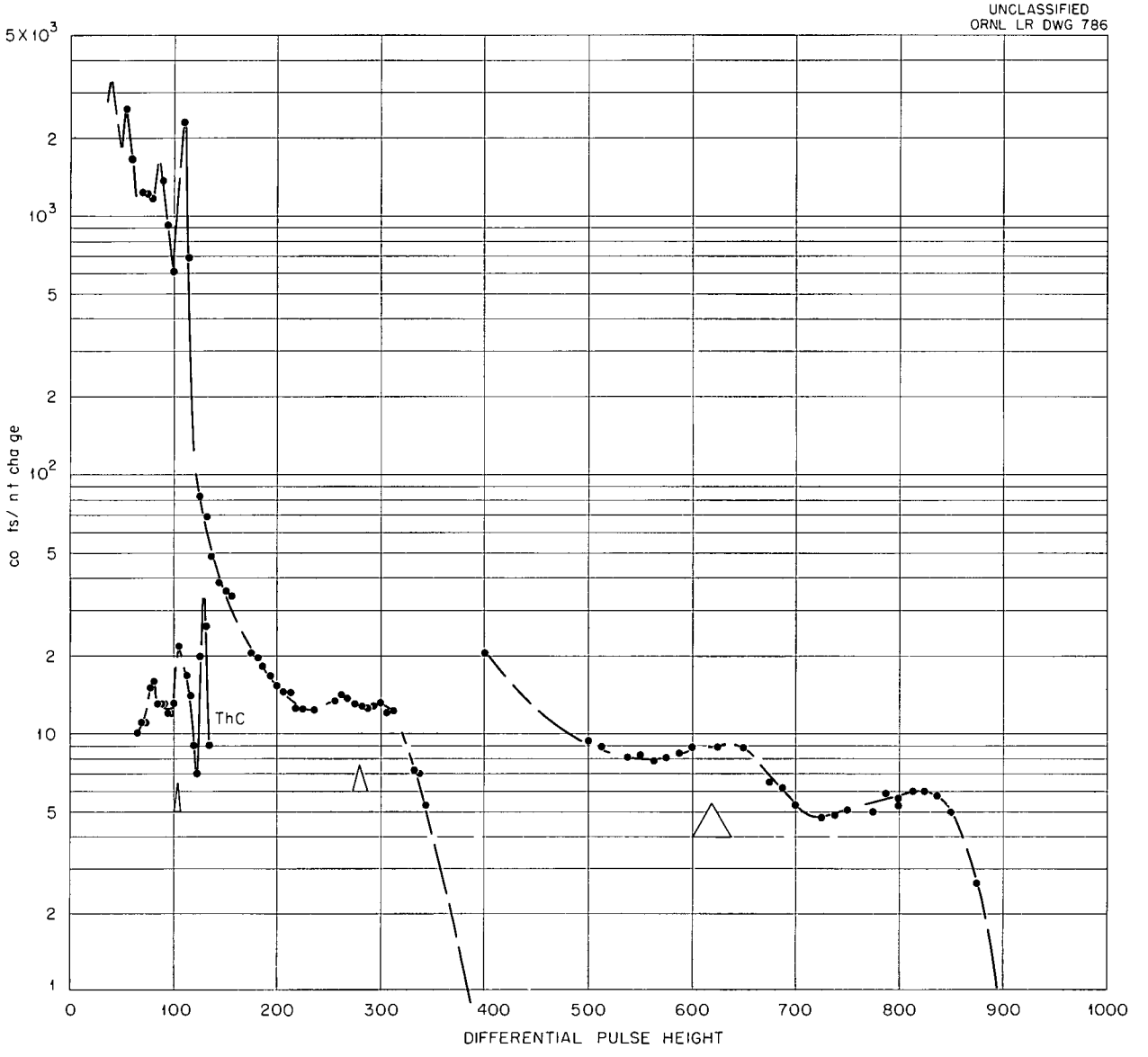

Fig 1 13 Pulse Spectrum Produced in NaI by the Gamma Rays from Boron Bombarded by Protons

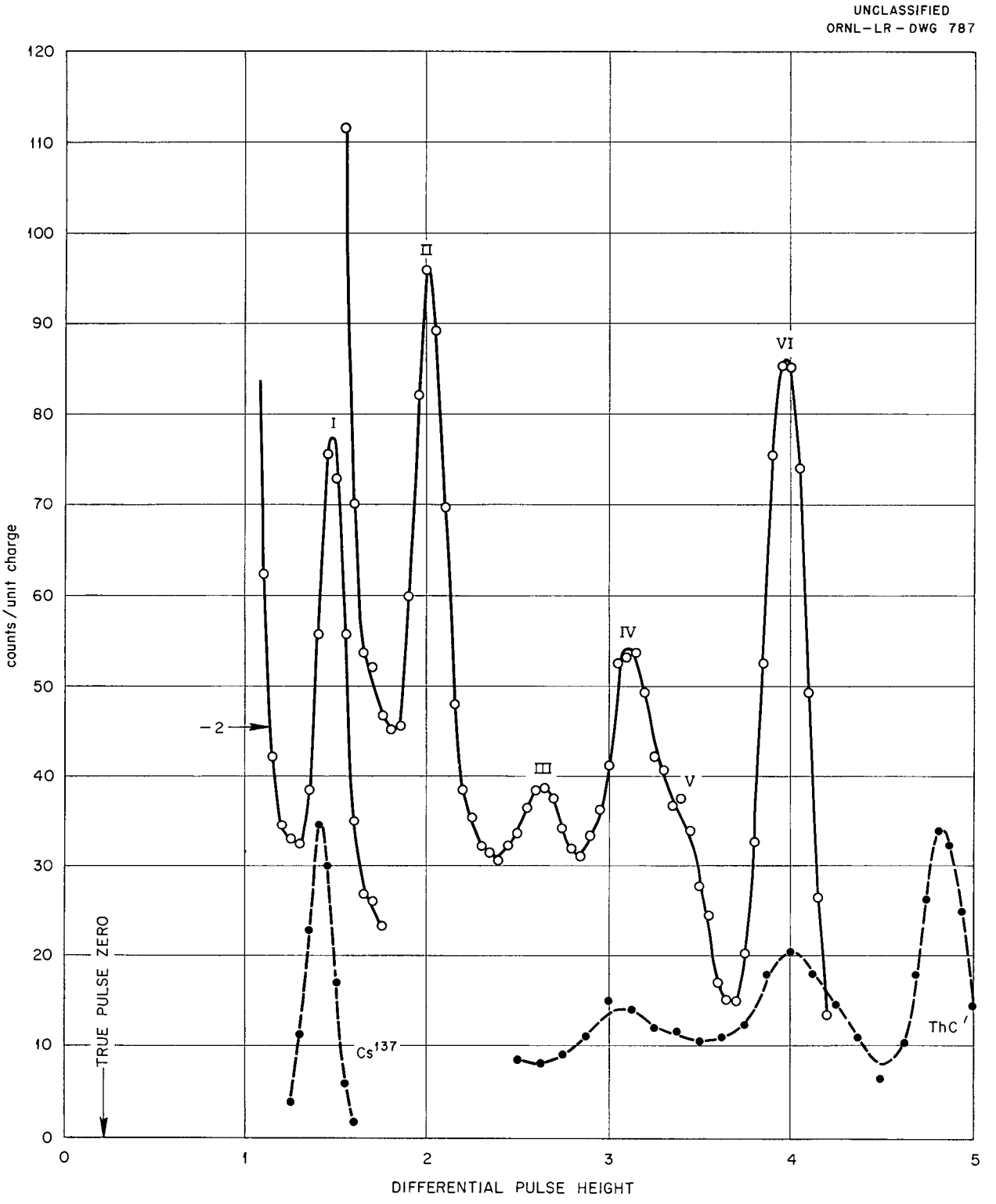

Fig 1 14 Pulse Spectrum at Low Pulse Height Produced in NaI by the Gamma Rays from Boron Bombarded by Protons

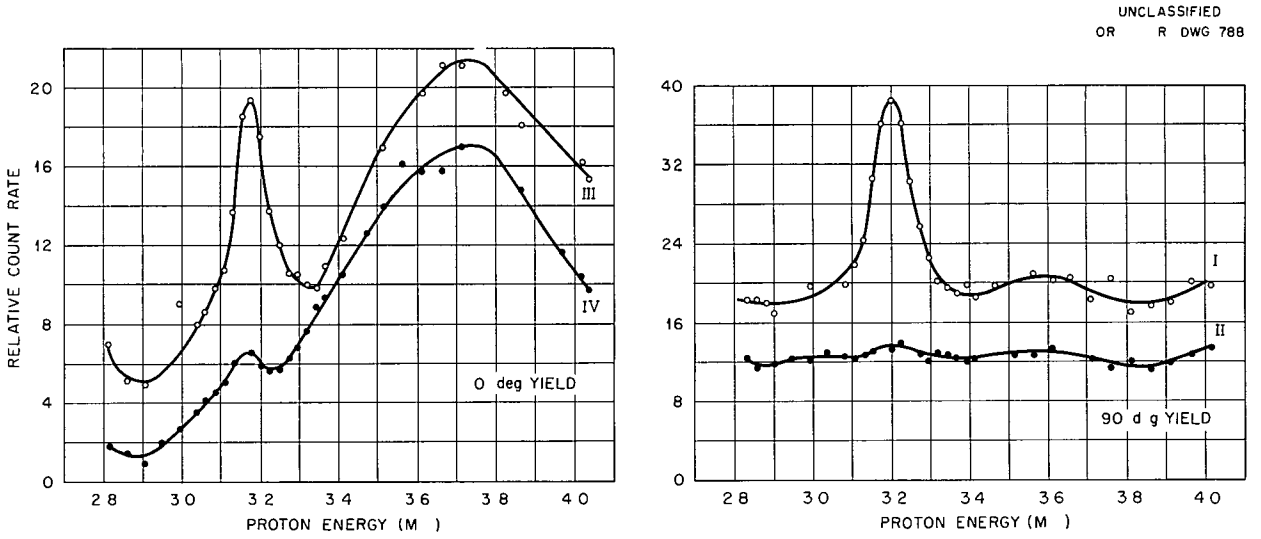

Fig 1 15 Yield with Energy of the C^{12} Ground Static Gamma Rays Following Proton Capture on B^{11}

2 RADIOACTIVITY AND NUCLEAR ISOMERISM

ANGULAR CORRELATION OF GAMMA RAYS

E D Klema F K McGowan

Neodymium 144

The directional angular correlation of the 1480–700 kev gamma-gamma cascade in Nd^{144} has been measured in a series of four experiments with a total of 10^5 coincidence counts obtained at 19 angular positions The correlation function obtained is

$$W(\theta) = 1 - (0\ 2534 \pm 0\ 0095)P_2(\cos\theta) + (0\ 033 \pm 0\ 013)P_4(\cos\theta)$$

The relative intensities of the 700 1480 and 2180 kev gamma rays have been measured and from this information the intensity of the beta spectrum to the 2180 kev level relative to that of the spectrum to the 700 kev level has been found to be 0 90 ± 0 14 Alburger and Kraushaar[1] had measured this gamma gamma cascade previously and had concluded that their data supported spin assignments $1\ D\ 1\ D\ 0$ $1\ Q\ 1\ D\ 0$ or $1\ D\ 2\ Q\ 0$ all of which lead to the same correlation function $W(\theta) = 1 - 0\ 2500\ P_2(\cos\theta)$ In the last spin sequence mentioned above they could not exclude up to 6% admixture of quadrupole radiation in the first transition The present measurement of the coefficient of $P_2(\cos\theta)$ excludes admixtures greater than 0 01%

Barium 134

The angular correlation of the 1367–603 kev gamma gamma cascade in Ba^{134} has been measured in a series of five experiments with a total of $1\ 1 \times 10^5$ coincidence counts The correlation function found is

$$W(\theta) = 1 + (0\ 0902 \pm 0\ 0086)P_2(\cos\theta) - (0\ 004 \pm 0\ 013)P_4(\cos\theta)$$

An experiment was performed which showed that the 1367 and 794 kev gamma rays in the decay scheme are not in coincidence An unambiguous spin assignment for the three energy levels involved cannot be made on the basis of these measurements alone Because of the small values of the coefficients of $P_2(\cos\theta)$ and $P_4(\cos\theta)$ in this correlation the precision of the determination is not sufficient to allow a selection from among the possibilities of $4\ Q\ 2\ Q\ 0$ $3(D+Q)2\ Q\ 0$ and $2(D+Q)2\ Q\ 0$ However the last of these assignments can be ruled out because the spin of the ground state of Cs^{134} has been measured[2] to be 4 and no beta rays have been observed leading to the 603 kev state in Ba^{134}

Lutetium 175

At the suggestion of M E Rose the angular correlation of the 54 kev x ray from ϵ capture in Hf^{175} and the 342 kev gamma ray in Lu^{175} was measured to make certain that the correlation is really isotropic as expected This experiment is also a good test of the apparatus since the counting rate is high in this case and a large number of coincidence counts can be obtained In a series of four experiments with a total of $1\ 85 \times 10^6$ coincidence counts the correlation function obtained is

$$W(\theta) = 1 - (0\ 0019 \pm 0\ 0022)P_2(\cos\theta) + (0\ 0034 \pm 0\ 0034)P_4(\cos\theta)$$

The angular correlation of the 89–342 kev gamma gamma cascade in Lu^{175} has been measured in a series of eight experiments with a total of $2\ 9 \times 10^5$ counts The correlation function found is

$$W(\theta) = 1 - (0\ 00056 \pm 0\ 0043)P_2(\cos\theta) + (0\ 0051 \pm 0\ 0074)P_4(\cos\theta)$$

The K shell internal conversion coefficient of the 342 kev gamma ray has been measured to be $9 \pm 1 \times 10^{-2}$ which indicates that the transition is probably mixed electric quadrupole and magnetic dipole radiation An upper limit on the lifetime of the state emitting the 342 kev gamma ray has been measured to be 10^{-9} sec Calculations are in progress to determine whether any spin assignment with the 89 kev gamma ray considered to be pure and the 342 kev considered to be mixed leads to the observed isotropic angular correlation function

Cesium 133

The angular correlations of the 357–82 kev and

[1] D E Alburger and J J Kr usha r *Phys Rev* **87** 448 (1952)

[2] V J ccarino B Bederson nd H H Stroke *Phys Rev* **87** 676 (1952)

the 300–82 kev gamma gamma cascades of the excited states of Cs^{133} have been measured For the 357–82 kev cascade the measured correlation function for a series of four experiments with a total of 9 2 × 10^5 coincidence counts is

$$W(\theta) = 1 + (0\ 0515 \pm 0\ 0028)P_2(\cos\theta) - (0\ 0091 \pm 0\ 0044)P_4(\cos\theta)$$

The correlation function for the 300–82 kev cascade obtained in a series of three experiments with a total of 4 2 × 10^5 counts is

$$W(\theta) = 1 + (0\ 0175 \pm 0\ 0039)P_2(\cos\theta) + (0\ 0004 \pm 0\ 0061)P_4(\cos\theta)$$

The interpretation of these experimental results is not unambiguous because of the smallness of the coefficients in both correlation functions and because the effect of the 357–82 kev cascade on the measurement of the 300–82 kev correlation has not yet been taken into account Since the 82 kev level is metastable with a half life of 6 × 10^{-9} sec the coefficients of the above correlation functions may be attenuated

Europium 153

Investigations have been made of the gamma rays from Eu^{153} with a delayed coincidence scintillation spectrometer which uses NaI detectors Samarium 153 (47 hr) decays by beta emission to Eu^{153} which emits gamma rays of 70 and 103 kev and while one of these excited states in Eu^{153} was known to be metastable the position of the metastable state and order of emission of the gamma rays were not known Recent measurements have shown conclusively that the 70 kev transition precedes the 103-kev isomeric transition and that the latter has a 3 4 × 10^{-9} sec half life Furthermore the 103 kev transition following the ϵ capture decay of Gd^{153} (225 d) decays with $T_{1/2}$ = 3 4 × 10^{-9} sec In addition the ϵ capture decay of Gd^{153} leads to another excited state in Eu^{153} within a few kev of the 103 kev level The gamma ray from the decay of this state is in prompt coincidence ($T_{1/2} < 10^{-9}$ sec) with the K x rays from ϵ capture and is 1 4 times as intense as the 103 kev gamma ray The cross over gamma ray of 173 kev for the 70–103 kev gamma ray cascade and a gamma ray of 530 kev were also observed to follow the beta decay of Sm^{153} The intensities of these two gamma rays relative to the 103 kev gamma ray are 0 22 and 0 42% respectively

The directional angular correlation of the 70–103 kev gamma ray cascade appears to be nearly isotropic Observed angular correlation coefficients of the various terms in the expansion of the correlation function in Legendre polynomials are

$$A_2 = -(0\ 0022 \pm 0\ 0029)$$

and

$$A_4 = 0\ 0124 \pm 0\ 0080$$

Both transitions are known[3] to be mixed multipole radiations from K shell internal conversion coefficient measurements The explicit form of the angular correlation function[4] for a mixed gamma–mixed gamma cascade is a function of δ_1 and δ_2 where δ_1^2 and δ_2^2 are defined as the intensity ratio (in this case) of quadrupole to dipole radiation in transitions 1 and 2 respectively The intensity ratio $E2/M1$ for the 70 kev transition is 2 0 The following spin sequences were examined for vanishing angular correlation coefficients with δ_1^2 = 2 0 $j_1 = j$ or $j \pm 1$ $(E2 + M1)$ j = 5/2 5/2 ± 1 $(Q + D)$ 5/2 All nine sequences lead to real roots for $|\delta_2|$ with 18 roots ranging between 0 09 and 0 39 and 6 roots equal to 3 23 Unfortunately the uncertainty in the internal conversion coefficient measurement which fixes $|\delta_2|$ makes it impossible to exclude any of these roots

BROAD BEAM GAMMA ATTENUATIONS

R Stephenson P R Bell

Experiments on the attenuation of gamma rays through thick absorbers as described in the previous report (ORNL 1620) are continuing and a satisfactory method has been developed for analyzing the data The detector is a standard 1½ in dia by 1 in thick sodium iodide scintillation counter resting inside a lead cubicle which is lined with a graded shield The signal from the scintillation counter is amplified by an Al linear amplifier and is then fed to the 20-channel analyzer to obtain the counting rate as a function of pulse height Sources of various energy can be suspended above the scintillation counter in a small polystyrene cup and large sheets of lead or aluminum are placed between the source and detector Experiments with the following gamma sources have now been completed for various thicknesses of both lead and aluminum Cs^{137}

[3] F K McGowan *Phys Rev* **93** 163 (1954)

[4] M E Rose *Phys Rev* **93** 477 (1954)

(661 kev) K^{42} (1 51 Mev) Na^{24} (2 76 and 1 38 Mev) and Po Be (4 44 Mev excited carbon)

Figures 2 1 and 2 2 show the attenuation in lead and aluminum of the 4 44 Mev excited carbon gamma from polonium beryllium The source was contained within a block of lithiated paraffin to minimize hydrogen capture gammas and paraffin scatterers were used to scatter out neutrons without appreciably attenuating the gammas Figure 2 3 gives the attenuation of Cs^{137} gammas in

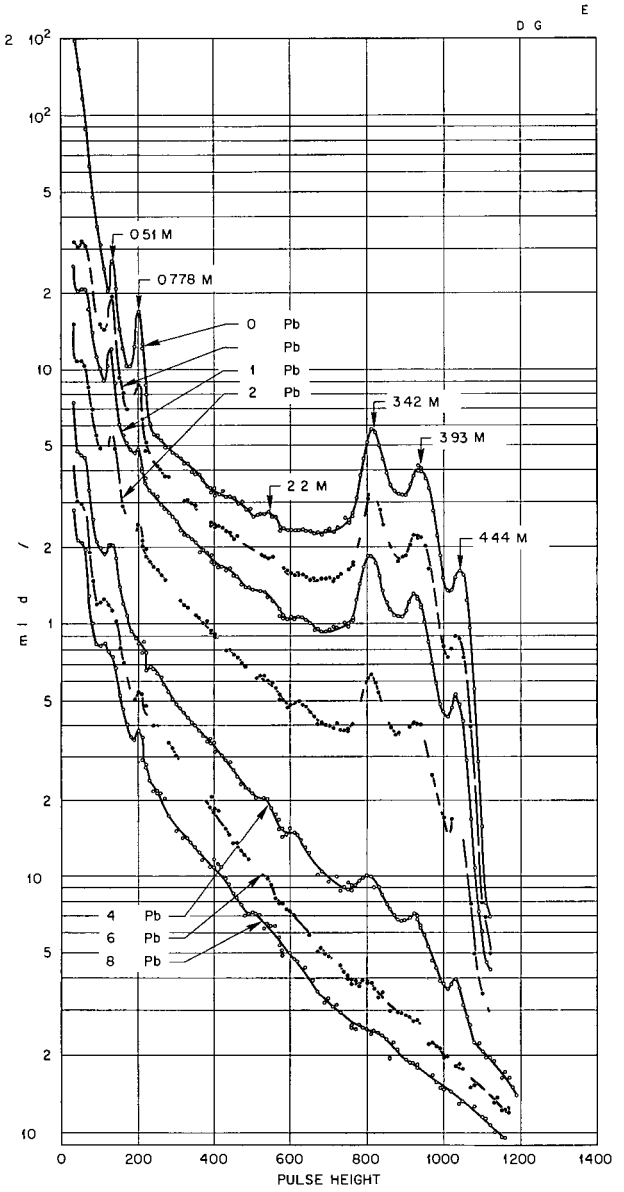

Fig 2 1 Broad Beam Attenuations 4 44-Mev Excited Carbon from Polonium Beryllium in Lead Runs AT 11 20 53 to AT 11 30-53

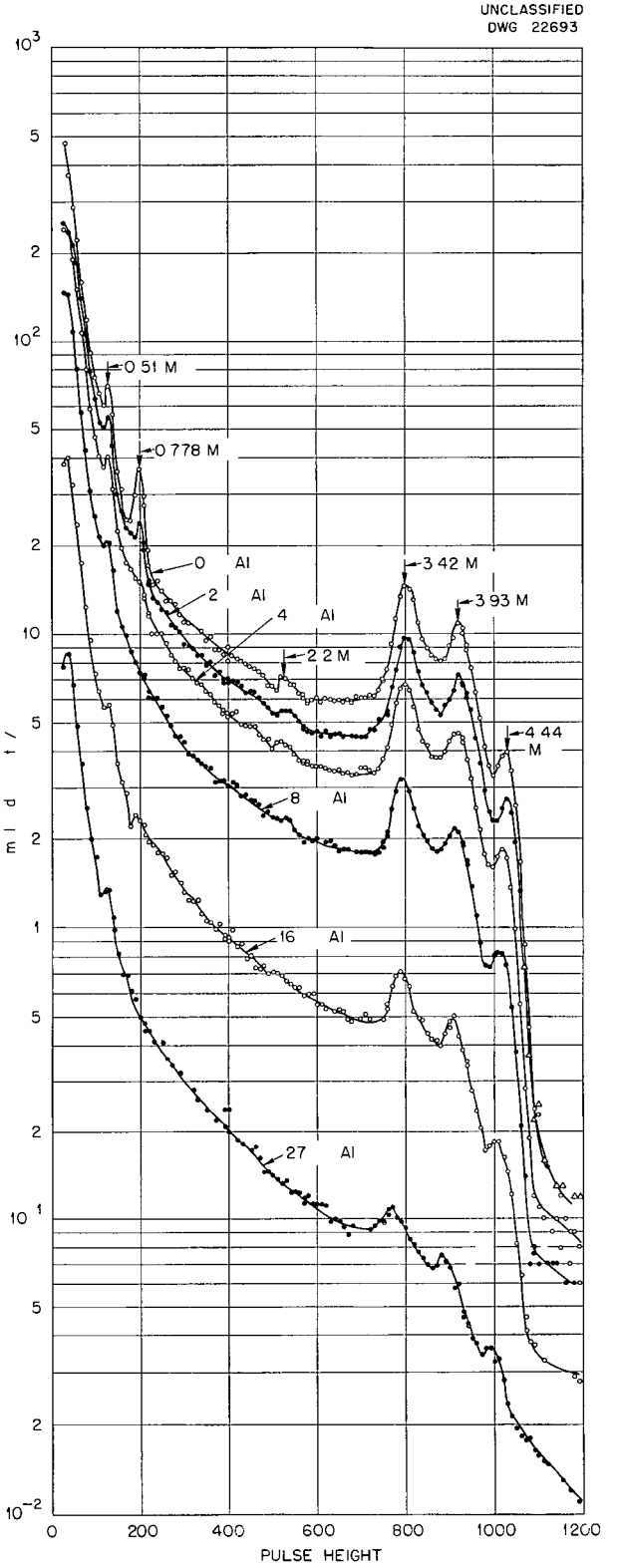

Fig 2 2 Broad Beam Attenuations 4 44 Mev Excited Carbon Gamma from Polonium Beryllium in Aluminum Runs AT 12 2 53 to AT 12 7 53

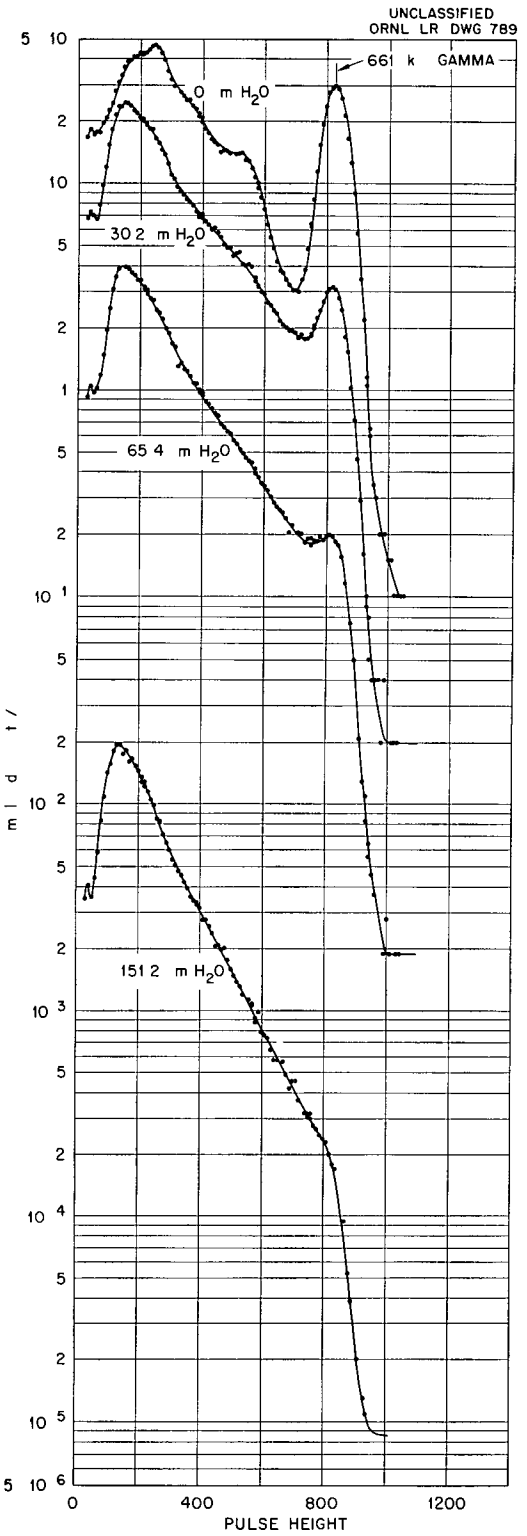

Fig 2 3 Broad Beam Attenuations Cs^{137} in Water – Source at 170 cm

water and Fig 2 4 gives the attenuation of K^{42} gammas in water

Values of absorption coefficient and build up factor derived from our experimental data are given in Table 2 1 together with theoretical values calculated by the National Bureau of Standards and NDA The agreement is very good Our values of absorption coefficient tend to be slightly lower than the NBS values indicating perhaps that coherent scattering may be higher under broad beam geometry Since the NDA build up factors are for a point source and detector within an infinite medium whereas our values are for a point source and detector separated by a slab shield the NDA values should be slightly higher because of back scattering

Theory

The theoretical response of a scintillation counter to monoenergetic gammas of energy E_0 is illustrated diagrammatically in Fig 2 5 Depending upon the gamma energy the possible reactions in the crystal are as follows

1 Photoelectric absorption – this produces a pulse equal to the full energy of the gamma photon

2 Compton scattering at any angle from 0 to 180 deg – this produces a continuum from an energy of zero to a maximum energy corresponding to 180-deg scattering of the gamma

3 Pair production – this gives pulses of three discrete energies If both annihilation gammas are absorbed in the crystal a pulse equal to the full energy is obtained If one annihilation gamma escapes a pulse is obtained of 0 51 Mev less than the full energy and if both annihilation gammas escape a pulse is obtained of 1 02 Mev less than the full energy There is also a possibility of Compton interaction of the 0 51 Mev gammas which produces a continuum down to 1 02 Mev less than the full energy

4 Coherent scattering by bound electrons in the crystal – there is negligible transfer of energy to the crystal negligible degradation of the photon energy and hence no crystal response from such an interaction Coherent scattering is more important than is commonly realized and it is significant in sodium iodide for energies as high as 2 Mev

The actual response of a crystal and its associated electronic circuit differs from the theoretical

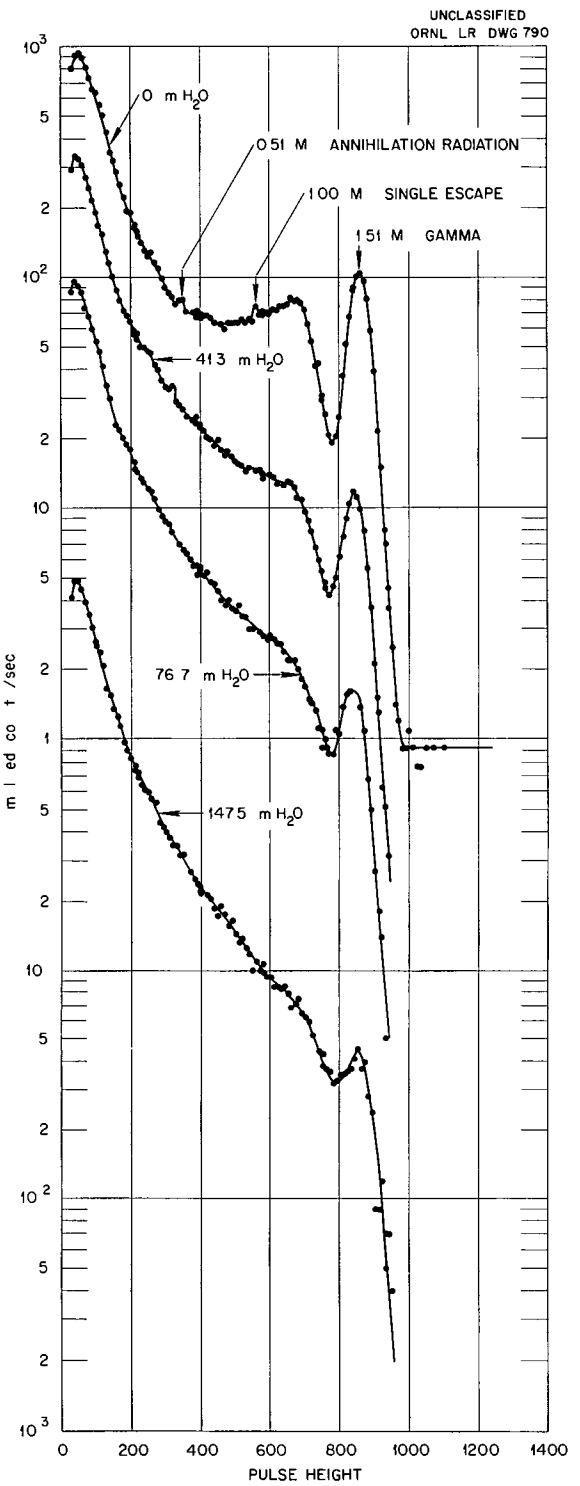

Fig 2 4 Broad Beam Attenuations – K^{42} in Water Runs AT 3 30-54 MCA 1 Through AT 4 1 54 MCA 1

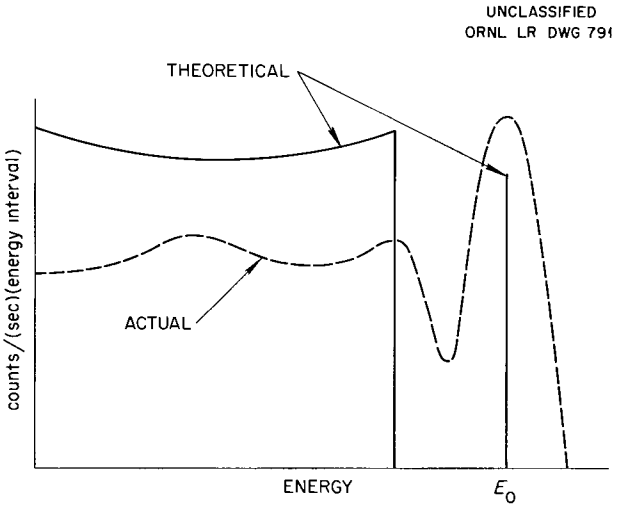

Fig 2 5 Theoretical and Actual Response of a Scintillation Counter

response in the following ways

1 Because of the finite resolution of the equipment pulses of a discrete energy will be smeared by a Gaussian distribution about that energy

2 When a gamma undergoes a Compton scattering the probability of photoelectric absorption of the scattered photon is increased because of its lower energy and multiple processes leading to the complete absorption of the incident gamma are possible Thus for a crystal of any appreciable size the relative number of full energy pulses will be much greater than predicted from the ratio of the photoelectric to the total cross section

3 Since the crystal is normally contained within a lead cubicle to minimize background radiation primary gammas may scatter from the surroundings to produce a back scatter spectrum which usually peaks at an energy corresponding to 180 deg scattering If a graded shield is not employed there will also be a peak corresponding to *K* shell x rays produced in the lead shield If the primary radiation is greater than 1 02 Mev in energy there will also be a peak at 0 51 Mev corresponding to annihilation radiation produced in the surroundings

4 For a large crystal the Compton distribution will be considerably reduced and those photons scattered in the top face of the crystal will have the greatest probability of escaping This causes a noticeable bulge in the Compton distribution at higher energies

5 At very low gamma energies the iodine photoelectric cross section is so large that the photons

TABLE 2 1 SUMMARY OF EXPERIMENTAL DATA

NUCLIDE	ENERGY (k)	SHIELD	SHIELD THICKNESS (m)	ABSORPTION COEFFICIENT (m ^{1})	NBS VALUE OF ABSORPTION COEFFICIENT	NUMBER BUILD UP FACTOR	DOSE BUILD UP FACTOR	NDA DOSE BUILD UP FACTOR	RELAXATION LENGTHS
C ^{137}	661	Al m m	74 97	0 203	0 203	213	64	60	15 2
C ^{137}	661	Al m m	41 69	0 200	0 203	34 3	13 4	24	8 34
C ^{137}	661	Al m m	20 91	0 197	0 203	10 7	5 12	8 2	4 11
C ^{137}	661	L d	10 39	1 146	1 143	2 50	2 22	3 2	11 91
C ^{137}	661	N I	18 12	0 262	0 270				4 75
K^{42}	1510	Al m m	36 49	0 136	0 136				4 96
K^{42}	1510	L d	13 12	0 568	0 574	3 98	3 20	3 5	7 45
K^{42}	1510	L d	6 46	0 565	0 574	2 53	2 07	2 27	3 65

do not penetrate very far into the crystal Under these conditions the 28 kev iodine K x rays may escape the crystal and an iodine escape peak is formed

If only the full energy or photopeak is considered the distribution about the energy E_0 is very closely Gaussian and the counting rate may be expressed by the equation

$$y = Ae^{-(V-V_0)^2/K^2V_0}$$

where

y = counts/(sec)(pulse height interval)
A = maximun counting rate
V = pulse height
V_0 = pulse height corresponding to the primary energy E_0
K = constant depending upon the resolution of the crystal and its associated electronic equipment

The pulse height is proportional to energy so that at any energy E

$$V = CE$$

where the constant C is determined by the voltage on the phototube and the gain of the linear amplifier

At half the maximum counting rate $y = A/2$ and

$$\frac{(V - V_0)^2}{K^2V_0} = \ln 2$$

The resolution is arbitrarily defined as the width of the Gaussian at half maximum divided by the peak pulse height for the gamma energy E_0 Thus

$$\text{Resolution} = \frac{2(V - V_0)}{V_0} = \frac{2K\sqrt{\ln 2}}{\sqrt{V_0}}$$

or

$$\text{Resolution} = \frac{2(E - E_0)}{E_0} = \frac{2K\sqrt{\ln 2}}{\sqrt{C}\sqrt{E_0}}$$

The smaller the resolution the less will be the smearing of the true spectrum and the easier will be the analysis of the data In our experiments the resolution was about 10% for Cs^{137} (661 kev) The resolution depends primarily upon the number of photoelectrons produced in the photomultiplier for a given total energy loss in the crystal At higher energies the percentage variation in the number of photoelectrons is smaller and the resolution becomes better As can be seen from the above equation the resolution is inversely proportional to the square root of the gamma energy

For two gammas of energy E_0 and E_1 measured under the same conditions the ratio of the widths of the Gaussians at half maximum is

$$\frac{2(E - E_0)}{2(E - E_1)} = \frac{2K\sqrt{E_0 \ln 2}/\sqrt{C}}{2K\sqrt{E_1 \ln 2}/\sqrt{C}} = \sqrt{\frac{E_0}{E_1}}$$

Thus the width of a Gaussian at a given fraction of the maximum counting rate is directly proportional to the square root of the energy If two gammas of different energy are counted simultaneously the lower energy Gaussian will be narrower but the resolution will be better at the higher energy

In analyzing the spectrum it is desirable that a line of any energy should have the same shape and width If the width of a Gaussian is considered as some fraction F of its maximum height

$$y = \frac{A}{F} = Ae^{-(V-V_0)^2/K^2V_0}$$

$$\ln A - \ln F = \ln A - \frac{(V - V_0)^2}{K^2V_0}$$

$$V - V_0 = K\sqrt{V_0}\ln F$$

But if the resolution of the system is of the order of 10% or less for Cs^{137} the value of the Gaussian will be very small except when V is close to V_0 Under these conditions this equation may be re written

$$\sqrt{V} - \sqrt{V_0} = \frac{\sqrt{V_0}}{\sqrt{V} + \sqrt{V_0}} K\sqrt{\ln F} \sim \frac{K\sqrt{\ln F}}{2}$$

Thus if the logarithm of the counting rate is plotted as a function of the square root of the pulse height the Gaussians will all have the same shape regardless of energy

Analysis of a Continuum

When an absorber is placed between source and detector single and multiple Compton scatterings in the absorber produce a continuum of degraded photons from zero energy to the full primary energy The crystal response to this continuum is now added to that of the primary radiation and for any appreciable attenuation the integrated number of degraded photons striking the crystal will be much larger than the number of primaries To obtain the build-up factor the spectrum of the primary radi ation must first be subtracted and the resultant degraded spectrum then separated into its com ponents

Consider now the response of a crystal to a continuum extending up to the full energy pulse height V_0 as illustrated in Fig 2 6 If $g(V)$ repre sents the actual pulse height distribution in the crystal the smeared pulse height spectrum will be

$$f(V) = \int_{V_1=0}^{V_1=V_0} \frac{1}{K\sqrt{\pi V_1}} \times g(V)\, e^{-(V-V_1)^2/K^2V_1}\, dV_1$$

where

$g(V)$ = true spectrum counts/(sec)(pulse height interval)

$f(V)$ = smeared spectrum counts/(sec)(pulse height interval)

V_1 = variable of intergration

It has been found experimentally that immediately below the primary energy $g(V)$ is nearly a straight line on semilogarithmic paper so that

$$g(V) = Be^{4DV/K^2}$$

where B and D are constants The equation is written in this form to simplify future calculations

But as before the Gaussian contributions are small except when V_1 is close to V Thus as an approximation

$$\frac{(V - V_1)^2}{V_1} = (\sqrt{V} - \sqrt{V_1})^2 \frac{(\sqrt{V} + \sqrt{V_1})^2}{V_1} \sim 4(\sqrt{V} - \sqrt{V_1})^2$$

and substituting the value of $g(V)$ at the pulse height V_1

$$f(V) = \frac{B}{K\sqrt{\pi V}} \int_{V_1=0}^{V_1=V_0} \exp\left[\frac{4}{K^2}(DV_1 - V + 2)\sqrt{VV_1} - V_1\right] dV_1$$

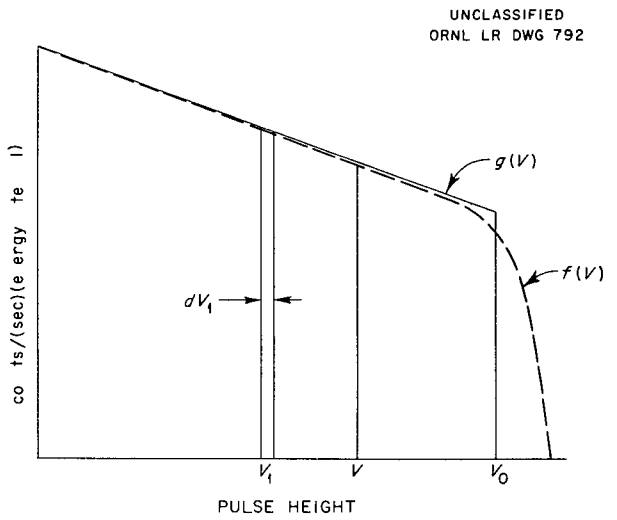

Fig 2 6 True and Smeared Pulse Distributions

which with the substitution

$$x = \frac{2\sqrt{1-D}\,\sqrt{V_1}}{K} - \frac{2\sqrt{V}}{K\sqrt{1-D}}$$

reduces to

$$f(V) = \frac{B}{K\sqrt{\pi V}}\, e^{4DV/K^2(1-D)} \int_{x_1}^{x_2} \left[\frac{K^2 x}{2(1-D)} + \frac{K\sqrt{V}}{(1-D)^{3/2}} \right] e^{-x^2}\, dx$$

Since pulse heights considerably greater than zero are being considered the solution is

$$f(V) = \frac{Be^{4DV/K^2(1-D)}}{(1-D)^{3/2}} \left[\frac{1}{2} + \frac{1}{\pi} \int_0^{x_2} e^{-x^2}\, dx - \frac{K(1-D)^{1/2}}{4\sqrt{\pi V}}\, e^{-x_2^2} \right]$$

where

$$x_2 = \frac{2(1-D)^{1/2}\sqrt{V_0}}{K} - \frac{2\sqrt{V}}{K(1-D)^{1/2}}$$

At pulse heights well below that height corresponding to the primary energy the quantity within the brackets becomes equal to unity and $f(V)$ is a straight line on semilogarithmic paper When $D = 0$ $f(V)$ and $g(V)$ are identical at energies well below the source energy

Analysis of Data

The first problem to be considered is that of peeling off the proper amount of primary One of the chief objects of this work is to measure experimentally the absorption coefficient under broad beam conditions which is given by the equation

$$\Sigma = \frac{\ln I_0/I}{x}$$

where

Σ = absorption coefficient of primary radiation cm^{-1}

I_0/I = ratio of intensities before and after shielding

x = thickness of shield

Because of the logarithmic term in the numerator the calculated value of the absorption coefficient will be more accurate at the larger attenuations which are also of greater interest to the shield designer Our values of absorption coefficients and build up factors are thus more precise at the higher attenuations

From the thickness of the shield and the absorption coefficient reported in the literature (with coherent scattering deducted) the attenuation of the primary radiation is first estimated The intensity without shield is then multiplied by this value and subtracted point by point from the spectrum with shield At high attenuations the relative amount to be subtracted is often small at energies less than the photopeak

The values of B and D are then determined from the slope of the degraded spectrum immediately below the photopeak The theoretical distribution is then calculated from the above equation and subtracted from the original curve to obtain the primary peak alone The absorption coefficient is calculated from the intensities with and without absorber Figure 2 7 shows a typical curve for the case of K^{42} in aluminum In this case the relative amount of degraded spectrum in the full energy peak is small

To analyze the degraded spectrum into its components the curve is replotted on a square root scale of pulse height and the Gaussian shape corresponding to the photopeak without any absorber is successively subtracted starting at the high energy end as illustrated in Fig 2 8 Each Gaussian subtraction must of course be accompanied by its Compton distribution as estimated from experimental measurements summarized in Fig 2 9

The gross spectrum falling on the crystal can then be determined by dividing the area of each subtracted Gaussian peak by the peak to total and by the crystal efficiency for a gamma of that particular energy Figures 2 10 2 11 and 2 12 give the values of these two quantities Degraded photon distributions for Cs^{137} in aluminum Cs^{137} in lead and K^{42} in lead are given in Figs 2 13 2 14 and 2 15

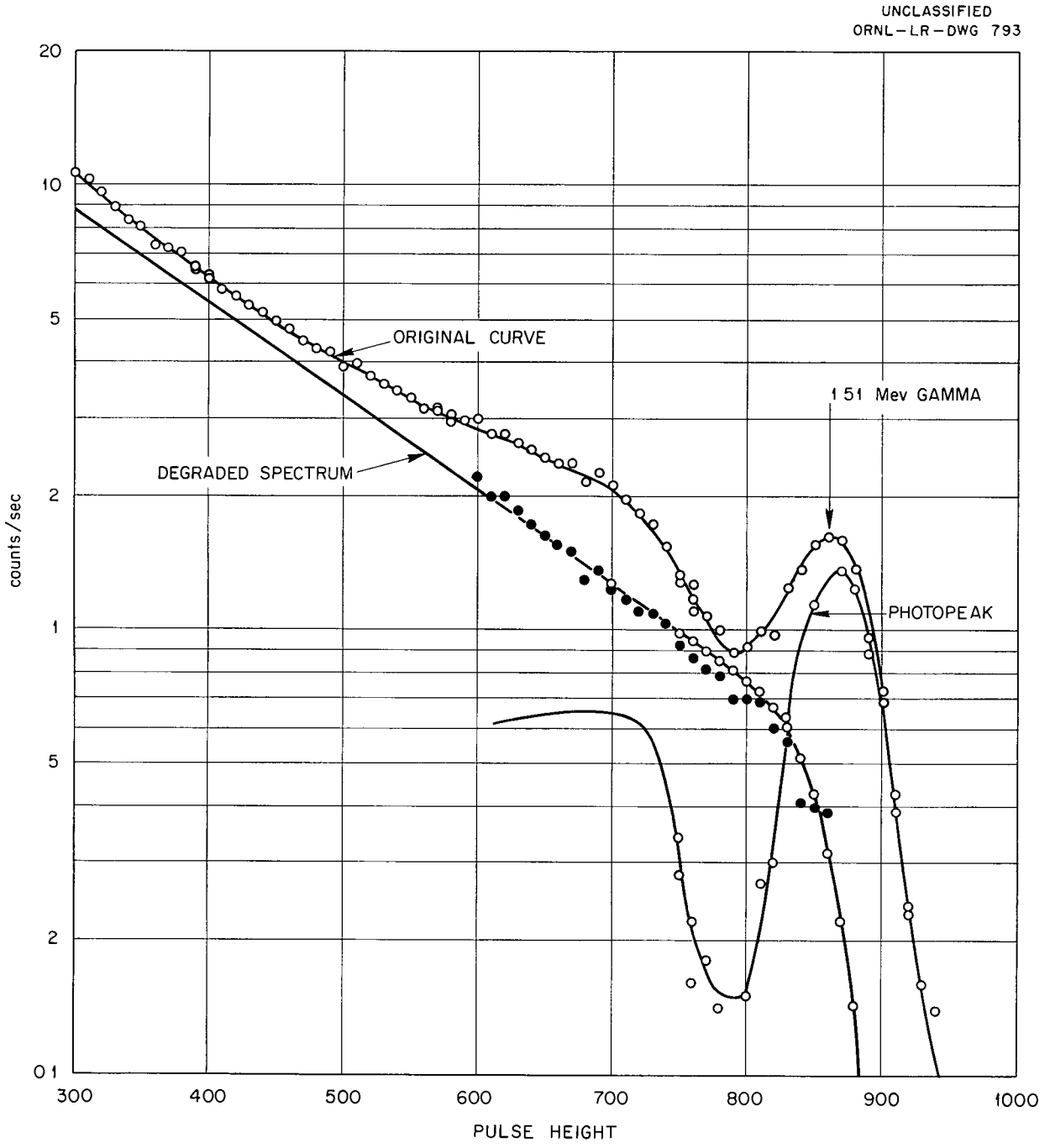

Fig 2 7 Broad Beam Attenuation – Typical Unscrambling K^{42} in Alum num – 36 49 cm of Aluminum Run AT 9 18-53 MC 2

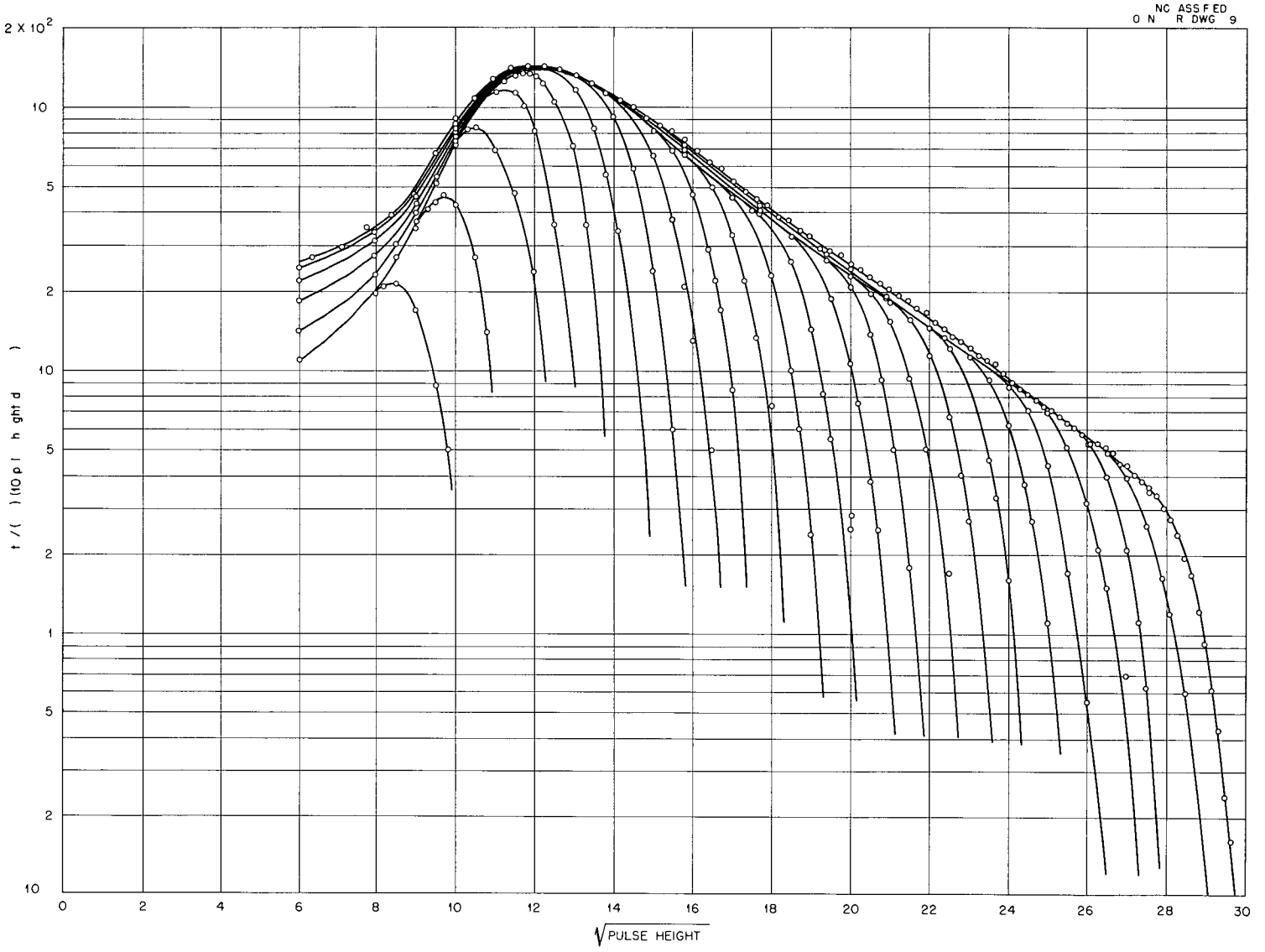

Fig 2 8 Broad Beam Attenuation Gaussian Peeling-Off Cs^{137} in Aluminum – 41 69 cm of Aluminum Run AT 7 17 53 MC 2

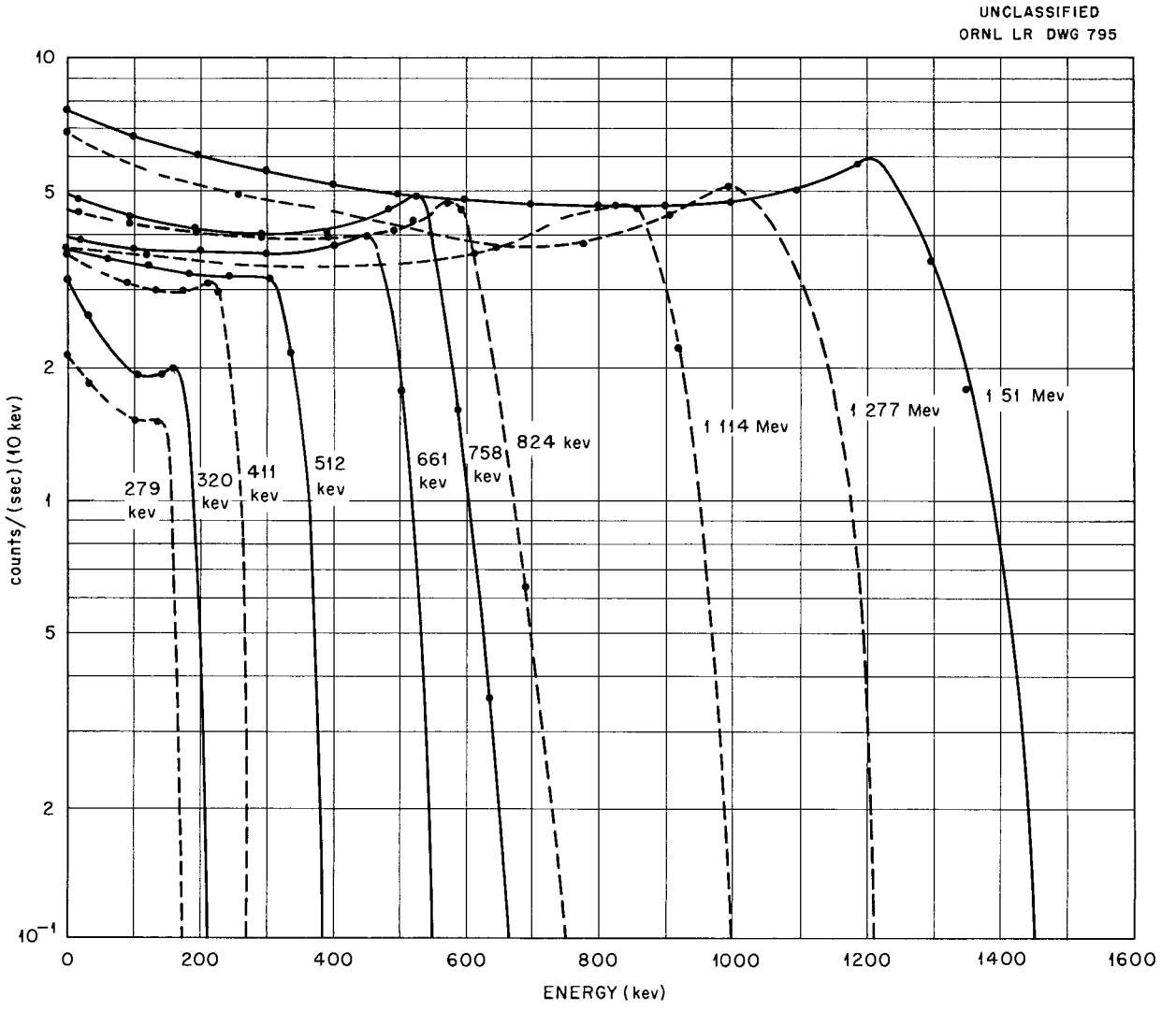

Fig 2 9 Normalized Compton Distribution Summary of experimental data for $1\frac{1}{2}$ in dia by 1 in thick NaI crystal based on photopeak counting rate = 100 counts/sec

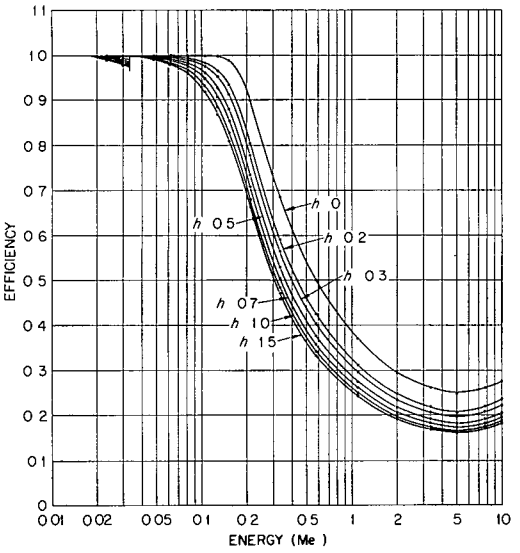

Fig 2 10 Calculated Efficiency of NaI Crystal 1½ in in Diameter and 1 in High h = cm from source to crystal (source centrally located above crystal)

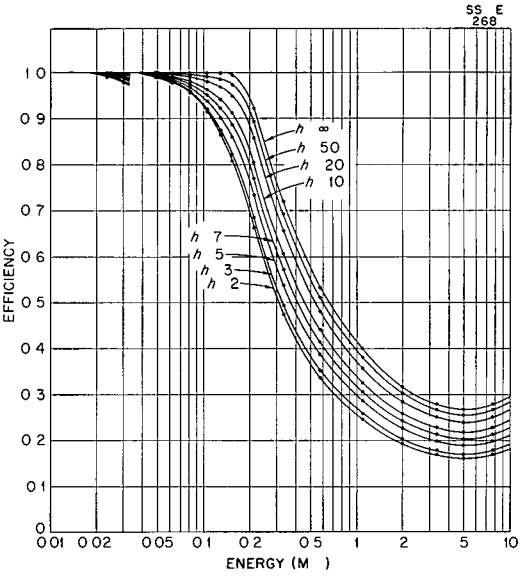

Fig 2 11 Calculated Efficiency of NaI Crystal 1½ in in Diameter and 1 in High h = cm from source to crystal (source centrally located above crystal)

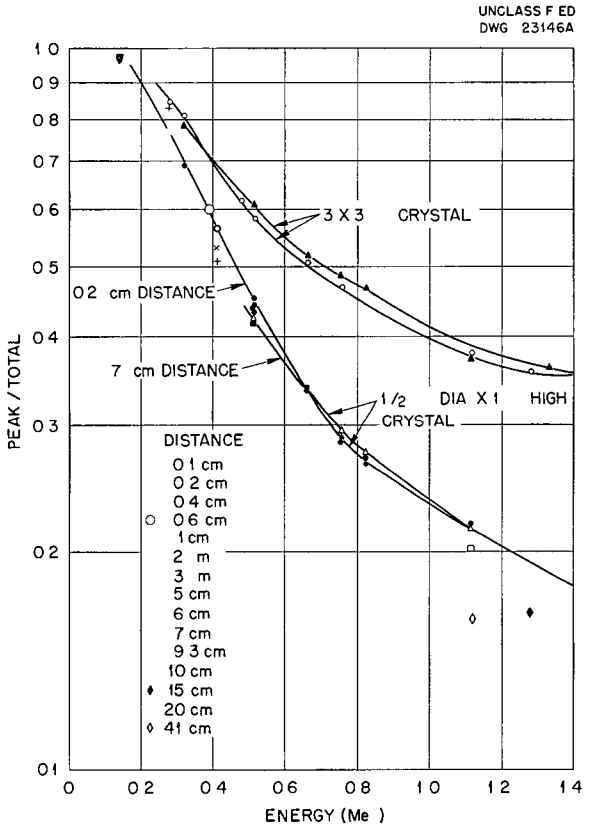

Fig 2 12 Peak to Total for NaI(Tl) Crystals (Summary of Experimental Data)

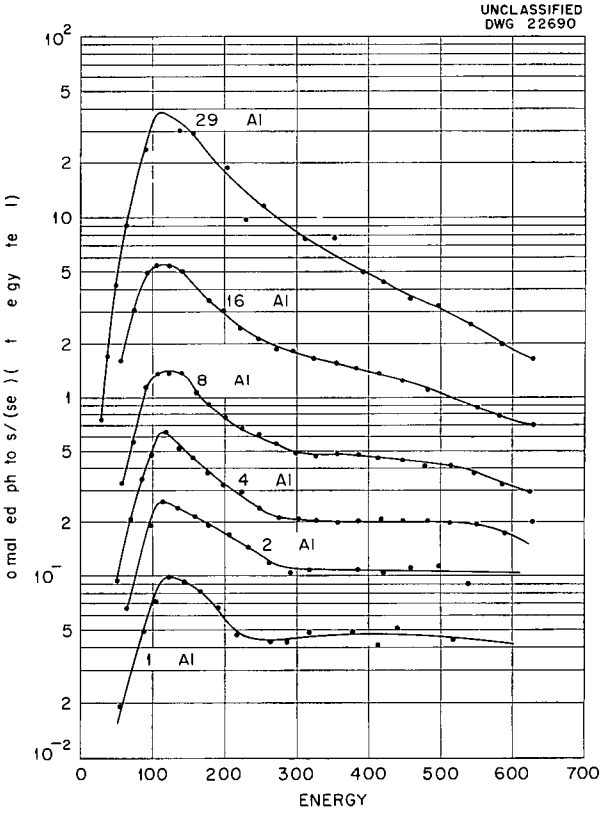

Fig 2 13 Degraded Spectrum Cs^{137} in Aluminum

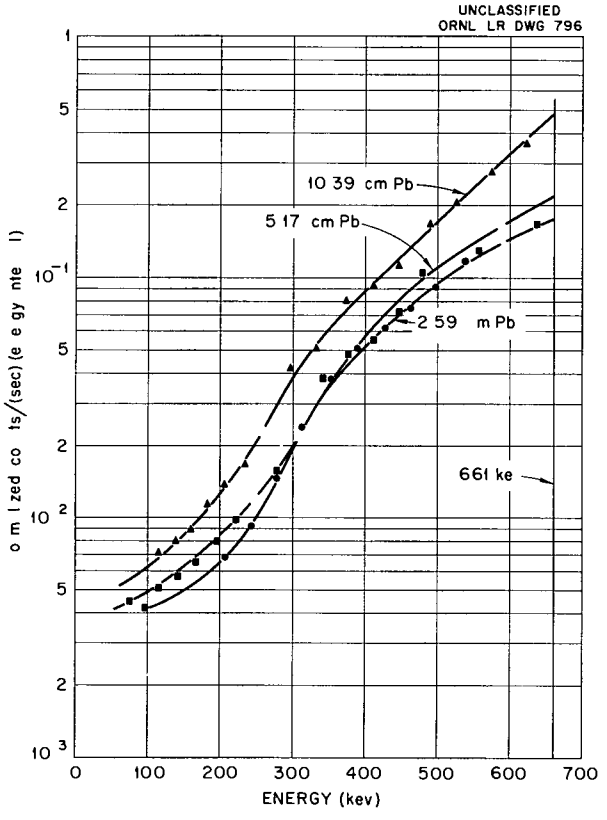

Fig 2 14 Broad Beam Attenuations – Degraded Spectrum Cs^{137} in Lead

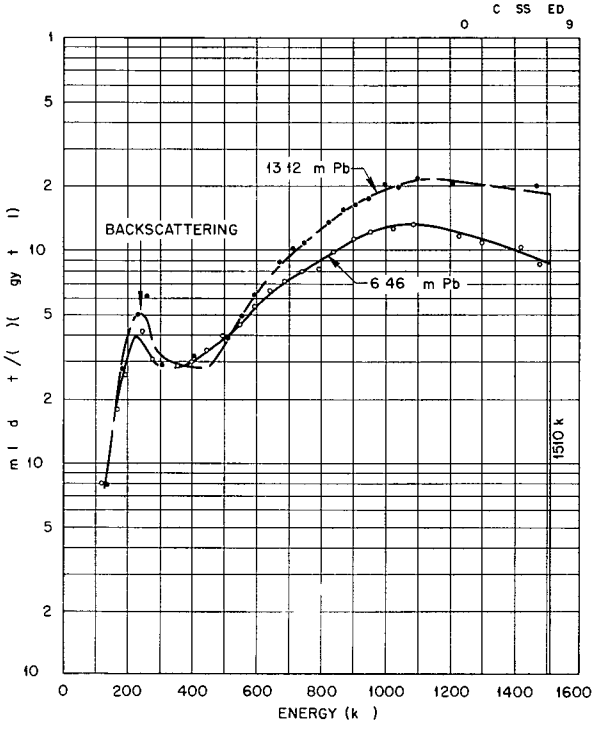

Fig 2 15 Broad Beam Attenuations – Degraded Spectrum K^{42} in Lead

3 NEUTRON DIFFRACTION

NEUTRON DIFFRACTION STUDIES ON IRON AT HIGH TEMPERATURES

M K Wilkinson C G Shull

Neutron diffraction patterns have been taken for iron at various temperatures up to about 1000°C in a study of the ferromagnetic disorder scattering below the Curie temperature (T_c = 770°C) and of the paramagnetic scattering above T_c The sample used for this study was cut from a polycrystalline block of Armco iron (purity 99 92%) Heating was accomplished with tantalum resistance wires in direct thermal contact with the sample and temperatures were measured with a calibrated (Pt Pt Rh) thermocouple The heated sample was surrounded by a number of floating radiation shields to minimize heat losses and the whole assembly was contained within a high vacuum envelope In order to minimize spurious neutron scattering vanadium windows were used in the shields and vacuum jacket at places where the neutron beam passed Figure 3 1 presents typical patterns taken at room temperature and at high temperature that show the transformation from a body centered cubic structure (α form) to the face centered cubic structure (γ form) which is known to occur at a temperature of

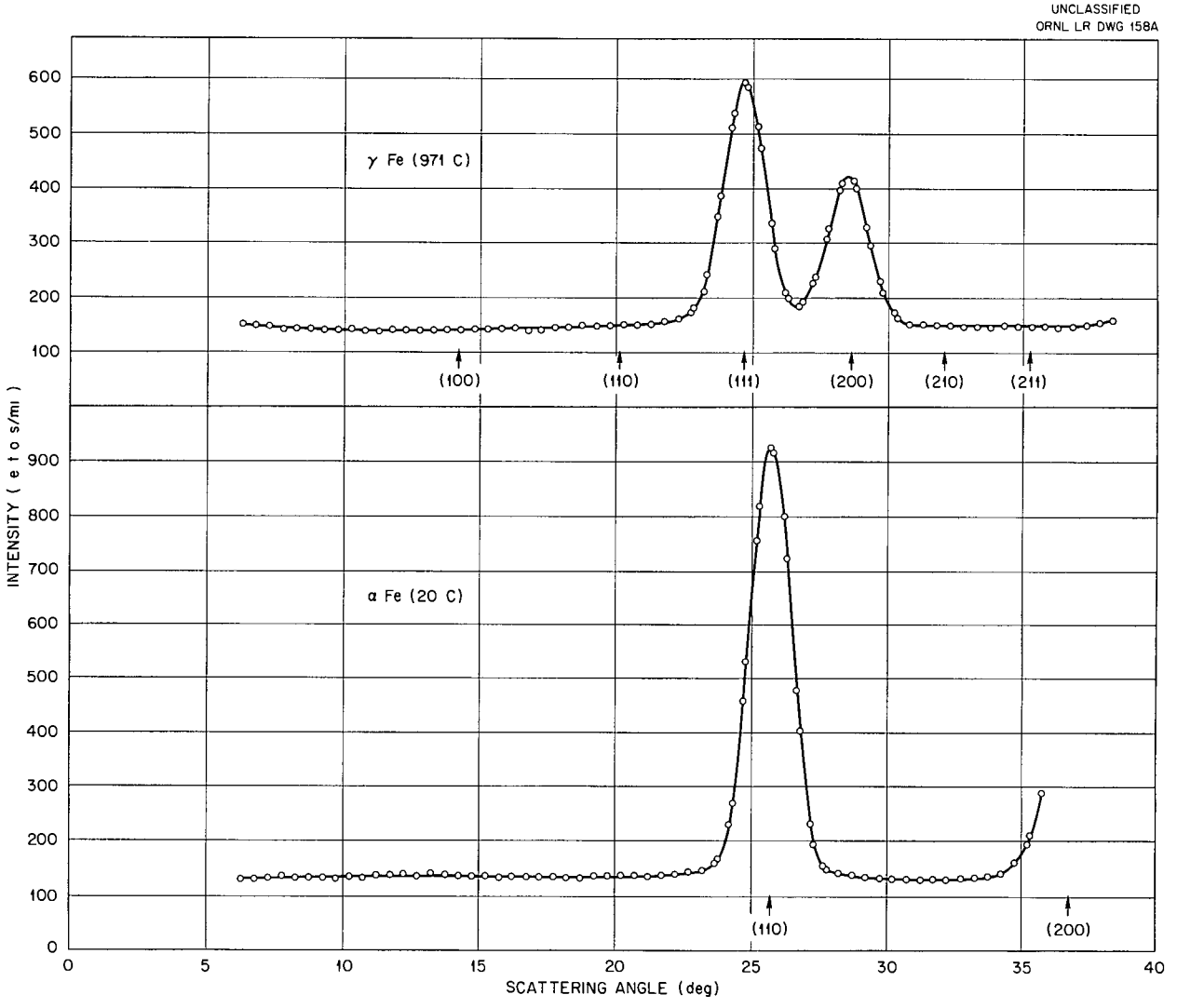

Fig 3 1 Neutron Diffraction Patterns from Iron

about 900°C These patterns have been corrected for instrumental and background scattering by standard procedures and they represent the true scattering by the iron sample

It is to be noticed that the γ iron pattern of Fig 3 1 shows no evidence of superstructure intensity at the (100) (110) etc positions and this fact eliminates the possibility that face centered cubic iron is antiferromagnetic as has been suggested in the literature a number of times The pattern for the ferromagnetic α iron phase contains both nuclear and ferromagnetic scattering components and Fig 3 2 illustrates how these two components can be recognized In Fig 3 2 is plotted the (110) reflection at two temperatures below T_c and two temperatures above T_c It is known that the intensity of such a reflection should decrease with increasing temperature because of enhanced thermal oscillation of the scattering centers in the lattice and the expected decrease in intensity due to this cause is indicated on the figure by the vertical arrows An additional intensity decrease is to be noted however and this is caused by the disappearance of the ferromagnetic scattering when the sample temperature reaches the vicinity of T_c A calculation of the ferromagnetic component by use of known values for the nuclear and magnetic scattering amplitudes agrees closely with the observed component

Most interest in the patterns of the type shown in Fig 3 1 resides in the diffuse scattering components since the ferromagnetic disorder scattering

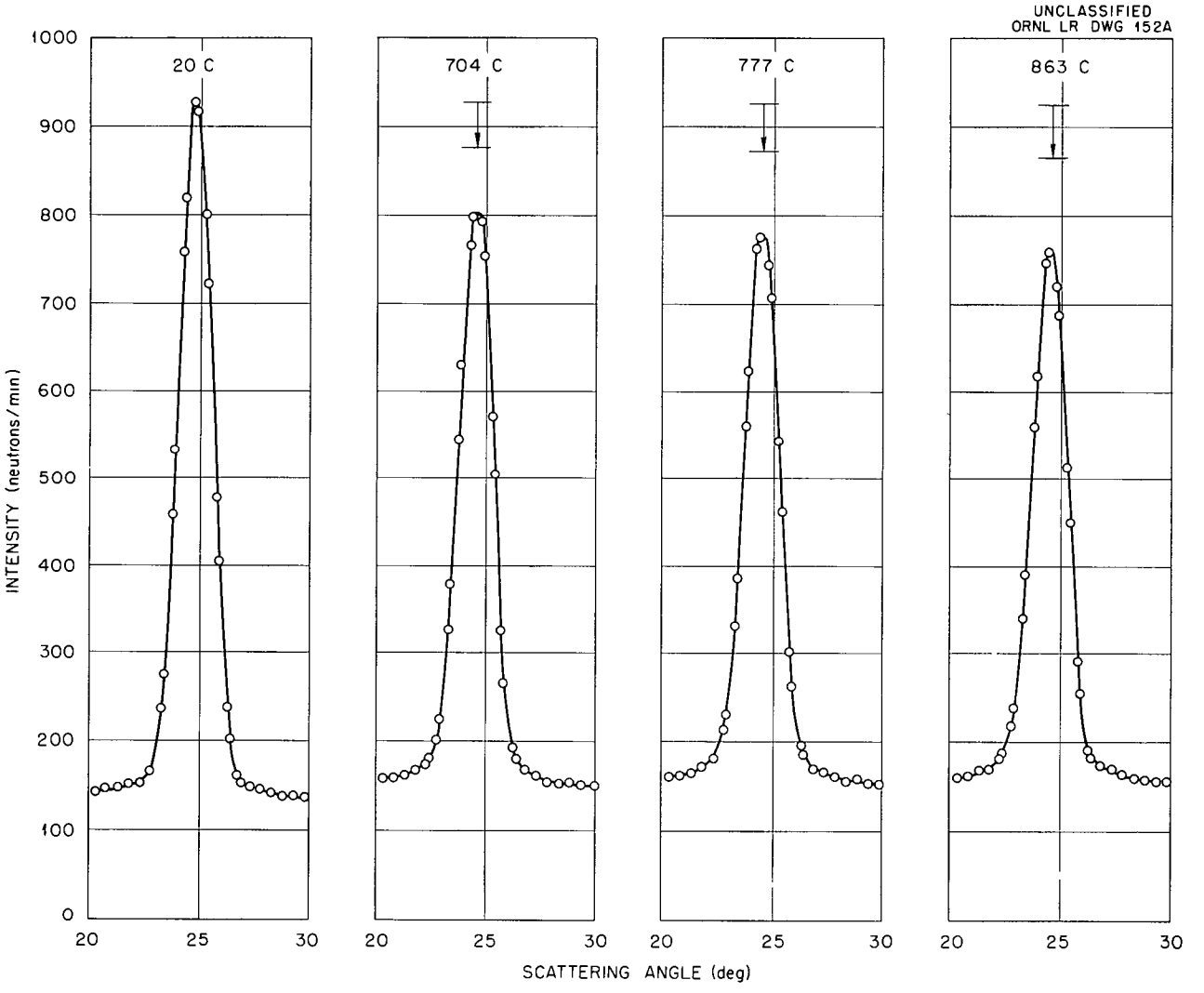

Fig 3 2 (110) Reflection from α Fe

and the paramagnetic scattering should be of diffuse character Figure 3 3 illustrates regions of the diffuse scattering as measured at a series of temperatures in the vicinity of T_c and well above T_c Most of the intensity change at the larger angles of scattering can be accounted for by the expected increase in thermal diffuse scattering whose calculated values for the different temperatures are shown in the bottom part of the figure There appears however an excess scattering in addition to the thermal scattering in the close vicinity of the coherent diffraction peak and even more pronouncedly in the small angle scattering region On the same intensity scale is placed the expected paramagnetic scattering (assuming the paramagnetic and ferromagnetic moments to be the same) and it is seen that the observed intensity change from below to well above T_c is much smaller than expected Before discussing the implications of this it will be advisable to consider in more detail the small angle scattering effects noted above

The data presented in Figs 3 1 to 3 3 have all been taken with the usual spectrometer resolution which does not permit study at angles below 4 or 5 deg because of pronounced background effects in this region In order to make this angular region accessible the primary beam width and collimation were successively reduced until it was possible to obtain significant data into scattering angles of slightly less than 1 deg Figure 3 4 illustrates the small angle scattering intensity which is obtained in excess of the intensity measured at room temperature Pronounced intensity is found to develop at a temperature of about 600°C and this intensity increases until the Curie temperature of 770°C is reached Above T_c it reverses itself and falls but it is still observable at the highest temperature studied about 970°C This small angle scattering is interpreted as being the result

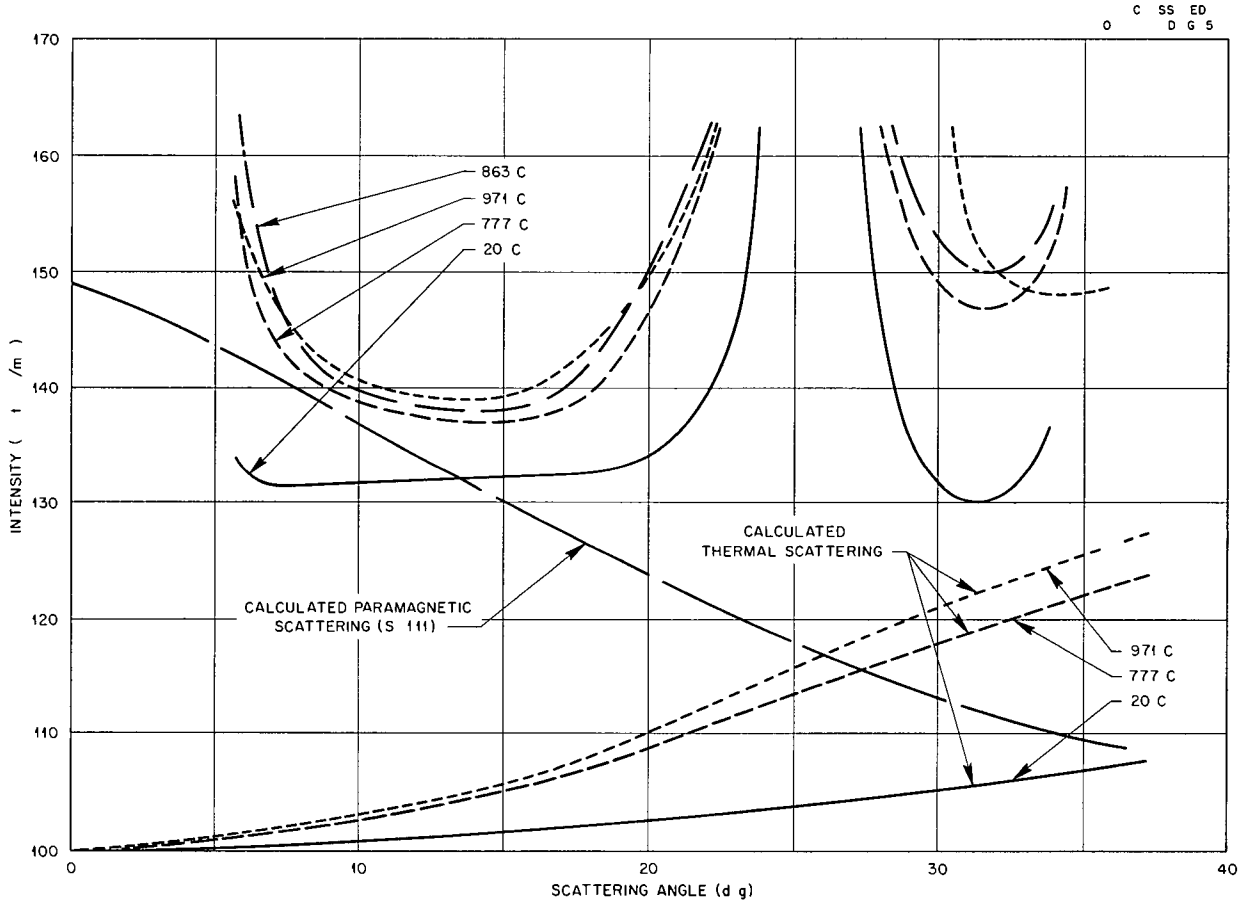

Fig 3 3 Diffuse Scattering from Iron

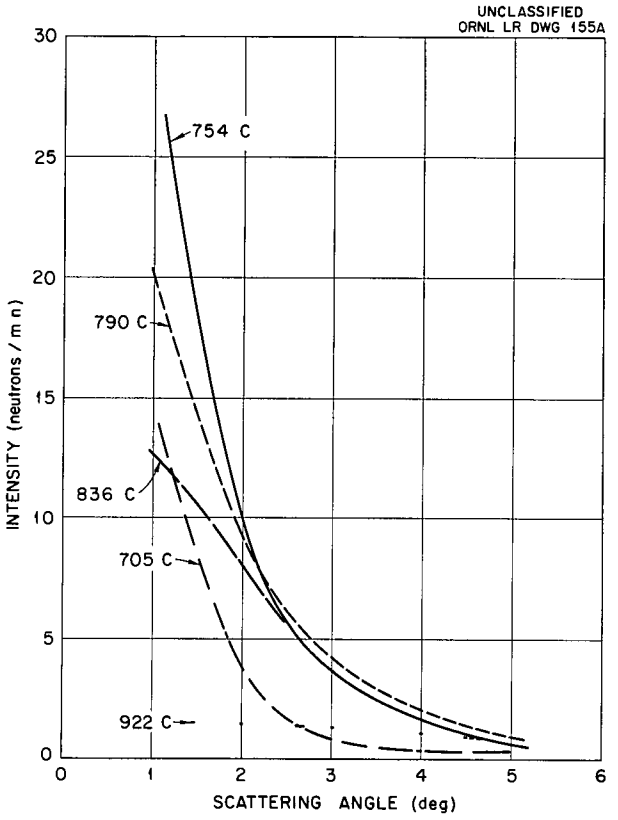

Fig 3 4 Iron Small Angle Scattering

of domain diffraction with the domain structure becoming more disrupted as the Curre temperature is approached Earlier work by Hughes Burgy Heller and Wallace[1] had shown the presence of domain scattering of neutrons into angles less than 1 min of arc for iron at room temperature where the domain size was about 10^{-3} cm With the resolution used in the present study such small angle scattering is unobservable at room temperature but at the higher temperatures the scattering becomes measurable in the 1 to 5 deg region

Figure 3 5 illustrates the logarithmic variation of the small angle scattering intensity plotted in absolute units of magnetic scattering cross section as a function of the square of the scattering angle The theory of small angle scattering by scattering discontinuities (in this case the regions of magnetic coherence or domains) yields a linear relationship between the logarithm of the intensity and the scattering angle squared if the discontinuities are all of the same size Pronounced curvature is to be noted in the data plot of Fig 3 5 and this would merely imply a distribution of domain sizes at a given temperature The slope of the outer part of the 750°C curve corresponds to a domain size of about 12 Å so that only a few unit cells would be magnetically coherent at this temperature near the Curie temperature

[1] D J Hughes M T Burgy R B Heller and J W Wallace *Phys Rev* 75 565 (1949)

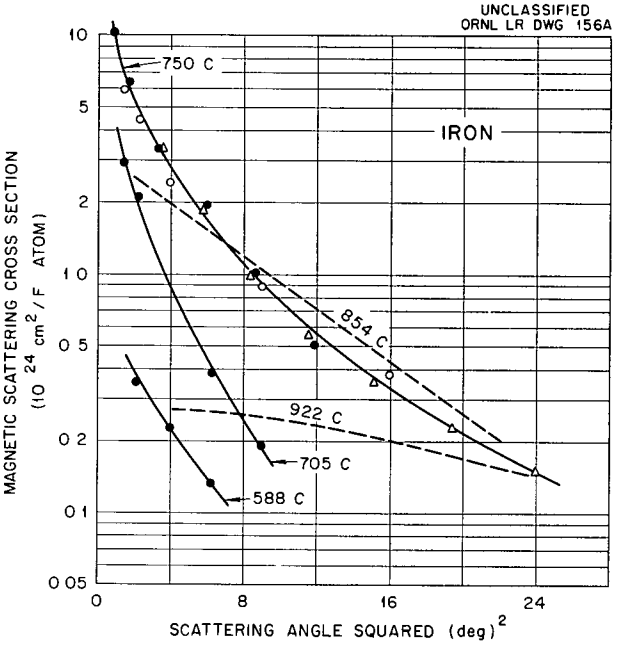

Fig 3 5 Iron

These data suggest then that the regions over which magnetic coherence occurs (the domains) get smaller and smaller as the Curie temperature is approached until finally they represent only a few magnetic unit cells coupled together There appears a gradual reorganization of the scattering pattern at the Curie temperature from such a domain scattering into short range order scattering with the short range order characteristics becoming less noticeable as T increases above T_c At the highest temperature studied 970°C there is still evidence of residual short range order

NEUTRON–MAGNETIC DIFFRACTION STUDY OF THE PEROVSKITE TYPE COMPOUNDS $(La\ Ca)MnO_3$

E O Wollan W C Koehler

A neutron diffraction study is being made of the magnetic properties of a series of compounds of the form $[xLa\ (1-x)Ca]MnO_3$ where x varies from

zero to unity For all values of the parameter x these mixed oxides crystallize in one or another modification of the perovskite structure The ideal unit cube of a perovskite contains one molecule ABO_3 where A is a large ion for example La^{3+} Nd^{3+} Ca^{2+} Sr^{2+} Ba^{2+} etc located at the cube center B is a small ion Mn^{3+} Co^{3+} Te^{4+} Mn^{4+} etc situated at cube corners and where the three oxygen ions are at the mid points of the cube edges Many examples of the perovskite structure are known only a few of which are perfectly cubic For the series above the structures are probably cubic only for a very narrow range of the parameter x

Jonker and Van Santen[2] have investigated the magnetic properties of a number of perovskite type compounds and have found that certain mixed oxides containing manganese or cobalt become ferromagnetic with Curie points ranging downward from about room temperature In particular their measurements of Curie temperature and saturation moments for the (La Ca)MnO_3 series are reproduced here as Fig 3 6 The $CaMnO_3$ content against which these quantities are plotted is a measure of the Mn^{4+} concentrations in the samples to which the magnetic properties are markedly sensi tive The saturation moments represented here are the average ferromagnetic moments of the macroscopic specimens The Curie points refer to the temperature of transition to the ferromagnetic state With the neutron diffraction technique the magnitude and alignment of individual atomic moments at temperatures below the Curie or Neel point can be observed To study the moment distri butions in these perovskites a number of samples of various compositions in the (La Ca)MnO_3 series have been examined The samples were prepared by a technique similar to that described by Jonker and Van Santen

Since complete analytical data on these prepa rations are not yet available the Mn^{3+} Mn^{4+} con tent of the samples cannot be reported This and the fact that the neutron measurements have shown results which are so startlingly dependent upon the composition and upon the temperature and atmos phere of firing of the samples require us to empha size that this is strictly a progress report

The technique has been to obtain diffraction patterns with good statistics from about 5 to 40 deg in scattering angle at room temperature (re ferred to as 300°K) and at one or more temperatures below the respective Curie or Neel points

An example of a low temperature pattern is shown in Fig 3 7 The data from the several runs at each temperature are averaged point by point and

[2] G H Jonker and J H Van Santen *Physica* **16** 337 (1950) G H Jonker and J H Va Santen *Physica* **19** 120 (1953)

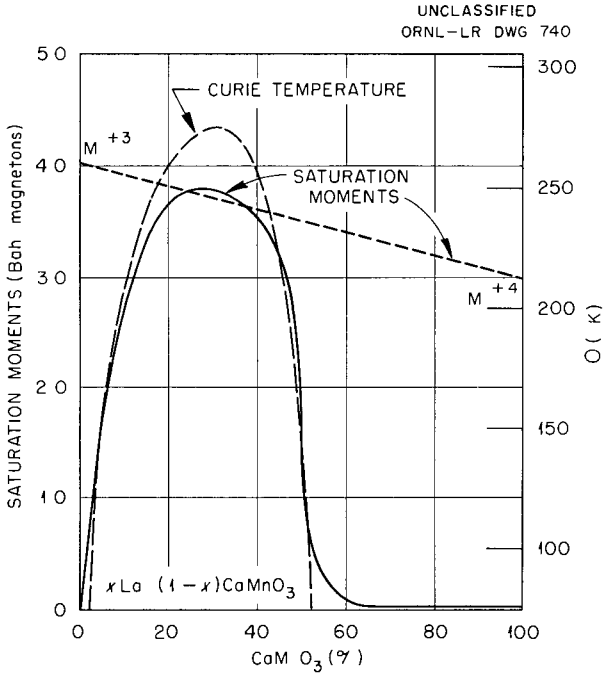

Fig 3 6 Curie Temperatures and Average Satu ration Moments per Manganese Ion (Jonker and Van Santen)

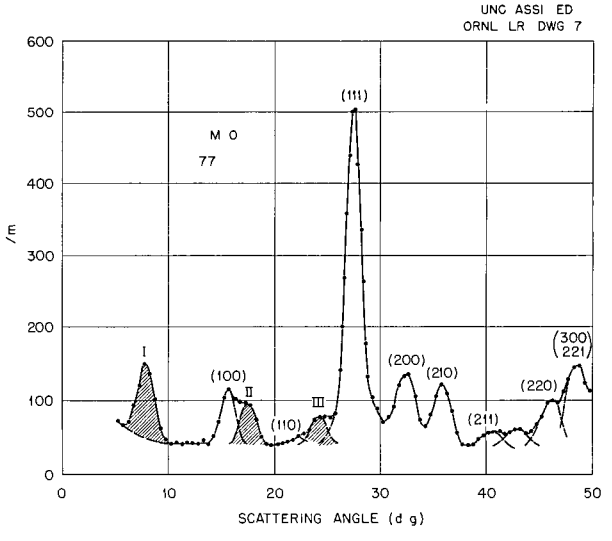

Fig 3 7 Diffraction Pattern of $LaMnO_3$ at 77°K

the room temperature data are then subtracted from the low temperature data and in plotting the points are averaged over an angular range up to 1 deg when this averaging does not lose detail to the pattern Since the magnetic diffuse scattering is larger at room temperature than below the Curie or Neel temperatures the diffuse scattering excess will appear as a negative contribution in the plot of $I_{T^\circ K} - I_{300^\circ K}$ vs scattering angle The results for several samples are shown in Figs 3 8 to 3 13

Figure 3 8 is for pure $LaMnO_3$ fired in 1% oxygen–99% nitrogen and the manganese in this sample should be almost entirely Mn^{3+} The temperatures at which the diffraction patterns were taken for this sample and for succeeding samples are shown on the figures For this case a saturation curve fitted by a Brillouin function is shown in Fig 3 14 The critical temperature can be seen to be near 140°K The three lines in this difference pattern can be accounted for by doubling the elementary cell along one of the cube edges The system is thus antiferromagnetic and from the intensities and line positions one finds the spins to be aligned as shown in Fig 3 15*a*

Figure 3 9 shows the case of $LaMnO_3$ fired in an oxygen atmosphere and at such a temperature as to give about 20% Mn^{4+} ions The unshaded peaks fall at the same positions as the nuclear peaks and hence represent ferromagnetic scattering The peaks at the larger scattering angles have some contribution arising from the smaller thermal motion effect at low temperatures and the intensities are such as to require also some nuclear contribution arising presumably from minor shifts in oxygen positions as one passes below the Curie point

The three peaks which have been shaded are evidently to be associated with the antiferromagnetic phase of Fig 3 8 Exactly how these dif

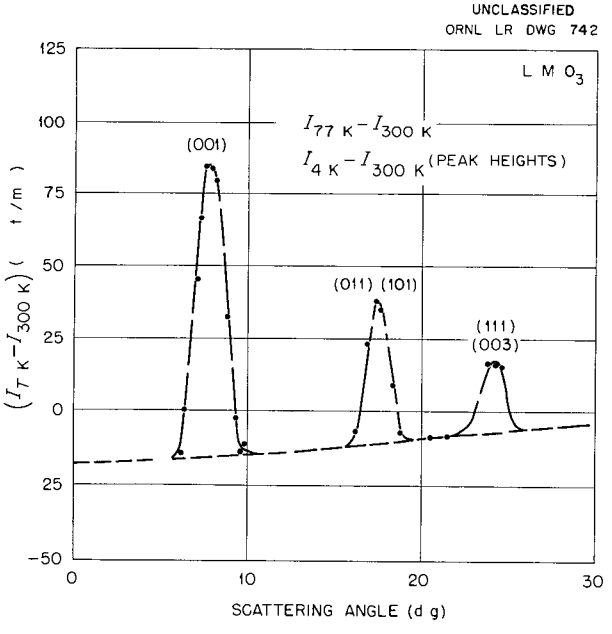

Fig 3 8 Difference Pattern Showing Antiferromagnetic Peaks of Fig 3 7 Indexed for a Cell Doubled Along C Axis

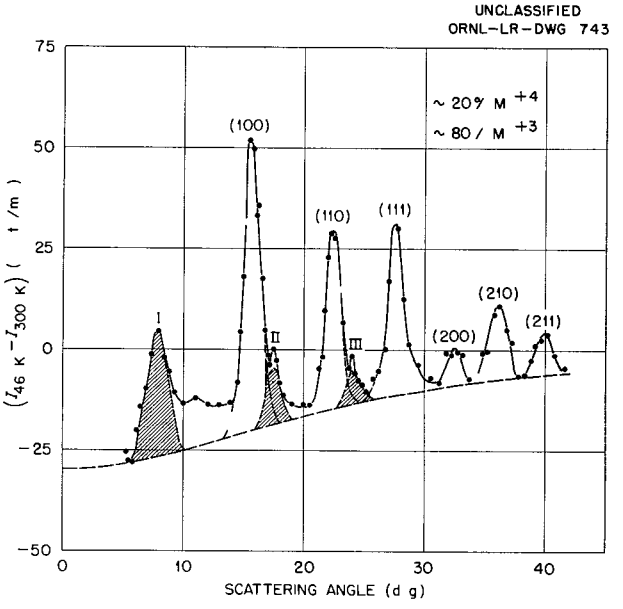

Fig 3 9 Difference Pattern for a Sample of $LaMnO_3$ Fired to Give About 20% Mn^{4+}

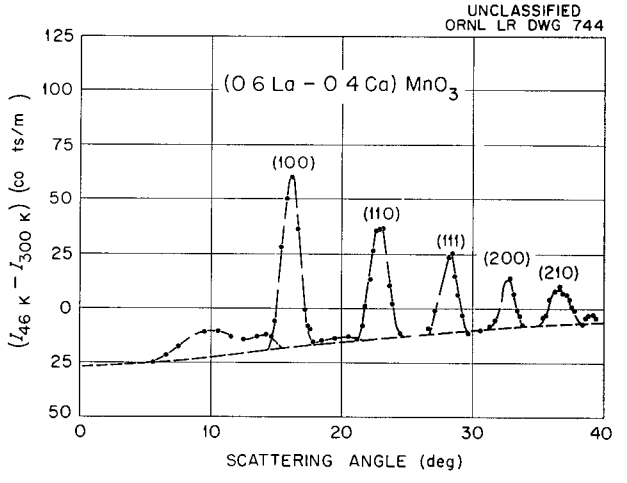

Fig 3 10 Difference Pattern for (0 6La 0 4Ca)MnO_3

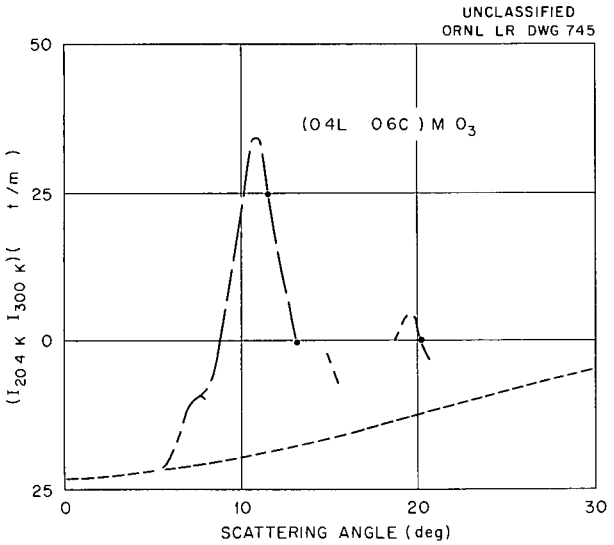

Fig 3 11 Difference Pattern for (0 4La 0 6Ca)MnO_3

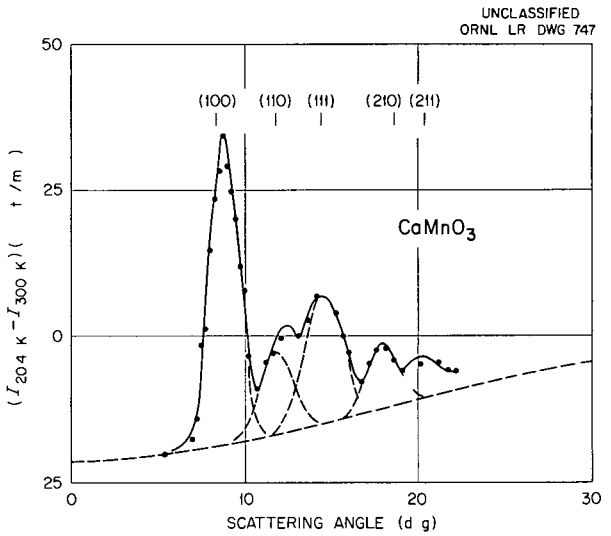

Fig 3 13 Difference Pattern for $CaMnO_3$ Indexed for a Cell Doubled Along All Cube Edges

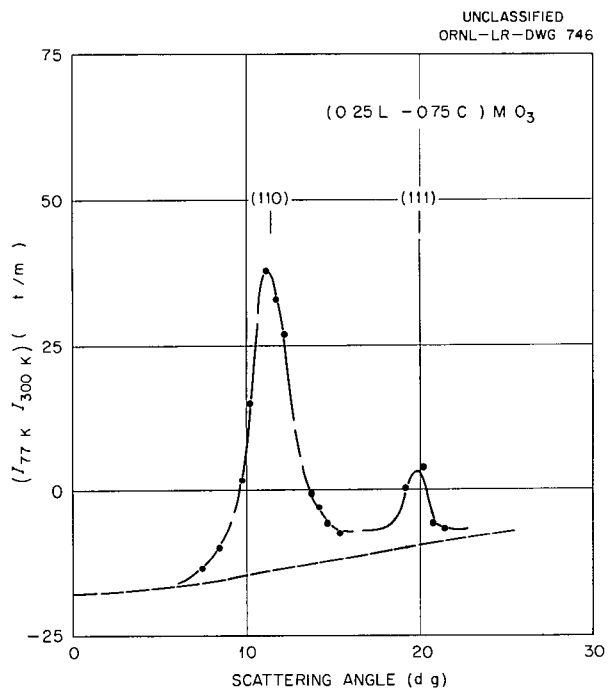

Fig 3 12 Difference Pattern for (0 25La 0 75Ca)MnO_3 Indexed for a Cell Doubled Along Two of the Cube Edges

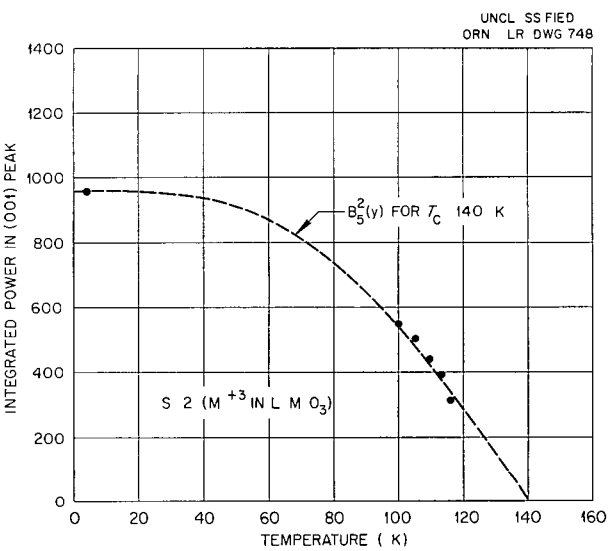

Fig 3 14 Neel Temperature for $LaMnO_3$ as Determined from (001) Peak

ferent magnetic phases are distributed in the sample or why a finely divided homogeneous mixture fired for 2 hr or more at high temperatures should be magnetically inhomogeneous is difficult to say A simple magnetic test at liquid nitrogen temperature showed the sample to be ferromagnetic to a scale comparable to the particle size (~ 100 mesh) It has been suggested by Jonker and Van Santen that the ferromagnetic coupling in these compounds should be between Mn^{4+} and Mn^{3+} ions (the coupling must of course be of the superex change type via the intervening oxygen ions) A small percentage of Mn^{4+} might then be insufficient

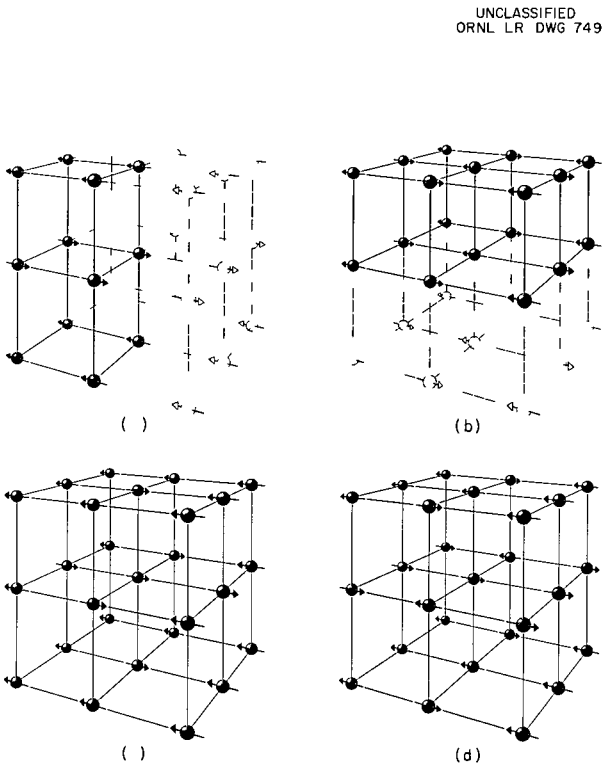

Fig 3 15 Cells Proposed for the Various Antiferromagnetic Patterns in This Series of Compounds

to produce ferromagnetism in the whole sample but electron shifts could take place between ions and the lowest energy could correspond to part of the sample on a small scale being ferromagnetic and part being antiferromagnetic The Curie and Neel points for the two phases in this sample both fall at about 140°K which was the value found for the single magnetic phase in Fig 3 8

The patterns for all the samples shown will not be discussed in detail and data obtained for other samples will not be described in this report However the coexistence of more than one magnetic phase seems to be characteristic of most of the samples Figure 3 10 shows primarily ferromagnetic scattering with a small unresolved antiferromagnetic contribution that suggests a build up of the phases appearing in later patterns

In Fig 3 12 there are primarily two lines which can best be accounted for on the basis of an antiferromagnetic cell doubled along two of the cube edges as shown in Fig 3 15*b* There may be some of this phase in the sample of Fig 3 11 also

A pattern for a pure $CaMnO_3$ sample is shown in Fig 3 13 This sample may have considerably less than 100% Mn^{4+} Another pure sample (not shown) although having the same lines shows a different intensity distribution The pattern for these samples requires a cell doubled along all three of the cube edges and the line intensities cannot be accounted for on the bases of a single cell consisting of two simple interpenetrating lattices with opposite spin orientation The cells shown in parts c and *d* of Fig 3 15 are capable of accounting for the lines shown and on the assumption that these two cells are not in this case energetically very different mixtures of these can account for variations in the line intensities from one sample to another In fact mixtures are required to account for the lines in Fig 3 13

The antiferromagnetic cells shown in Fig 3 15 all have closest neighbor relations involving both ferro and antiferromagnetic coupling in different amounts There is also a region of stability involving purely ferromagnetic coupling and it is conceivable that a cell of two interpenetrating lattices having opposite spins and involving only antiferromagnetic coupling between neighbors may also exist

Preliminary study has also been made of the crystallographic features of the problem Although the structures in all cases are close to cubic with the oxygens in the mid points of the edges (or of the faces if the manganese atom is taken at the center of the cube) the perovskite structure itself ($CaTiO_3$) has small displacements of the oxygens from these special positions and this is also true for this system In some cases the room temperature x ray patterns show a small line splitting and also in some cases there are weak lines which require doubling of the unit cell dimensions In the case of the mainly ferromagnetic patterns of Figs 3 9 and 3 10 there seems to be no measurable line shift as one goes below the Curie point as evidenced by the clean nature of the difference lines In other cases the difference pattern over the nuclear peaks shows an easily observable shift at the low temperatures

The nature of the superexchange responsible for the complex magnetic character of these compounds will certainly not be easily ascertained It was suggested by Jonker and Van Santen that the exchange Mn^{4+}–O–Mn^{3+} is ferromagnetic and the exchange between like ions is of antiferromagnetic

character Zener has postulated a resonance type of superexchange in which an electron moves from the Mn^{4+} ion to the oxygen and simultaneously from the oxygen to the Mn^{3+} ion in a rapid back and forth alternation of this process Undoubtedly the irregular displacements of the oxygen ions from their special positions also bear some relation to the type of magnetic coupling Detailed consideration of the type of magnetic coupling must however wait for more complete experimental data

SEARCH FOR ANTIFERROMAGNETISM IN THE SILICIDES V_3Si Cr_3Si AND Mo_3Si

W C Koehler E O Wollan

Neutron diffraction data at room temperature and at 20 4°K have been obtained for the isostructural silicides V_3Si Cr_3Si and Mo_3Si for which the structure is shown in Fig 3 16 In no case has an antiferromagnetic structure been detected nor is there any indication of paramagnetic scattering The situation with regard to the coherent scattering is illustrated for V_3Si in Fig 3 17 and the absence of paramagnetic scattering is seen in Fig 3 18 An upper limit of 0 2 μ_B is found for the moments of the V Cr and Mo ions in these crystal lattices As a side aspect the silicon coherent neutron scattering cross section has been redetermined as 2 16 ± 0 06 barns

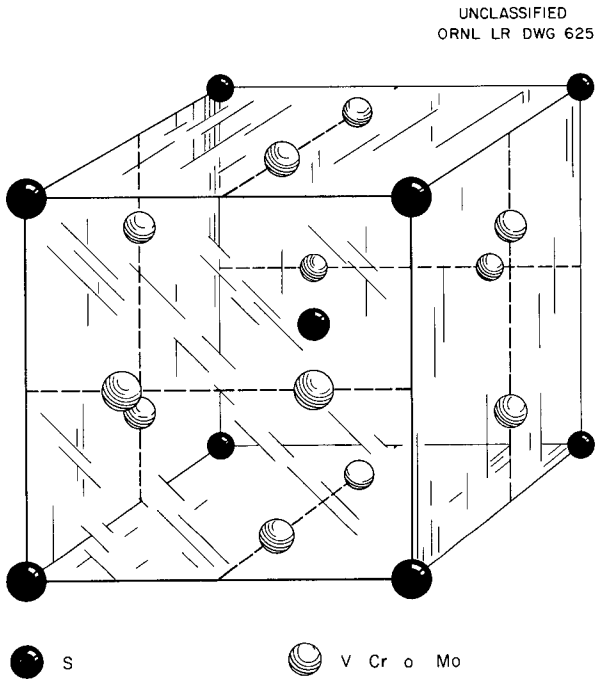

Fig 3 16 Structure of V_3Si Cr_3Si and Mo_3Si In the model proposed by Zener the spins of the transition group atoms are assumed to alternate along the linear chains in the crystal so that this would represent $\frac{1}{8}$ of the magnetic unit cell

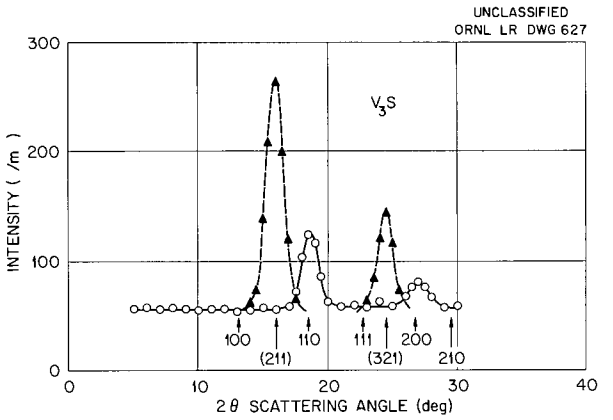

Fig 3 17 Room Temperature Diffraction Pattern of V_3Si The dashed curves are antiferromagnetic intensities to be expected on Zener s model

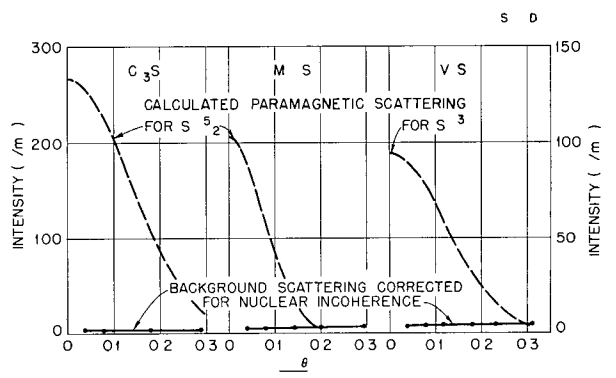

Fig 3 18 Comparison of Observed and Expected Diffuse Scattering The observed scattering has been corrected for nuclear incoherent effects

4 LOW TEMPERATURE PHYSICS

AN APPROXIMATE PARTITION FUNCTION FOR CERTAIN IRON GROUP SALTS AT LOW TEMPERATURES

L D Roberts J W T Dabbs

For certain paramagnetic salts of the iron group the predominant interaction in the spin Hamiltonian of the magnetic ion is that due to the crystalline electric field This term will produce an anisotropy in the magnetic thermodynamic properties of the salt as for example in the adiabatic dependence of temperature on magnetic field and entropy Assuming the Hamiltonian $H = g_1\beta H_1 S_1 + g_2\beta H_2 S_2 + g_3\beta H_3 S_3 + DS_3^2$ where the g_i H_i and S_i are components of the spectroscopic splitting factor magnetic field and electron spin operator where β is the Bohr magneton and D is the electric field splitting coefficient this anisotropy may be estimated Assuming the D term large compared to the terms in H and using the interaction representation of Schwinger the partition function Z can be obtained

$$Z = \sum_{m=-S}^{S} e^{-m^2/\theta}\left(1 + \frac{1}{2}\frac{m^2 h_3^2}{\theta^2}\right) + \frac{1}{2}\left(h_1^2 + h_2^2\right)\left\{\left[S(S+1) + \frac{1}{4}\right]\frac{e^{-1/4\theta}}{2\theta^2} \sum_{\substack{m=-S \\ m\neq -1/2}}^{S}\left[S(S+1) - m(m+1)\right]\left[\frac{e^{-m^2/\theta}}{\theta(2m+1)} + \frac{e^{-(m+1)^2/\theta} - e^{-m^2/\theta}}{(2m+1)^2}\right]\right\}$$

where m is the magnetic quantum number $h_i = g_i\beta H_i/D$ and $\theta = kT/D$ Figure 4 1 gives a calculation of the entropy as a function of temperature at $h = 0\ 3$ at three angles to the polar axis and with $S = 5/2$

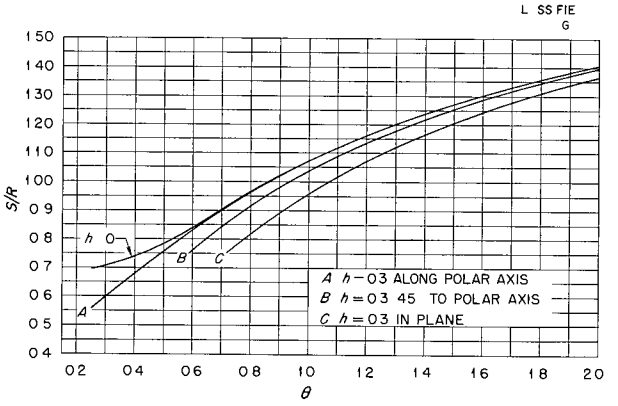

Fig 4 1 Specific Heat of $MnCl_2$ (0 2 mole) as a Function of Temperature

METHOD FOR BRUTE FORCE POLARIZATION OF HYDROGEN NUCLEI

J W T Dabbs L D Roberts

Certain anisotropic paramagnetic salts containing hydrogen allow adiabatic demagnetization by rotation of a magnetic field H from the direction of large spectroscopic splitting factor g_l to the direction of small splitting factor g_s at constant H Starting at an initial temperature T_i the proton polarization obtained by brute force is given by $f_p = 1\ 0 \times 10^{-7}\, Hg_l/T_i g_s$ for small polarizations in an ideal case Values of H/T_i up to about 2×10^5 are available using techniques of indirect cooling[1] together with the superconducting heat switch [2] for thermal isolation after cooling to T_i and before rotation

The salt $Ce_2Mg_3(NO_3)_{12}\ 24H_2O$ has a magnetic anisotropy[3] given by $g_l/g_s \approx 7$ and for this case values of f_p in the range 0 055 to 0 07 are available taking into account both the electron and proton spin system (Schottky) specific heats which arise from the Zeeman splittings ΔE (electronic) = $2g_s\beta SH$ and ΔE (protons) = $2\mu_p H$ these are the only important specific heats in the region of interest Calculations on this basis indicate that proton polarizations of about 6 to 7% probably could be maintained for reasonable times It is assumed that the ortho para energy difference is small compared to kT

[1] L D Roberts S Bernstein J W T Dabbs and C P Stanford *Phys Rev* (n p ess)

[2] J Da by J Hatto B V Roll n E F W Seymo and H B Silsbee *Proc Phys Soc (London)* **A64** 861 (1951)

[3] A H Cooke H J Duff s and W P Wolf *Phil Mag* 44 623 (1953)

It is interesting to note that if a similar material with $g_s \approx 0$ were available a proton polarization of about 0 20 would be attainable Theoretical calculations[4] of the magnetic properties of ytterbium and dysprosium in the ethyl sulfates suggest that here $g_s = 0$ Since no thermodynamic measurements have been made on these salts below 1°K it is not yet possible to design a polarization experiment around these salts

LOW TEMPERATURE SPECIFIC HEAT ANOMALY OF $MnCl_2$

R B Murray

The specific heat of a polycrystalline sample of anhydrous $MnCl_2$ has been measured from 1 3 to 4 2°K by the techniques of adiabatic calorimetry The sample was prepared by the dehydration of pure $MnCl_2 \cdot 4H_2O$ in a dry HCl atmosphere The anhydrous $MnCl_2$ was then fused ground to a coarse powder and sealed with a small amount of helium exchange gas in the calorimeter cup Specific heat measurements were carried out by observing the rise in temperature of the sample associated with the input of a measured amount of heat from an electrical heater coil Sample temperatures were measured with a carbon resistance thermometer whose resistance was carefully calibrated against the temperature of the liquid helium bath at the beginning of each experiment The thermometer resistance as a function of temperature (in the liquid helium temperature range) may be accurately described by a function of the form

$$\ln R = A + B \ln T + \frac{C}{T} + DT$$

where the parameters A B C and D are evaluated by a least squares fit of the calibration data Such a treatment permits an accurate measurement of temperature increments of the order of 0 05°K

Six specific heat experiments have been carried out in the liquid helium range on an approximately 0 2 mole sample The results are shown in Fig 4 2 The measurements show an anomalously large specific heat throughout this region the maxima are located at 1 8 and 2 0°K The specific heat is falling very slowly at 1 4°K and suggests the possibility of further anomalies at even lower temperatures

The observed anomalies are tentatively associated with a transition from the paramagnetic state to the antiferromagnetic state Such transitions however are usually accompanied by a single specific heat maximum The observation of two maxima suggests the existence of two separate phases in the crystal lattice A two phase structure might arise from the mechanical grinding of the fused $MnCl_2$ before filling the calorimeter cup X ray diffraction patterns of ground $MnCl_2$ are being studied in this laboratory to examine this possibility

[4] B Bleaney and K W H Stevens *Repts Progr in Phys* XVI 108 (1953)

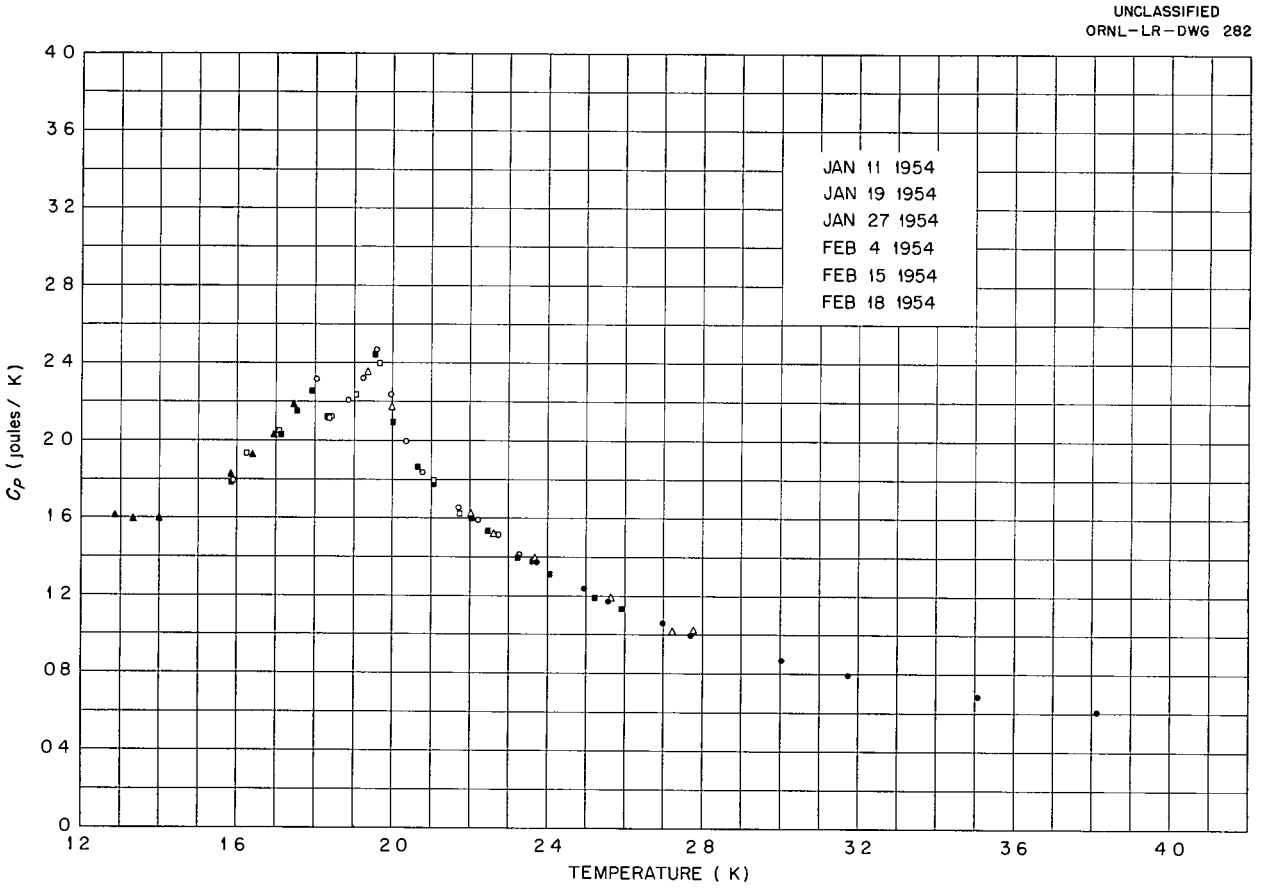

Fig 4 2 Specific Heat of $MnCl_2$ Sample 0 2 mole $MnCl_2$

5 HEAVY ION PHYSICS

INVESTIGATION OF ELECTRON CAPTURE AND LOSS FOR HEAVY IONS PASSING THROUGH GASES

P M Stier C F Barnett
G E Evans[1]

During the past six months the energy dependence of the equilibrium charge distribution has been determined for the ions H^+ He^+ N^+ Ne^+ and A^+ with energies of from 20 to 250 kev passing through each of the following gases hydrogen helium nitrogen oxygen neon and argon A description of the equipment and preliminary results were given in the preceding semiannual report [2]

The results of the determinations of the fraction of the particle beam which was neutral at charge equilibrium are displayed in Figs 5 1 to 5 6 The ratios of the charge +2 to charge +1 components are given in Figs 5 7 to 5 10

The number of negative ions formed in the charge exchange chamber was below the detectable limit (about 0 1% of the total beam at 30 kev 0 01% at 100 kev) for the incident ions He^+ N^+ Ne^+ and A^+ The energy dependence of the H^- component formed by the passage of protons through nitrogen is shown in Fig 5 11

Interpretation of the results of experiments which measure the equilibrium charge distribution is difficult because only the ratio of the electron capture to electron loss cross sections is determined These cross sections are for different types of interactions the energy dependence of

[1] On leave to Union Carbide and Carbon Corporation Cleveland Ohio

[2] P M Stier C F Barnett G E Evans and V L DiRito *Phys Semiann Prog Rep Sept 10 1953* ORNL 1620 p 37

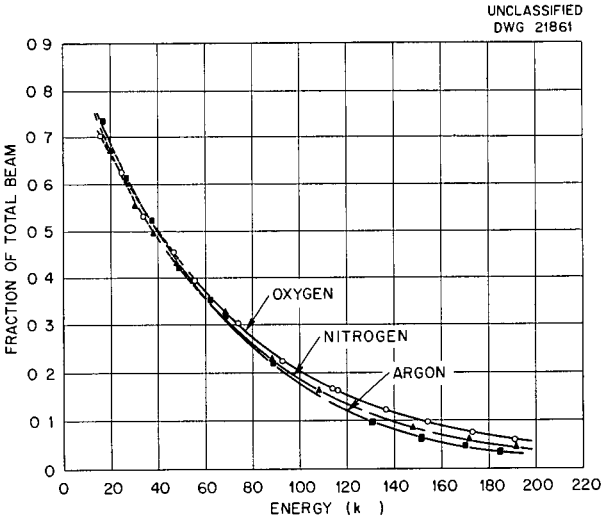

Fig 5 1 Equilibrium Fraction of H^0 in Various Gases

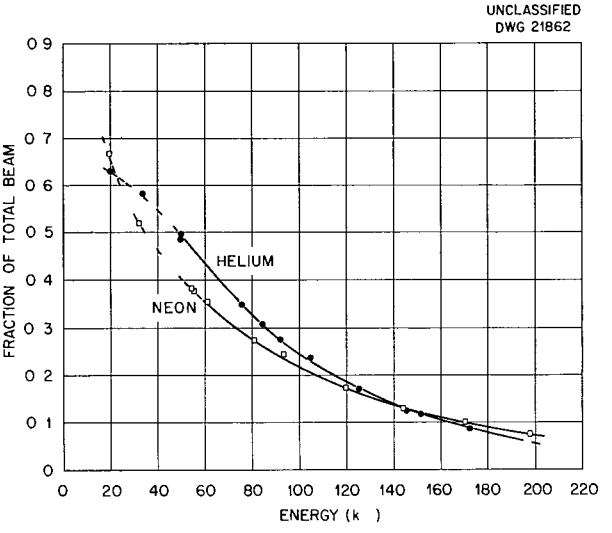

Fig 5 2 Equilibrium Fraction of H^0 in Various Gases

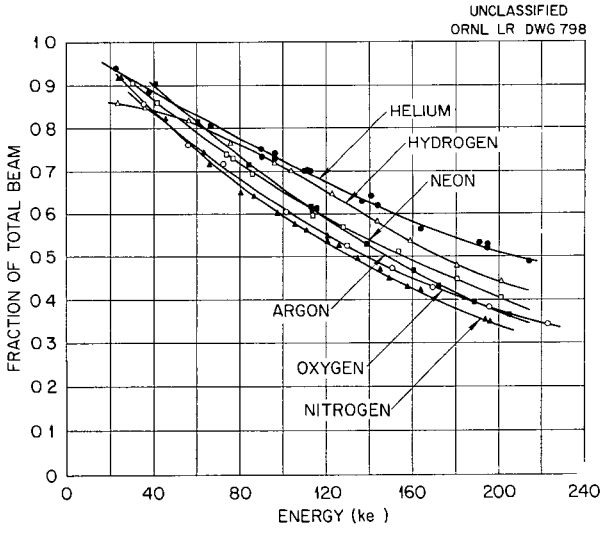

Fig 5 3 Equilibrium Fraction of He^0 in Various Gases

which is expected to differ The electron loss is ionization of a fast atom by the target atom and therefore the loss cross section is expected to increase to a maximum and then decrease slowly at higher energies The capture cross section which is the cross section for the transfer of an electron from the target atom to the projectile ion will in this low energy region be largely determined by the relative ionization potential of the target and projectile atoms This low energy behavior is not to be confused with the behavior expected at high energy

If it s assumed that the probability is small that two electrons are transferred in a single collision the ratio of the number of particles in charge states + 1 and 0 (or in + 2 and + 1) is the same as the ratio of the complementary cross sections for transitions between these states The ratios [3] σ_{01}/σ_{10} calculated from the values taken from the smooth curves

[3] C oss sect o not t on the fi st s bs r pt refe s to the n t al charge state the second to the f nal state

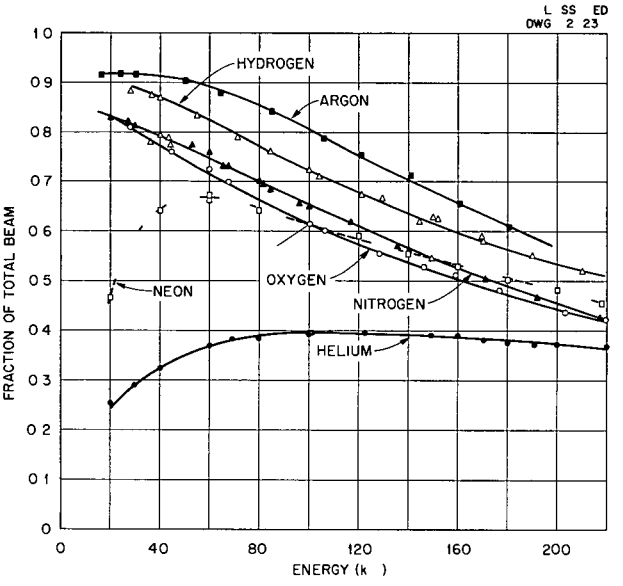

Fig 5 4 Equilibrium Fraction of N^0 in Various Gases

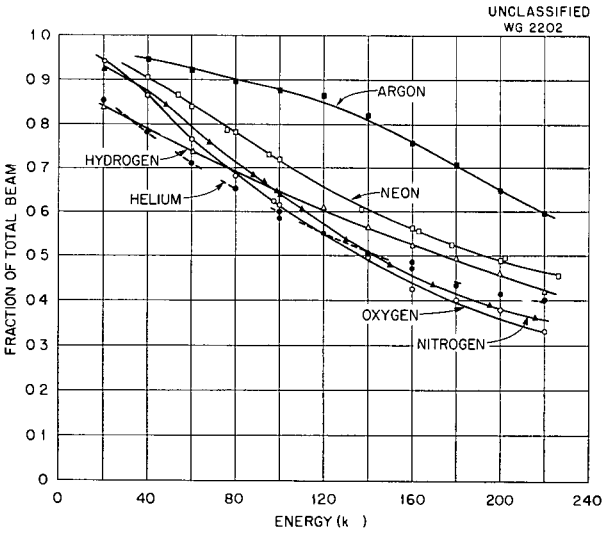

Fig 5 5 Equilibrium Fraction of Ne^0 in Various Gases

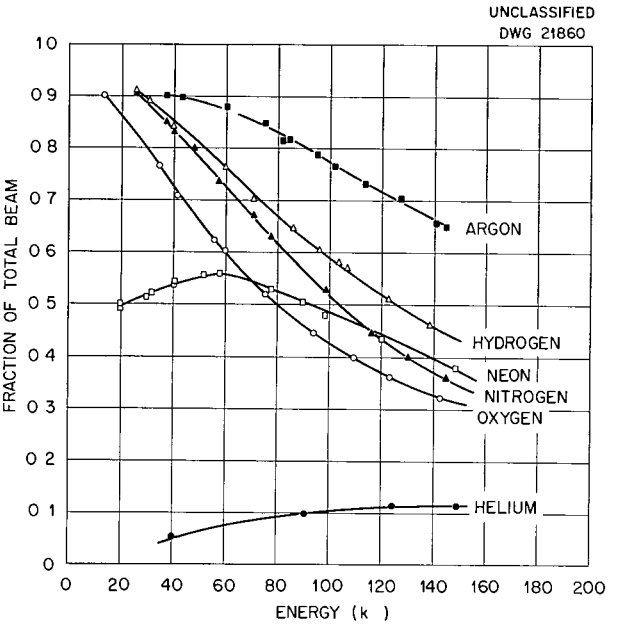

Fig 5 6 Equilibrium Fraction of A^0 in Various Gases

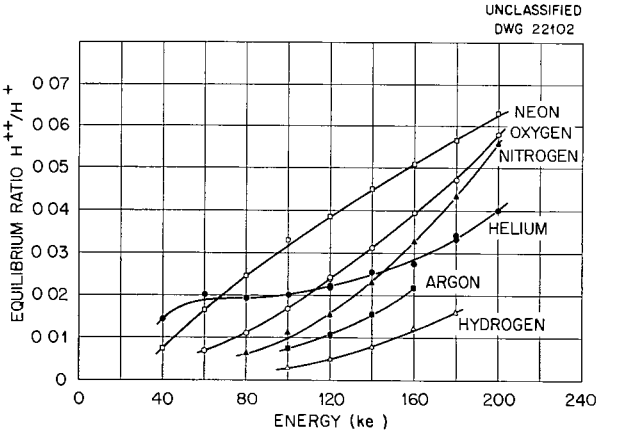

Fig 5 7 Equilibrium Ratio of H^{++} to H^+ in Various Gases

in Figs 5 1 to 5 6 are plotted as a function of the incident ion velocity in Figs 5 12 and 5 13 It is seen that much of the experimental data is well represented in this energy range by a formula of the type $\sigma_{01}/\sigma_{10} = K_1 v^m$ where v is the particle velocity and K_1 and m are empirically determined constants Values of m are listed in Table 5 1 for each ion gas combination for which the data could be represented by a straight line over a reasonable portion of the velocity range The interesting behavior of the relatively easily ionized heavy ions (nitrogen and argon) passing through the gases of high ionization potential (helium and neon) is to be noted As discussed above the velocity dependence of the reactions involved is expected to differ therefore it would seem that detailed discussion of the shapes of these curves should be deferred until the separate cross sections have been measured

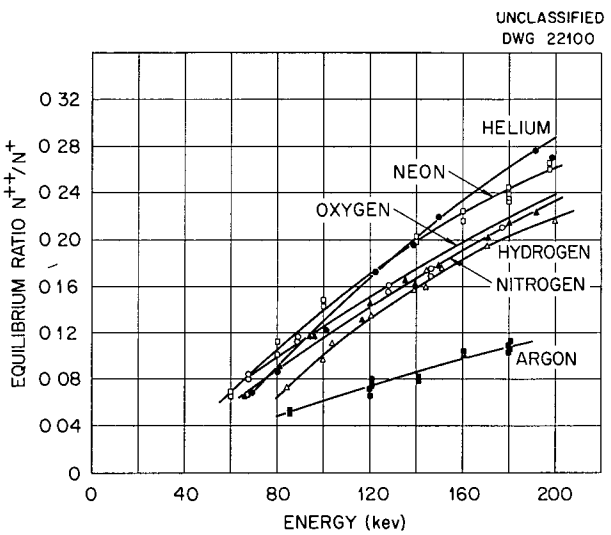

Fig 5 8 Equilibrium Ratio of N^{++} to N^{+} in Various Gases

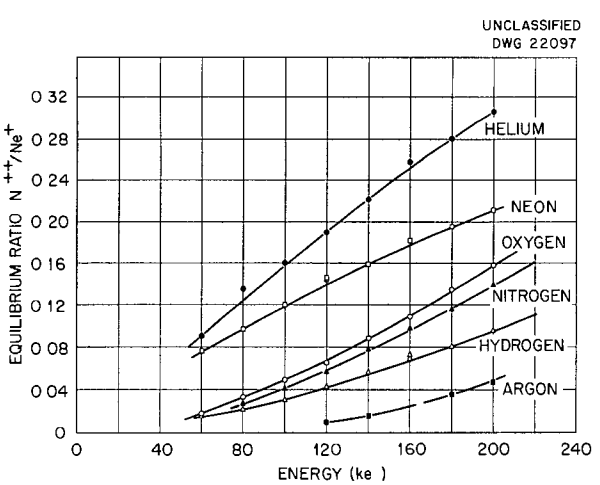

Fig 5 9 Equilibrium Ratio of Ne^{++} to Ne^{+} in Various Gases

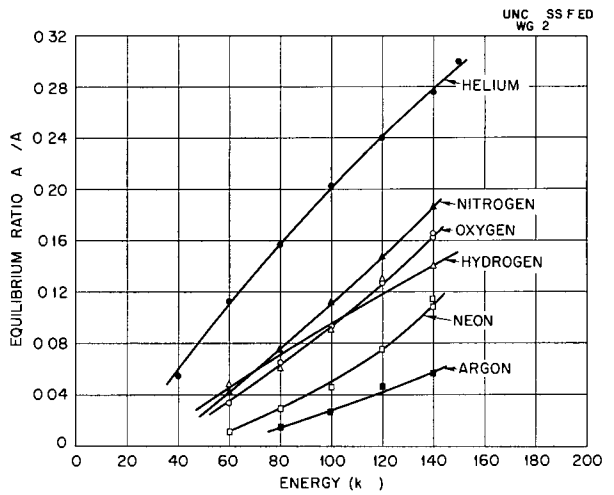

Fig 5 10 Equilibrium Ratio of A^{++} to A^{+} in Various Gases

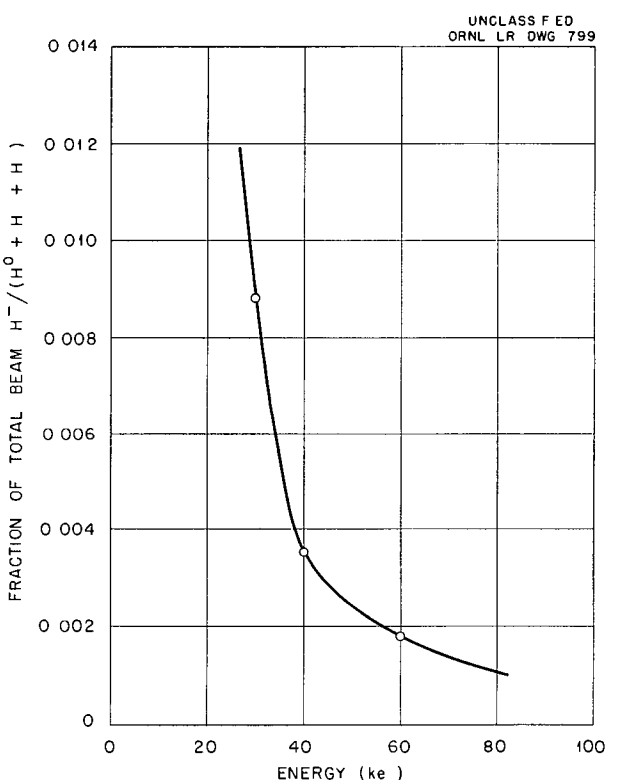

Fig 5 11 Equilibrium Fraction of Beam Which Is H^{-} After Passing Through Nitrogen

TABLE 5 1 VALUES OF THE EXPONENT m IN THE RELATION $\sigma_{01}/\sigma_{10} = K_1 v^m$ FOR THE VARIOUS ION GAS COMBINATIONS

GAS	ION				
	H^+	He^+	N^+	Ne^+	A^+
H_2	6 5	3 3	2 0	2 2	2 8
He	4 7	2 6		1 9	
N_2	5 4	2 9	2 2	2 9	3 3
O_2	4 6	2 6	1 7	2 8	2 5
Ne	3 7	2 8		2 5	
A	5 8	3 5	3 1	4 3	3 7

No straight sect on

It is evident from Figs 5 7 to 5 10 that in many cases the ratios of the cross sections for transitions between charge states 2 and 1 cannot be represented by a simple power law in the velocity over the energy range studied since the curves do not extrapolate to $n^{++}/n^{+} = \sigma_{12}/\sigma_{21} = 0$ at zero energy However the data are well represented by formula of the type $\sigma_{12}/\sigma_{21} = K_2(v - v_c)^m$ as is shown in Figs 5 14 and 5 15 The empirically determined values for the constants m and v_c are given in Table 5 2. The constant v_c corresponds to a threshold velocity below which there is very little probability of forming the doubly charged ion Here again it is difficult to interpret the details of this table because of the unknown and different velocity dependence of the two cross sections involved

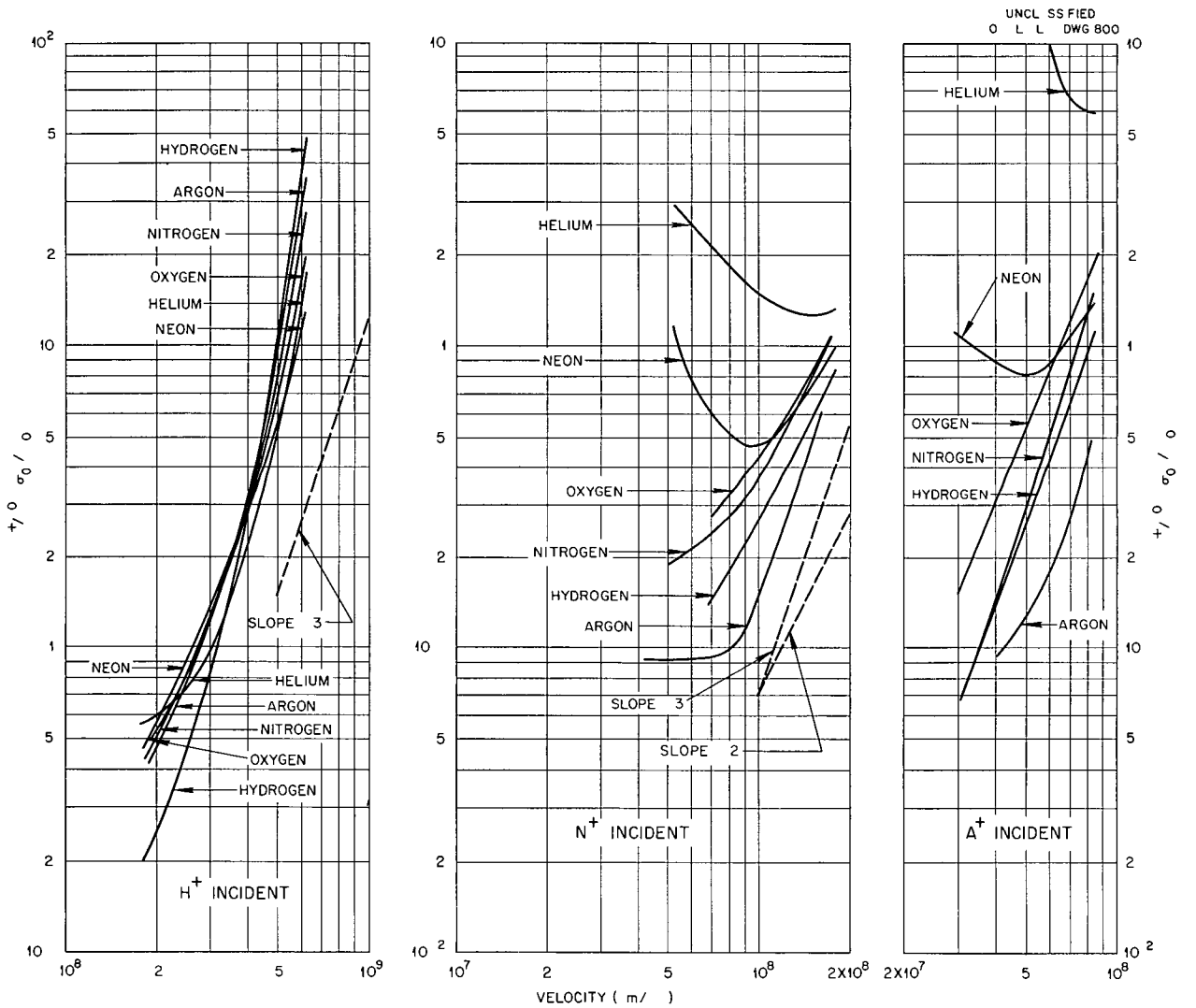

Fig 5 12 Ratio of Loss to Capture Cross Sections for H^+ N^+ and A^+ Ions Passing Through Various Gases

Experiments are now in progress in which the cross section for electron loss by fast atoms in this energy range is being measured From these data and the reported ratios of loss to capture cross sections the electron capture cross section and the rate of loss of energy due to charge exchange can be calculated

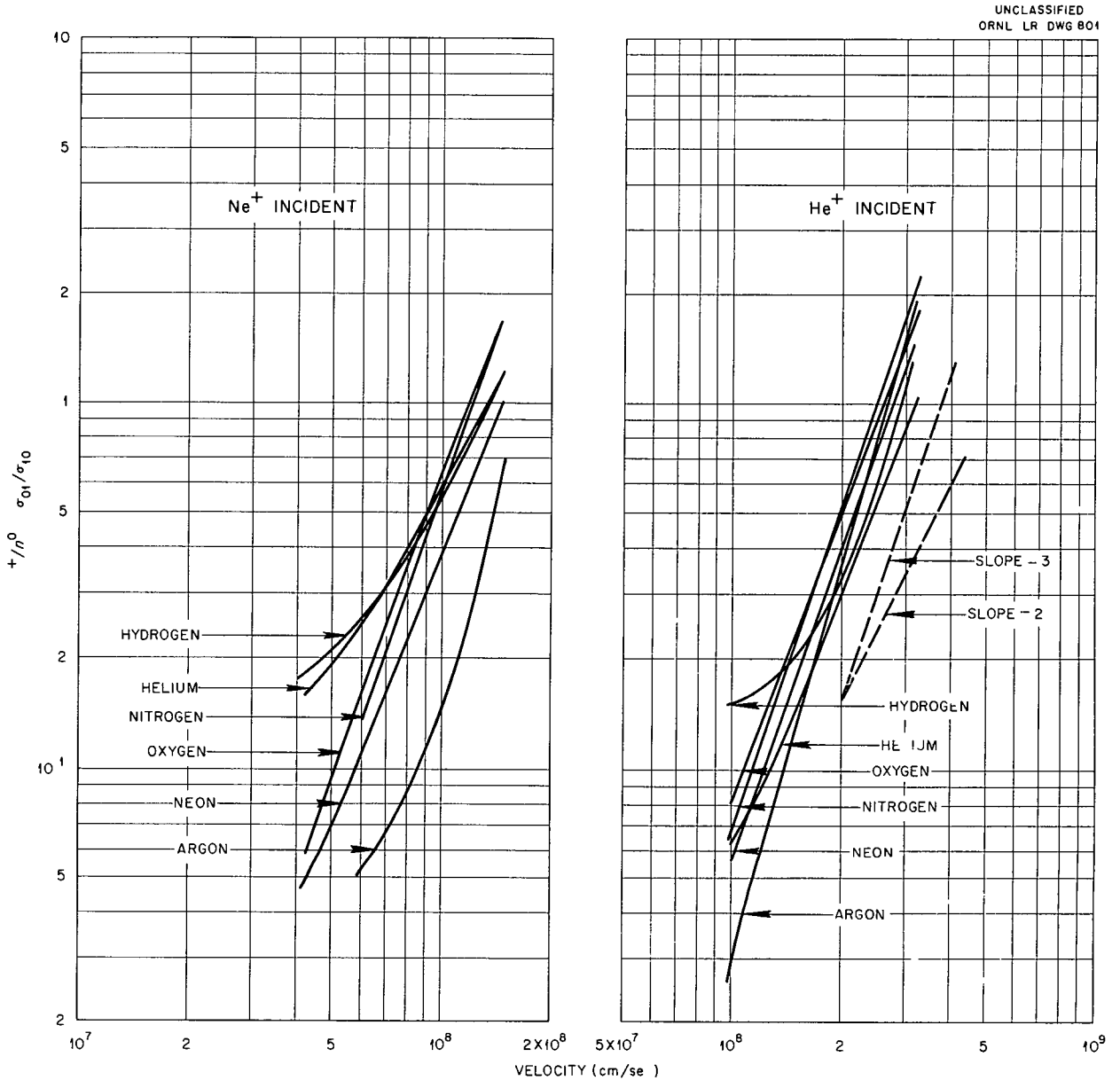

Fig 5 13 Ratio of Loss to Capture Cross Sections for He^+ and Ne^+ Ions Passing Through Various Gases

TABLE 5 2 VALUES OF THE THRESHOLD VELOCITY v_c AND THE EXPONENT m IN THE RELATION $\sigma_{12}/\sigma_{21} = K_2(v - v_c)^m$ FOR THE VARIOUS ION GAS COMBINATIONS

GAS	VALUES OF m FOR				VALUES OF v_c (cm/sec × 10^{-8}) FOR			
	He^+	N^+	Ne^+	A^+	He^+	N^+	Ne^+	A^+
H_2	5 7	0 6	3 0	1 3	0 2	1 0	0	0 3
He		1 1	1 3	1 3		0 7	0 4	0 3
N_2	4 7	1 0	2 8	1 7	0 1	0 7	0 2	0 3
O_2	3 4	1 0	2 7	2 3	0	0 6	0 3	0 2
Ne	1 1	0 8	1 4	2 9	1 1	0 8	0 2	0 3
A	4 7	1 1	3 8	1 3	0	0 6	0 5	0 5

No st a ght sect o

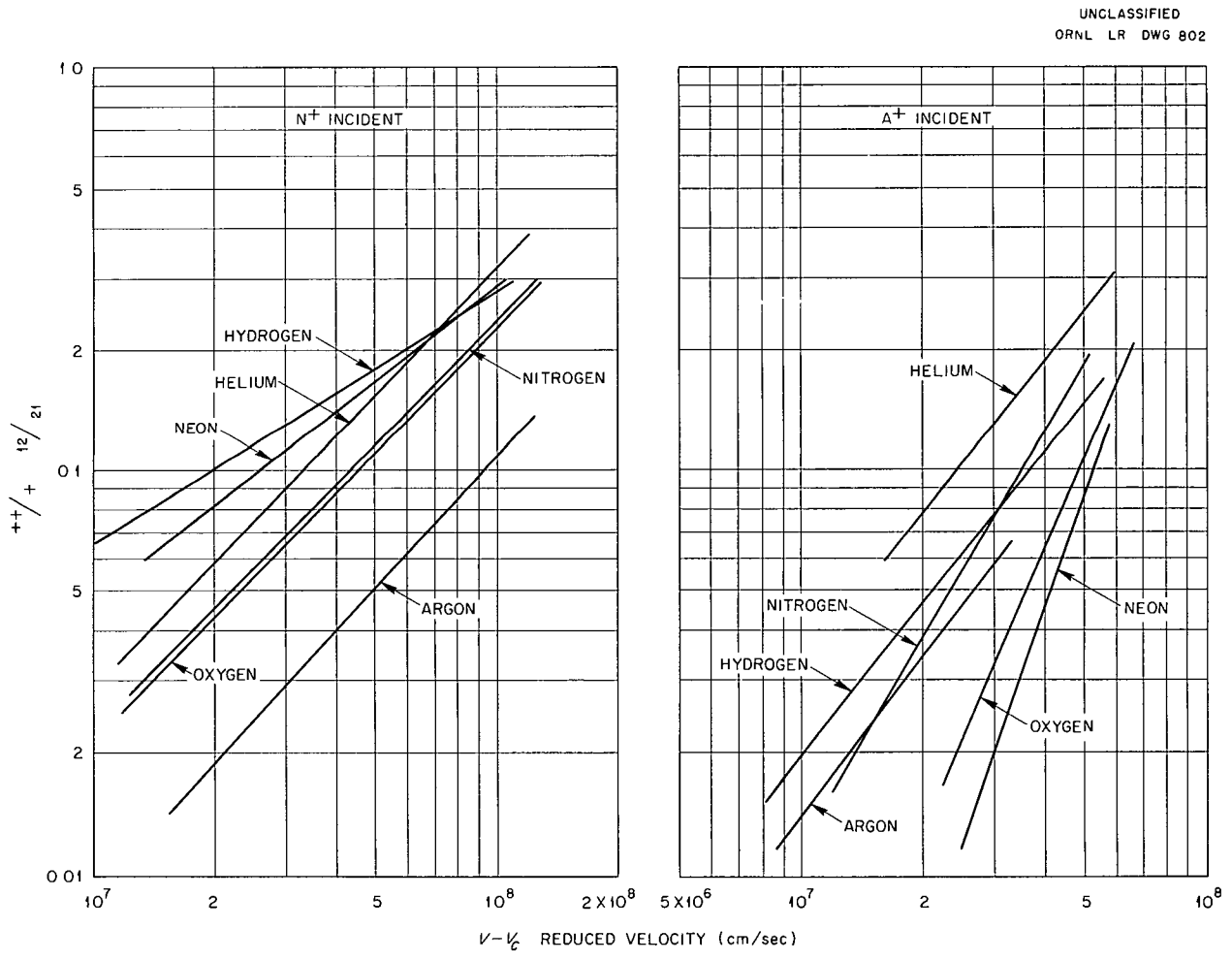

Fig 5 14 Ratio of Second Loss to Capture Cross Sections for N^+ and A^+ Ions Passing Through Various Gases

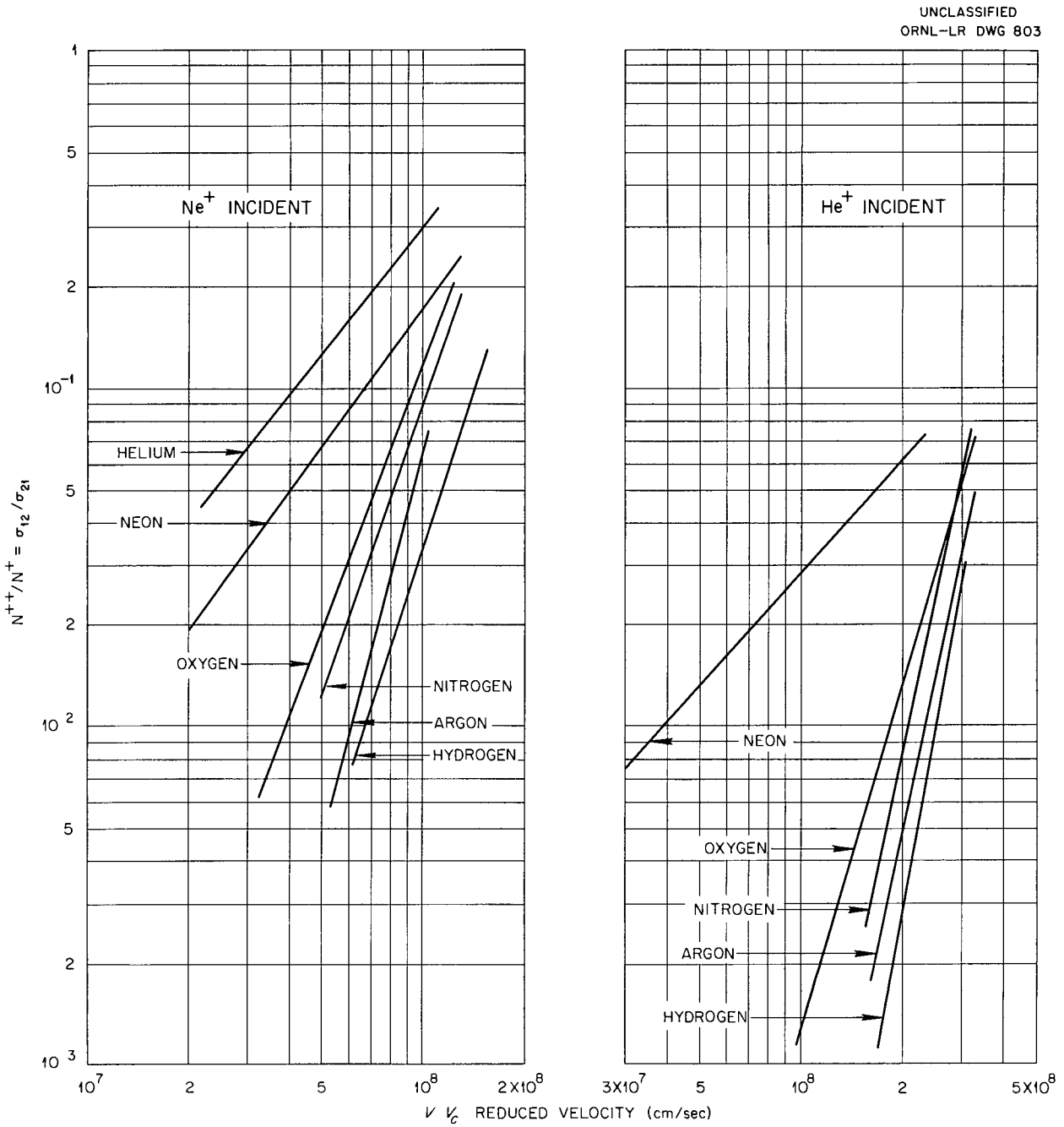

Fig 5 15 Ratio of Second Loss to Capture Cross Sections for Ne^+ and He^+ Ions Passing Through Various Gases

6 NEUTRON PHYSICS

DEMONSTRATION OF NEUTRON SPIN FROM BLOCH ALVAREZ TYPE OF EXPERIMENT

C P Stanford T E Stephenson
S Bernstein

Rabi[1] developed the magnetic resonance method of measuring the gyromagnetic ratio of molecular beams This type of experiment was modified for use in the measurement of the neutron gyromagnetic ratio Alvarez and Bloch[2] selected a given neutron spin state by transmission through a magnetically saturated piece of iron instead of passing the beam through an inhomogeneous magnetic field as is usual with molecular beams This magnetic resonance type of experiment has been extended to give a demonstration of the neutron spin

Two magnetized single crystals of magnetite were used for the neutron polarizer and analyzer as shown in Fig 6 1 Use of magnetite has distinct advantages over the transmission method mentioned above in the selection of a particular spin state in that a monoergic neutron beam is produced which has a high degree of polarization [3 4] Between these two magnetite crystals a constant field H_0 of several hundred oersteds is maintained parallel to the field applied to the crystals Transitions between neutron energy levels in the constant field are induced by an oscillating field H_1 perpendicular to H_0 The frequency ω of H_1 is adjusted so as to satisfy the relation

$$\omega_0 = (\mu/S)H_0$$

where μ/S is the gyromagnetic ratio of the neutron with μ and S expressed in fundamental units

The transition probability[5] in a rotating magnetic field of a particle possessing a magnetic moment is a function of the frequency and amplitude of the rotating field and of the length of time spent by the particle in this field The transition probability also depends upon the angular momentum J of the particle and upon its initial and final magnetic quantum numbers M and M The shape of the transition probability curve plotted against the amplitude of the oscillating magnetic field is distinctly different for the different values of J Using these calculated transition probabilities and the calculated reflectivity of the magnetite crystals for different values of neutron spin the neutron intensity reflected from the two magnetite crystals can be calculated as a function of the amplitude of the oscillating magnetic field for various assumed values of neutron spin With $\omega = \omega_0$ the transition probability curve for spin $\frac{1}{2}$ is of the form $T = \sin^2 \alpha/2$ where α is proportional to the amplitude H_1 of the oscillating magnetic field The intensity reflected from the second magnetite crystal is then proportional to $1 - A \sin^2 \alpha/2$ where for identical magnetite crystals A is a function of the polarization P produced by either crystal alone $A = (2P^2)/(1 + P^2)$

With $\omega = \omega_0$ the intensity reflected from the two magnetite crystals was measured as a function of the amplitude of the oscillating magnetic field the measured values are shown in Fig 6 2. The solid curve shows the calculated intensity for spin $\frac{1}{2}$ that is $1 - A \sin^2 \alpha/2$ the curve is adjusted to give the best fit to the experimental points The observed close agreement of Fig 6 2 cannot be approached by using any other value of neutron spin

The straight line in Fig 6 2 gives the measured counting rate when the neutron beam is depolarized between the two crystals The fact that the $\sin^2$

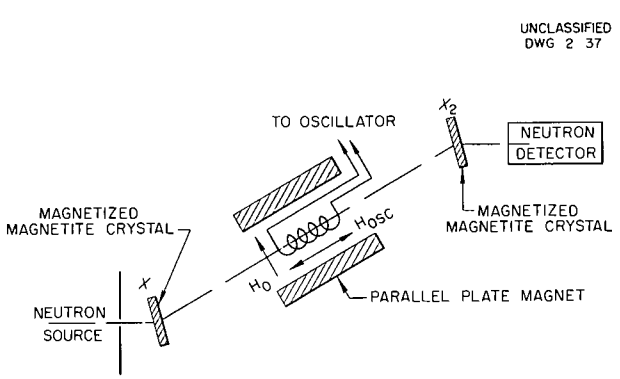

Fig 6 1 Arrangement for Measuring Polarization Using Two Magnetite Crystals and Magnetic Resonance Method

[1] I I Rabi J R Zacharias S M Ilma and P Kusch *Phys Rev* 53 318 (1938)

[2] L W Alvare nd F Bloch *Phys Rev* 57 111 (1940)

[3] C G Sh ll *Phys Rev* 81 626 (1951)

[4] C P Sta ford T E Stephenson L W Cochran and S Be n te p e ented fo publ cat on *The Phys cal Rev ew*

[5] E Majorana *Nuovo cimento* 9 43 (1932)

$\alpha/2$ portion of the best fit calculated curve is symmetrical about this line demonstrates that the maximum transition probability obtained was 100%

The neutron polarization produced by reflection from either magnetite crystal alone as determined by this work is 86%

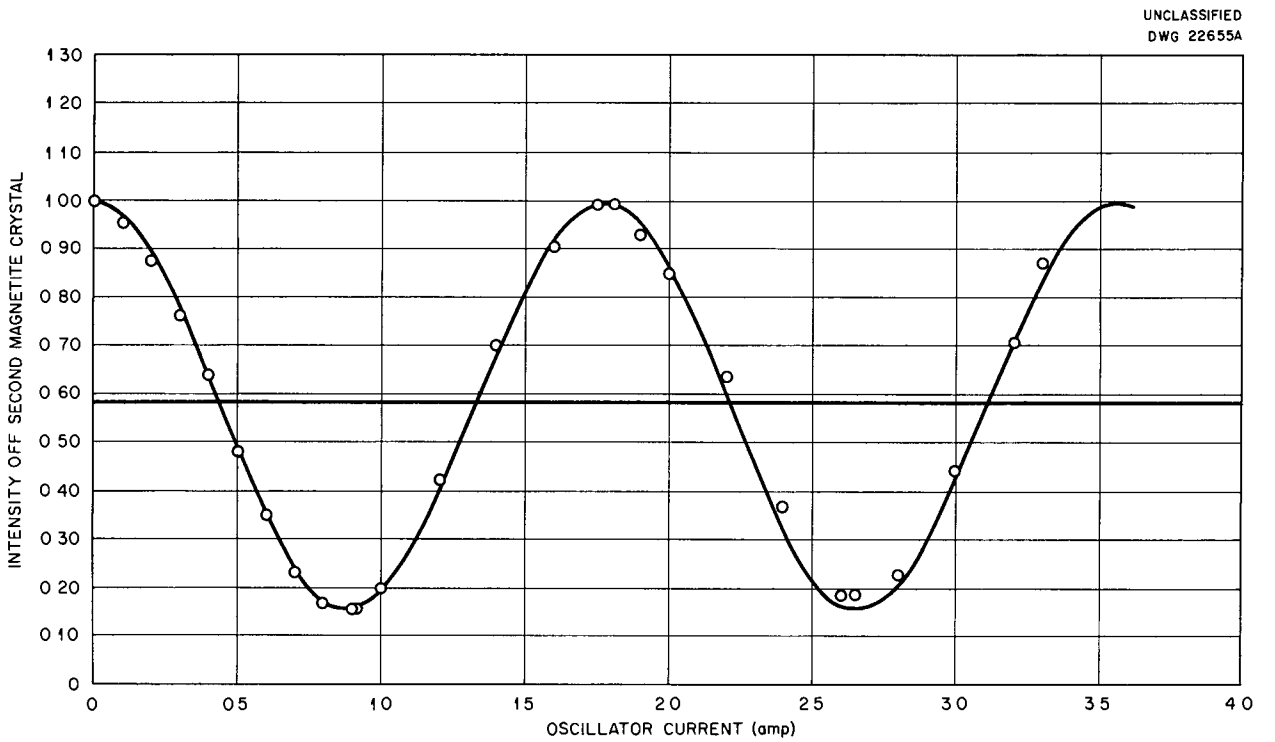

Fig 6 2 Intensity off Second Magnetite Crystal vs Oscillator Current for $\omega = \omega_0$ The solid curve is the best fitting $(1 - A \sin^2 \alpha/2)$ curve obtained using $P(\frac{1}{2}\ \frac{1}{2}\ -\frac{1}{2})$ and polarization of 87%

7 THEORETICAL PHYSICS

TABULATION OF ANGULAR MOMENTUM FUNCTIONS

A Simon

UNIVAC tabulation of the numerical values of the Racah function $W(abcd\,ef)$ is now complete The tables were printed out by the UNIVAC in completely edited form and are being photographically reproduced for final distribution as ORNL 1679 The Racah functions are given to 10 places after the decimal point while the range of arguments is as follows

$$a\,c = 0\ \frac{1}{2}\ 1 \qquad \frac{15}{2}$$

$$b\,d = 0\ \frac{1}{2}\ 1 \qquad \frac{9}{2}$$

$$e = 0\ \frac{1}{2}\ 1 \qquad 3$$

$$f = 0\ 1\ 2 \qquad 8$$

A similar (but much simpler) tabulation of the Clebsch Gordan coefficient $C^{abc}_{\alpha\beta\gamma}$ is also now complete All coefficients which have no argument greater than $\frac{9}{2}$ are tabulated Distribution of this report will follow shortly after the Racah tables

Machine tabulation of the X and G functions is now in the planning stage

MACHINE COMPUTATION OF HIGH ENERGY ELECTRON SCATTERING

G T Trammell

The ORACLE is being programed to calculate the elastic scattering which would be expected to result from high energy electrons – of the order of 100 Mev – falling on various static continuous distributions of positive charge It is hoped that a comparison of these results with the elastic scattering cross sections of heavy nuclei for high energy electrons which have been measured by Hofstadter and collaborators at Stanford will improve the knowledge of nuclear charge distributions A portion of the program has been completed and performed by the ORACLE and the complete program is expected to be ready soon

MAXIMUM VALUES FOR RESONANCE CROSS SECTIONS

A Simon T A Welton

An old controversy as to the maximum permissible resonance cross sections has been resolved Suppose that only a single compound state contributes (definite J and parity) and that potential scattering is ignored From simple statistical arguments (or from the general properties of the scattering matrix) it can be shown that for elastic scattering ($\alpha = \alpha$ with α and α designating initial and final channels) the maximum value of the cross section is

$$(1) \qquad \sigma_{\alpha\alpha} = \frac{4\pi}{k^2}\,\frac{2J + 1}{(2i + 1)(2I + 1)}\,N_s N_l$$

where I and i are target and projectile spins and N_s and N_l are the numbers of possible incident channel spins and orbital angular momenta If $\alpha \neq \alpha$

$$(2) \qquad \sigma_{\alpha\alpha} \leqq \frac{\pi}{k^2}\,\frac{2J + 1}{(2i + 1)(2I + 1)}\,N_s N_l$$

Unless N_s and $N_l = 1$ the results are at variance with those which follow from the simple Breit Wigner formula The resolution of the apparent paradox lies in the fact that if N_s and $N_l \neq 1$ there exists a degeneracy with more than one state having the same energy J and parity (various eigenfunctions of the scattering matrix) Except by accident however only one of these degenerate states will be resonant in a given energy range This implies that a cross section curve of Breit Wigner shape must satisfy Eqs 1 and 2 with $N_s = N_l = 1$ The energy dependence *may* be complicated by the accidental near coincidence of resonances of two or more of these degenerate states in which case Eqs 1 and 2 *must* be used It is interesting to note that in such cases the angular distribution will be that appropriate to a single level

POLARIZATION FROM ISOLATED RESONANCES

A Simon T A Welton

Previous work on polarization arising from nuclear reaction has been specialized to the interesting

case where only a single resonant compound state (definite J and parity) contributes In this case constant (and perhaps large) fractional polarization can be observed across the resonance if $J \neq 0$ and if two different values of orbital angular momentum contribute for either the incident or outgoing beam This resonance polarization is discussed in a paper to appear shortly in *The Physical Review*

THEORY OF NUCLEAR REACTIONS WITH RADIOACTIVE PRODUCTS

T A Welton

A number of nuclear reactions have been observed which yield a stable product and a short lived unstable product Under these conditions even monoenergetic bombardment will yield a spectrum of energies for the stable product This arises because the decay of the unstable product makes its energy uncertain and this uncertainty must be reflected in the energy spectrum for the stable product It has been previously assumed (without proof) that the spectrum is essentially identical with the energy variation of the resonance cross section for scattering of one of the products by the other This speculation has been confirmed by calculation of a simple model and detailed results are being obtained by extension of the Wigner Eisenbud formalism

QUANTUM ELECTRODYNAMICS

T A Welton

An extremely symmetrical and simple formulation of quantum electrodynamics has been found by treating relativistic quantum mechanics as a direct extension of nonrelativistic quantum mechanics This extension is made by treating the motion of hypothetical particles of mass n in a space of four completely equivalent dimensions The motion is specified in terms of a fifth variable which plays the same role as time in nonrelativistic calculations Corresponding to any physical problem a related problem can be found in the hypothetical space The computation procedure is then to calculate the appropriate result for the related problem and finally set the quantity n equal to im where m is the actual electron mass The formalism offers several definite advantages and in spite of its bizarre appearance gives completely sensible results in the usual elementary calculations Application has been made to the level shift calculation with the result that the electrodynamic shift of order $Z^4\alpha^5 m$ is unchanged from previous results The electrodynamic shift of order $Z^5\alpha^6 m$ is completely altered in detail and very much reduced if previously used approximation methods are adhered to The term of order $Z^4\alpha^5 m$ arising from positron theory is eliminated if a plausible reformulation is made along the lines indicated above The net result is very poor agreement with experiment and the formulation may be only an interesting curiosity Further investigation of the approximations entering the calculation is however being made

OSCILLATION FREQUENCIES OF CHARGED PARTICLES IN AXIALLY SYMMETRIC ELECTROSTATIC FIELDS

E C Campbell

A charged particle moves with constant angular frequency ω_0 in an axially symmetric electrostatic field Its orbit is a circle perpendicular to the axis of symmetry and with its center on the axis If the field shape is such that the orbit is stable then small impulses applied to the particle in the axial and radial directions will result in small amplitude oscillations of frequency ω_z and ω_ρ respectively about the original orbit It is shown then that

$$\omega_\rho^2 + \omega_z^2 = 2\omega_0^2 \tag{1}$$

and the stability condition is that $1 < n_E < 3$ where

$$n_E = -\frac{\rho}{E_\rho}\frac{\partial E_\rho}{\partial \rho}$$

at the orbit

Two limiting cases in which the equation is satisfied are well known

1 For the purely cylindrical potential $V = \log \rho$ there is no restoring force in the z direction For this case Eq 1 reduces to $\omega_\rho = \sqrt{2}\,\omega_0$ Therefore in a time equal to a radial oscillation half period

$$\frac{T}{2} = \frac{\pi}{\omega_\rho} = \frac{\pi}{\sqrt{2}\,\omega_0}$$

the particle moves through an angle

$$\omega_0 \frac{T}{2} = \frac{\pi}{\sqrt{2}} \simeq 127 \text{ deg}$$

This radial focusing property of the cylindrical potential was discovered by Hughes and Rojansky in 1929

2 The focusing properties of the spherical field

$$V = \frac{1}{r} = (\rho^2 + z^2)^{-1/2}$$

follow from the circumstance that for this field $\omega_\rho = \omega_z$ Equation 1 implies that $\omega_\rho = \omega_z = \omega_0$ which is just the condition for 180 deg focusing

In order to prove Eq 1 expand the potential $V(\rho\ z)$ in the vicinity of the equilibrium orbit $\rho = \rho_0$ $z = 0$ The result is

$$(2) \quad V(\rho\ z) = (\rho - \rho_0)\left(\frac{\partial V}{\partial \rho}\right)_0 + \frac{1}{2!}(\rho - \rho_0)^2\left(\frac{\partial^2 V}{\partial \rho^2}\right)_0 + \frac{z^2}{2!}\left(\frac{\partial^2 V}{\partial z^2}\right)_0 +$$

The term linear in z is omitted since the z component of the field should vanish at the equilibrium orbit The equations of motion are

$$(3) \quad \rho - \rho\phi^2 = -\frac{\partial V}{\partial \rho}$$

$$(4) \quad z = -\frac{\partial V}{\partial z}$$

and

$$(5) \quad \frac{d}{dt}(\rho^2\phi) = 0$$

Since the component of angular momentum about the axis is constant set

$$(5\ ) \quad \rho^2\phi = \rho_0^2\omega_0$$

and obtain

$$(3\ ) \quad \rho - \frac{\rho_0^4\omega_0^2}{\rho^3} = -\left(\frac{\partial V}{\partial \rho}\right)_0 - (\rho - \rho_0)\left(\frac{\partial^2 V}{\partial \rho^2}\right)_0$$

and

$$(4\ ) \quad z = -z\left(\frac{\partial^2 V}{\partial z^2}\right)_0$$

Now let $y = (\rho - \rho_0)/\rho_0$ and expand the second term of Eq 3 for $y \ll 1$ Then

$$(3\ ) \quad y - \omega_0^2(1 - 3y) = -\frac{1}{\rho_0}\left(\frac{\partial V}{\partial \rho}\right)_0 - y\left(\frac{\partial^2 V}{\partial \rho^2}\right)_0$$

From the equilibrium condition that $y = 0$ at $y = 0$

$$(6) \quad \omega_0^2 = \frac{1}{\rho_0}\left(\frac{\partial V}{\partial \rho}\right)_0$$

and Eq 3 reduces to

$$(3\ ) \quad y = -y\left[\left(\frac{\partial_0^2 V}{\partial \rho^2}\right)_0 + 3\omega_0^2\right]$$

By comparing Eqs 4 and 3 with the equations for oscillatory motion it is found that

$$(7) \quad \omega_z^2 = \left(\frac{\partial^2 V}{\partial z^2}\right)_0$$

and

$$(8) \quad \omega_\rho^2 = \left(\frac{\partial^2 V}{\partial \rho^2}\right)_0 + 3\omega_0^2$$

But the derivatives of the potential must satisfy Laplace s equation

$$(9) \quad \frac{\partial^2 V}{\partial \rho^2} + \frac{1}{\rho}\frac{\partial V}{\partial \rho} + \frac{\partial^2 V}{\partial z^2} = 0$$

On substitution of Eqs 6 7 ana 8 into Eq 9

$$\omega_\rho^2 - 3\omega_0^2 + \omega_0^2 + \omega_z^2 = 0$$

or

$$\omega_\rho^2 + \omega_z^2 = 2\omega_0^2$$

is obtained which is the result stated in Eq 1

The conditions for radial and axial stability are most simply expressed in terms of the index of the

radial component of the electric field

$$n_E = -\frac{\rho}{E_\rho}\frac{\partial E_\rho}{\partial \rho}$$

where of course $E_\rho = -\partial V/\partial \rho$ Equations 7 and 8 are thus transformed into

(7) $$\omega_z^2 = (n_E - 1)\omega_0^2$$

and

(8) $$\omega_\rho^2 = (3 - n_E)\omega_0^2$$

In order that the motion be stable (both frequencies real) n_E must satisfy the condition

(10) $$1 < n_E < 3$$

It is of interest to compare these expressions with the analogous ones for stable orbits in a *magnetic* field Expressed in terms of the magnetic field index

$$n_H = -\frac{\rho}{H_z}\frac{\partial H_z}{\partial \rho}$$

these are

(11) $$\omega_z^2 = n_H\omega_0^2$$

and

(12) $$\omega_\rho^2 = (1 - n_H)\omega_0^2$$

whence

(13) $$0 < n_H < 1$$

is the stability condition and

(14) $$\omega_z^2 + \omega_\rho^2 = \omega_0^2$$

is the relation analogous to Eq 1 It is evident that the electric field stability conditions permit somewhat greater stability for particle orbits associated with a given angular velocity than do those for a shaped magnetic field The restoring forces for the transverse motion (proportional to the square of the frequency) are in fact twice as large in the electric as in the corresponding magnetic case

By combining appropriate axially symmetric solutions of Laplace s equation a potential function

$$V(\rho\, z) = z^2 - \frac{1}{2}\rho^2 + \frac{n_E + 1}{n_E - 1}\log \rho$$

can be obtained which has certain desirable properties and which contains the electric field index n_E as an adjustable parameter In particular the axial field component is independent of ρ and the radial field component is independent ot z so that the dynamical equations are simple If the magnitude of the field is adjusted so that the equilibrium orbit is a circle of radius $\rho = 1$ lying in the plane $z = 0$ then it can be shown that the frequencies of the small amplitude transverse oscillations are given explicitly by Eqs 7 and 8 For $n_E \rightarrow 1$ the field approaches the purely cylindrical field $E_z = 0$ $|E_\rho| = 1/\rho$ while for $n_E = 2$ the field in the neighborhood of the equilibrium orbit is spherical

It is of interest in view of certain applications of these fields to show how the kinetic energy E and the angular velocity ω of the particles in stable circular orbits depend on the radius of the orbit in a fixed field For the magnetic case

$$\frac{dE}{E} = 2(1 - n_H)\frac{d\rho}{\rho}$$

and

$$\frac{d\omega}{\omega} = -n_H\frac{d\rho}{\rho}$$

are obtained For the electric field the corresponding expressions are

$$\frac{dE}{E} = (1 - n_E)\frac{d\rho}{\rho}$$

and

$$\frac{d\omega}{\omega} = -\left(\frac{n_E + 1}{2}\right)\frac{d\rho}{\rho}$$